



NEAR EAST UNIVERSITY
INSTITUTE OF GRADUATE STUDIES
DEPARTMENT OF MECHATRONICS ENGINEERING

**EFFECTIVE ENERGY CONVERSION DESIGN FOR
AN ELECTRIC VEHICLE INTEGRATING SOLAR
ENERGY WITH EFFECTIVE BRAKING SYSTEM: A
CASE STUDY IN NICOSIA**

M.Sc. THESIS

Adeleye Adeoluwa OTEPOLA

Nicosia

January 2023

**ADELEYE ADEOLUWA
OTEPOLA**

**EFFECTIVE ENERGY CONVERSION
DESIGN FOR AN ELECTRIC
VEHICLE INTEGRATING SOLAR
ENERGY WITH AN EFFECTIVE
BRAKING SYSTEM**

MASTER THESIS

2023

**NEAR EAST UNIVERSITY
INSTITUTE OF GRADUATE STUDIES
DEPARTMENT OF MECHATRONICS ENGINEERING**

**EFFECTIVE ENERGY CONVERSION DESIGN FOR ELECTRIC
VEHICLE INTEGRATING SOLAR ENERGY WITH EFFECTIVE
BRAKING SYSTEM IN : A CASE STUDY IN NICOSIA**

M.Sc. THESIS

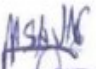

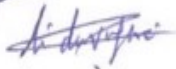
Adeleye Adeoluwa OTEPOLA

**Supervisor
Assist. Prof. Dr. Lida Ebrahimi Vafaei**

**Nicosia
January 2023**

Approval

We certify that we have read the thesis submitted by **Adeleye Adeoluwa Otepola** titled **“Efficient Energy Conversion Design for an Electric Vehicle Integrating Solar Energy with an Effective Braking System: A case study in Nicosia”** and that in our combined opinion it is fully adequate, in scope and in quality, as a thesis for the degree of Master of Educational Sciences.

Examining Committee	Name-Surname	Signature
Head of the Committee:	Prof. Dr. Mahmut Ahsen Savas	
Committee Member:	Prof. Dr. Melike Shah Direkoglu	
Supervisor:	Assist. Prof. Dr. Lida Ebrahimi Vafaei	

Approved by the Head of the Department



Assoc. Prof. Dr. Huseyin Haci
Head of Department

Approved by the Institute of Graduate Studies



Prof. Dr. Kemal Hüsni Çakır Baser
Head of the Institute



Declaration

I hereby declare that all information, documents, analysis, and results in this thesis have been collected and presented according to the academic rules and ethical guidelines of Institute of Graduate Studies, Near East University. I also declare that as required by these rules and conduct, I have fully cited and referenced information and data that are not original to this study.

Adeleye Adeoluwa Otepola

07/01/2023
Day/Month/Year

Acknowledgments

Without the assistance, support, and patience of my instructor, Assist. Prof. Dr. Lida Ebrahimi Vafaei, for her lectures and advice, my thesis would not have been feasible. She has guided me through the whole process of writing a conventional thesis, from beginning to end. This thesis template would not exist if it hadn't been for her constant and profound directions.

Above all, I'd want to express my deep gratitude and love to my beloved family for their patience and faith in me. I'd want to express my gratitude to my mother for her unwavering support, encouragement, and unconditional love that has supported me throughout my life. I owe my gratitude to my wife Omolara, for being my inspiration and for her support always.

Finally, I'd want to express my gratitude to a lengthy number of friends. I can't name everyone, but I want to thank them all from the bottom of my heart for their invaluable assistance and support from the beginning of my studies till now.

And I wish to add a few colleagues at Near East University, Dr. Parveneh Esmaili, Dr Marzieh Rezaei, Dr. Cemal Kavalcioglu, Dr. Serife Kaba, Dr. Huseyin Haci (my HOD), Professor Bulent Bilgehan (My admirable Dean) for the opportunity to work as assistant in the department of Mechatronics Engineering. I appreciate your support always.

Adeleye Adeoluwa Otepola

Abstract

Efficient Energy Conversion Design for an Electric Vehicle Integrating Solar Energy with an Effective Braking System in Nicosia

Assist. Prof. Dr. Lida Ebrahimi Vafaei

MSc, Department of Mechatronics Engineering

January 2023, 140 pages

The goal of this study is to develop a solar-powered electric vehicle that is entirely powered by solar panels mounted on its horizontal surfaces. Solar cars help to reduce consumption of currently renewable energy sources because they lessen reliance on fossil fuels. Solar-powered vehicles will rule the automotive industry in the future because they are more attainable, simple to build, incredibly user-friendly, and need less maintenance than other conventional vehicles. Economical and environmentally friendly features are additional benefits of solar vehicles. A travel survey has been done to study the energy consumption required for the thesis. The design was therefore based on the correspondence feedback at a particular location in Cyprus. Solar energy for the Nicosia location region was considered as input into the simulation design, while the energy and power required to move the vehicle was mathematically modelled. To further add to the powertrain in driving the car, the integration of antilocking and regenerative braking system were being designed to further move the vehicle for longer range and provide additional energy to the vehicle. It is also considered that the vehicle can choose what braking system is needed to obtain the required braking torque energy. The integration of both sources of energy , that is the solar energy and braking energy further produced enough power required in driving the vehicle as designed from the mathematical model.

Key Words: Solar Energy, MPPT, RBS, Simulink.

Summary

Efficient Energy Conversion Design for an Electric Vehicle Integrating Solar Energy with an Effective Braking System in Nicosia

Otepolo, Adeleye Adeoluwa

MSc, Department of Mechatronics Engineering

January 2023, 140 pages

The goal of this study is to develop a solar-powered electric vehicle that is entirely powered by solar panels mounted on its horizontal surfaces. Solar cars help to reduce consumption of currently renewable energy sources because they lessen reliance on fossil fuels. Solar-powered vehicles will rule the automotive industry in the future because they are more attainable, simple to build, incredibly user-friendly, and need less maintenance than other conventional vehicles. Economical and environmentally friendly features are additional benefits of solar vehicles. A travel survey has been done to study the energy consumption required for the thesis. The design was therefore based on the correspondence feedback at a particular location in Cyprus. Solar energy for the Nicosia location region was considered as input into the simulation design, while the energy and power required to move the vehicle was mathematically modelled. To further add to the powertrain in driving the car, the integration of antilocking and regenerative braking system were being designed to further move the vehicle for longer range and provide additional energy to the vehicle. It is also considered that the vehicle can choose what braking system is needed to obtain the required braking torque energy. The integration of both sources of energy, that is the solar energy and braking energy further produced enough power required in driving the vehicle as designed from the mathematical model.

Key Words: Solar Energy, MPPT, RBS, Simulink.

Table of Contents

Declaration.....	3
Acknowledgments.....	4
Abstract.....	5
Table of Contents.....	vii
List of Tables.....	xi
List of Figures.....	xii
List of Abbreviations.....	xv
CHAPTER I.....	16
Introduction.....	16
1.1 Background of Study	16
1.2 Problem Statement	17
1.3 Significance of the Thesis	18
1.4 Aims and Objectives	18
1.5 Scope of the Thesis	19
CHAPTER II.....	20
Literature Review.....	20
2.1 Solar Irradiance	20
2.2 Solar Panels	22

2.3 Electric vehicle (EV) Operation Description	23
2.4 Solar Electric Vehicle and its Main Design Components	24
2.4.1 Solar Array.....	24
2.4.2 Maximum Power Point Tracker (MPPT)	25
2.4.3 System of Energy Storage	26
2.4.4 Electric Motor	29
2.5 Types of Electric Vehicles.....	31
2.5.1 Battery electric vehicle.....	31
2.5.2 Hybrid electric vehicles (HEV)	31
2.5.3 sources of energy for hybrid electric vehicles.....	34
2.6 Brakes.....	34
2.6.1 Anti-lock braking system	35
2.6.2 Braking system in electric vehicles	37
2.7 Related Research.....	43
CHAPTER III	47
Methodology.....	47
3.1 Architectural model of the study	47
3.2 Northern Cyprus Climate Analysis	48
3.3 Travel Survey within North Cyprus.....	52
<i>Analysis of Survey for winter and summer seasons</i>	56

3.3.1 The load profiles.	60
3.4 Solar powered vehicle design.....	61
3.4.1 Design specifications of vehicle model	62
3.4.2 Mathematical Modelling of the Solar Electric Vehicle for Power and Energy required.....	64
3.4.3 Mathematical Modelling of the SEV for the Electric Motor.....	68
3.4.4 Mathematical Modelling of the SEV for the Battery Capacity	68
3.4.5 Mathematical Modelling of the SEV from the Solar Panel.....	69
3.5 Pv Design Analysis	70
3.6 Solar Energy mathematical model for Nicosia	72
3.6.1 Mathematical of the Temperature input from irradiance to PV Panel	75
3.6.2 Solar panel General Mathematical Model	78
3.7 Dc-Dc Boost Converter.....	80
3.8 Mppt Modelling Design	81
3.9 Energy Management System.....	84
3.10 Brake Design.....	85
3.10.1 ABS Mathematical modelling using third vehicle dynamics / analysis.	85
3.10.2 Parallel RBS Mathematical modelling	92
3.10.3 Novel Regenerative Braking Control Strategy.....	95
3.10.4 Mathematical Determination of Required Braking Torque.....	99

3.10.5 Mathematical Determination of Torque produced by vehicle.....	101
3.10.6 Mathematical Modelling of Novel Regenerative Braking Control Strategy	102
CHAPTER IV	104
Results and Discussion	104
4.1 Forces exerted on the SEV Simulink Model Result	104
4. 2 Energy Management System for Batteries	106
4.3 Braking System Simulink Model Result	109
4.4 RBS Power Output integration with PV Load Power Output.....	114
CHAPTER V	116
Conclusion and Recommendations.....	116
References.....	118
Appendices.....	124
Appendix A (Answers from the Survey).....	124
Appendix B (Fuzzy Logic Inference for MPPT model)	124
Appendix C (Plagiarism report).....	131

List of Tables

Table 3.1 Survey Transportation Mode	55
Table 3.2 Travel Purpose List	56
Table 3.3 Mechanical Specification of Tesla Model S	67
Table 3.4 Technical Specification of Lightyear0	68
Table 3.5 Solar Panel Specification of SunPower X-Series	75
Table 3.6 Pv Technology as Regards to Factor a Dependency	84
Table 3.7 Variation in The Ratio of Wheel Slip to The Coefficient of Traction in The Road	91
Table 3.8 Meaning of Lamp Colours	97
Table 4.,1 Technical Input Data of SEV Simulink Model	103
Table 4.2 Simulink Energy Management Output Power Design	109
Table 4.3 Table of Parameters	111
Table 4.4 Road of Surface Type Against and Corresponding Slip Ratio	112
Table 4.5 Matlab Simulink Table of Simulation	114
Table 4.6 Integration of PV Power Source with RBS Power Source	125

List of Figures

Figure 2.1 Solar Insolation on a typical Sunny Day	19
Figure 2.2 Breakdown of Solar Energy	19
<u>figure 2.3 Solar Panel Diagram</u>	<u>20</u>
Figure <u>2.4 Solar Panl Diagram</u>	<u>21</u>
Figure <u>2.5 Solar Car Design</u>	<u>23</u>
Figure <u>2.6 Hierachy of Solar PV Array</u>	<u>23</u>
Figure <u>2.7 MPPT Block Diagram</u>	<u>23</u>
Figure <u>2.8 Lithium ion Battery type comparison</u>	<u>26</u>
<u>Figure 2.9 View from the top of an electric car</u>	<u>29</u>
Figure <u>2.10 Series HEV Schematic</u>	<u>30</u>
Figure <u>2.11 Parallel HEV Schmatic</u>	<u>30</u>
Figure <u>2.12 Series-Parallel HEV Schematic</u>	<u>31</u>
Figure 2.13 Automotive Braking System	33
<u>Figure 2.14 ABS Operation</u>	<u>34</u>
<u>Figure 2.15 Energy flow in braking system</u>	<u>35</u>
Figure 2.16 Brake Torque blending overview	36
<u>Figure 2.17 Braking Distribution Coefficient</u>	<u>38</u>
<u>Figure 2.18 IC engines and electric regeneration system</u>	<u>39</u>
Figure 2.19 Energy usage from the battery	40
<u>Figure 2.20 when the brake is applied , battery charges</u>	<u>40</u>
<u>Figure 2.21 The generation which is the electric motor in reverse direction stores the energy in the vehicle's battery</u>	<u>41</u>
<u>Figure 3.1 Block diagram design of SEV</u>	<u>46</u>
<u>Figure 3.2 Global Horizontal irradiation GHI of Cyprus Island</u>	<u>46</u>
<u>Figure 3.3 Day light graph in Cyprus</u>	<u>47</u>
<u>Figure 3.4 Sun hours graph of Cyprus Island</u>	<u>47</u>
<u>Figure 3.5 Monthly Average Temperature</u>	<u>48</u>
<u>Figure 3.6 Historical mean temperature of Cyprus for 20 years</u>	<u>48</u>
<u>Figure 3.7 Cyprus max-min temperature</u>	<u>49</u>
<u>Figure 3.8 Energy radiation graph in Cyprus</u>	<u>50</u>
<u>Figure 3.9 Survey Gender Chart</u>	<u>53</u>
<u>Figure 3.10 Correspondence location Statistics</u>	<u>53</u>
<u>Figure 3.11 Correspondence work nature</u>	<u>54</u>
<u>Figure 3.12 Timeline factor of the survey</u>	<u>54</u>
<u>Figure 3.13 Purpose of trip during summer</u>	<u>55</u>
<u>Figure 3.14 Purpose of tri during winter</u>	<u>56</u>
<u>Figure 3.15 Distance travelled during summer</u>	<u>56</u>
<u>Figure 3.16 Distance travelled during winter</u>	<u>57</u>
<u>Figure 3.17 Mode of transportation during the summer</u>	<u>57</u>

Figure 3.18 Mode of transportation during the winter	57
Figure 3.19 Summer load profile	59
Figure 3.20 Winter load profile	59
Figure 3.21 Vehicle Design Illustration with solar panels	60
Figure 3.22 Solar working principle	60
Figure 3.23 Tesla Model S Body Specification	61
Figure 3.24 Forces acting on SEV on an inclined plane	63
Figure 3.25 Geographical View of Nicosia	64
Figure 3.26 Simulink Model of forces acting on the SEV	66
Figure 3.27 Monthly Solar irradiation in Nicosia	67
Figure 3.28 Average daily Meteo data in Nicosia	68
Figure 3.29 Nicosia geographical area	70
Figure 3.30 Pv cell circuit diagram	77
Figure 3.31 Energy Management system of three sourced input	78
Figure 3.32 DC-DC Converter	78
Figure 3.33 Three input converter model	79
Figure 3.34 I,V, Irradiance characteristics graph	80
Figure 3.35 P&O MPPT algorithm	81
Figure 3.36 Fuzzy Logic Mppt design model	81
Figure 3.37 Simulink energy management system design	82
Figure 3.38 Third Vehicle Model	83
Figure 3.39 Road friction coefficient versus wheel slip ratio	86
Figure 3.40 System for feedback control in ABS block diagram	87
Figure 3.41 Simulation of ABS governing equations	88
Figure 3.42 Calculation of slip ratio subgroup	88
Figure 3.43 Coefficient of friction computation subgroup	88
Figure 3.44 Model for the ABS feedback control system	90
Figure 3.45 Distance covered by ultrasonic pulse	94
Figure 3.46 Ultrasonics sensor operation sending	94
Figure 3.47 Ultrasonics sensor operation receiving	94
Figure 3.48 TIDA-00151 ultrasonic sensor circuit diagram	95
Figure 3.49 Single turn rotary type potentiometer circuit diagram	96
Figure 3.50 OCU flowchart	97
Figure 3.51 OCU block diagram	97
Figure 3.52 Matlab Simulink Simulation of required braking torque	99
Figure 3.53 Matlab Simulink Simulation of RBS braking torque	100
Figure 3.54 Matlab Simulink of overall control unit	101
Figure 4.1 Simulink Model of forces acting on the SEV	102
Figure 4.2 Simulink Result of SEV required power	103
Figure 4.3 Battery Management Systems	104

<u>Figure 4.4 Overall Power Simulation from the average irradiance input</u>	105
<u>Figure 4.5 Summer Power Output</u>	105
<u>Figure 4.6 Winter Power output</u>	106
<u>Figure 4.7 Coefficient of road friction against wheel slip ratio</u>	108
<u>Figure 4.8 Matlab Simulink Simulation result of required braking torque</u>	109
<u>Figure 4.9 Matlab Simulink simulation result of RBS braking torque</u>	109
<u>Figure 4.10 Matlab Simulink simulations of braking system integration</u>	110
<u>Figure 4.11 Energy Sources Integration</u>	112

List of Abbreviations

ABS – Anti-lock braking system

RBS – Regenerative braking system

ECU – Electronic control unit

PCB – Printed circuit board

MDF – Medium density fiber board

PWM – Pulse width modulation

OCU – Overall control unit

DC – Direct current

EMF – Electromotive force

G-CODE – Numerical programming language for automating machine tools

IDE – Integrated development environ

SEV – Solar electric vehicle

MPPT- Maximum Power Point Transmission

CHAPTER I

Introduction

1.1 Background of Study

One of the most urgent engineering problems at the moment is the need for clean energy sources. Electricity is frequently produced using coal and natural gas in many regions of the world. It has been demonstrated that this power source, despite being plentiful, increases global warming. Furthermore, it has been demonstrated that extraction techniques like fracking harm the environment, particularly earthquakes. One type of energy that is the subject of extensive research is solar energy. Prior to now, solar energy wasn't a viable substitute for fossil fuel-based energy because solar panels' efficiency was too low. Utilizing solar energy as a renewable resource that is progressively meeting society's energy needs is now possible thanks to modern materials. Transportation accounted for 26% of all greenhouse gas emissions in 2014, according to the US Environmental Protection Agency (EPA). (Manivannan & Kaleeswaran, 2017).

Over the past 12 years, there has been a rise in demand for renewable energy sources due to various global factors such as the declining availability of fossil fuels, instability in fuel-producing countries, intensifying impact of climate change, and declining costs of renewable energy technologies. These developments have led nations to reevaluate their energy sources. The increasing adoption of photovoltaic systems is largely attributed to the lower cost of installation and greater government support in the form of renewable energy programs, tariffs, tax incentives, etc. Similarly, the growing popularity of electric vehicles can be attributed to advancements in battery and electric drive technology, as well as the pressing need to reduce air pollution in cities. (Bhusal, 2018).

Ndyamukama; (2017)The transition to renewable energy sources today is facilitated by several factors, including government policies encouraging its use, business competition for market share, and homeowners' lower energy costs as a result of renewable energy sources' lower cost. In contrast to conventional energy sources, renewable energy sources are more difficult to manage because it is difficult to balance production with generation when there is unpredictable generation. But we can strike a balance by overseeing our consumption.

This study focuses on the incorporation of solar PV energy into an electric vehicle that is entirely powered by solar PV panels fixed to its horizontal surfaces. Because solar cars reduce reliance on fossil fuels, they help to reduce consumption of currently renewable energy sources. The automotive industry will be dominated by solar-powered vehicles in the future because they are highly

realizable, easy to construct, incredibly user-friendly, and require less maintenance than other conventional vehicles. Economical and environmentally friendly features are additional benefits of solar vehicles. The drawbacks of solar vehicles include high initial costs, a restricted range of speeds, and an unsatisfactory energy conversion rate of around 17% (Connors, 2007).

Photovoltaic (PV) panels, which are another name for solar cells, are merely converters. The ability of solar cells to produce electricity when exposed to light without endangering the environment or the device suggests that power can be generated for a long time with little maintenance and operating costs (Bhatti & Salam, 2013). Due to their lack of tailpipe emissions, which enhance air quality and reduce health risks, electric vehicles also assist the country in reducing its reliance on foreign fossil fuels (Robinson et al., 2014). Electric cars are essential for reducing carbon emissions and keeping the environment clean. When your electric vehicle (EV) or pure electric vehicle (PEV) is charged using a photovoltaic system (PV) with photovoltaic solar panels, which are typical grid sources, it will produce less pollution (Valero et al., 2013). The integration of PV with the electric vehicle (EV) charging system has increased due to several factors, including the ongoing decline in the cost of PV modules, the quick growth of EVs, and concern over the effects of greenhouse gases (Bhatti et al., 2016). A thesis titled "An Electric Charging Method for Automobiles Using Photovoltaic Cells" has been started to design and implement a dependable system to charge the vehicle using solar energy power sources (Latha et al., 2014).

In this thesis, I will analyze the daily energy demands of passenger vehicles in Cyprus to create a load profile. Then I determine how much energy the electric car's solar panels can produce at each of the locations. Finally, we calculate the amount of energy that can be produced to meet the energy needs of passenger vehicles.

1.2 Problem Statement

At the background of this chapter, some problems were highlighted to the need of solar electric vehicle. The Environmental pollution or hazards; noise and air pollution by fossil fuel vehicles is a challenge that needs to be treated, but with the advancement in the use of renewable energy as seen in solar, there are Shortage of Solar Charging Stations, with these shortages, we have High cost of charging at the few Charging Stations provided because of the scarcity of charging stations. As a fact we have high cost in building a solar charging station as well. With this scarcity, there is the problem of the electric vehicle recharging at longer distance, this has posed the problem of long-range distance movement deficiency with limited speed range, and this can all be attributed to Energy management systems knowledge Limitations.

In addition to these problems, it should be noted that, electric vehicles which are recently gaining acclaim and use due to their environment friendly operation,

require a braking system that allows for short braking distance, manoeuvrability while braking, as well as a means for reducing the heat energy being dissipated to the environment when the brake callipers clamp on the rotating tyres. This braking system should also have a means of energy conservation by converting this wasted heat energy into a form useful energy to the vehicle, in terms of electrical energy.

1.3 Significance of the Thesis

This thesis seeks to provide an energy management system that solves the design of solar electric vehicles in Cyprus. This is accomplishable by gathering load data for vehicles in the region and solar energy potential, in turn how much energy needed can be generated to meet the energy demand of passenger vehicles. The design will help to provide longer distance range electric vehicles in the region. To further boost the design longer distance and overcome speed limitations, the thesis seeks to provide control strategies for the synergistic integration of the two important braking system types being equipped in electric vehicles; the Antilocking braking system which provides a means of emergency braking without skidding, and the Regenerative braking system for energy conservation and conversion while still providing smooth steering control while braking to avoid collision with obstacles. The result of this synergy also provides a braking system that brings the vehicle to rest in short braking distances, while considering the intentions of the driver as to which braking system would be of priority, but mostly the choice braking system will be the regenerative braking system for energy conversion system.

1.4 Aims and Objectives

The aim of this thesis is to enhance the efficiency of an Electric Vehicle using Solar PV energy for longer range distance and design an effective braking system for sustainable energy supply when the Electric Vehicle is in motion and storage to battery.

To meet these aims, the following Objectives are highlighted as a means of designing an efficient solar electric vehicle based on the solar energy in Cyprus.

- Data Collection of Solar Energy in Cyprus.
- Analysis of data collated for optimization design.
- System design of solar PV inputs
- Design of efficient braking system
- Battery modelling and SOC design
- Integration of Solar and Braking systems Energy

1.5 Scope of the Thesis

The main scope of the thesis is to design a Solar electric Vehicle for longer range distance, providing an efficient braking system and an energy management system for electric vehicles using solar by;

- analyzing passenger vehicle travel patterns in Nicosia, Cyprus
- and then developing a load profile based on the energy demand of the passenger vehicle per day.
- Then calculate how much energy the solar panels on the electric vehicle can generate in the location.
- Finally, estimate how much energy can be generated to meet the energy demand of passenger vehicles.

CHAPTER II

Literature Review

Solar energy is becoming more and more popular due to the abundance of solar energy on Earth's surface as well as its non-polluting and silent properties. The weather and environment have an impact on how much electricity the PV system produces, and the PV system operating on its own is typically unreliable. Contrarily, PV modules stand out due to their straightforward design, compact size, light weight, and stability during installation and transport. Additionally, the PV system is easily installed with other power sources, has a quick construction time, and can be used in homes or public areas. A charging station-based energy storage device can significantly reduce the variability of PV power output [(Han et al., 2018), (Hill et al., 2012)]. PV solar panels are used to charge EVs for a variety of reasons, including:

1. Solar PV costs have steadily declined in recent decades.
2. In addition to parking spaces close to electric vehicle charging stations, rooftops can also be used to install PV panels.
3. Because the charging power is generated in part by PV panels, the peak demand for EV charging is reduced on the grid.
4. PV charging systems store the energy produced by PV panels using an ultracapacitor and lithium batteries. By doing so, daytime, and seasonal climate variations that have an impact on solar production can be managed.
5. Solar energy is less expensive than grid-based systems for charging EVs.

As a result, the utilization of a solar PV system and the addition of other energy sources is designed in this thesis. Incorporating a regenerative braking system and energy storage that encourages a greater range of velocity for the EV, this chapter provides a thorough literature review of the many topics involved in the design of a solar electric vehicle.

2.1 Solar Irradiance

The sun provides energy to the earth every day. On the other hand, the amount of energy varies with the time of day, the environment, and the place. It is common to measure solar energy insolation or irradiance in terms of watts per square meter, or w/m^2 (Chukwuka, 2013). The figure 2.1 below shows an example image graph of solar isolation.

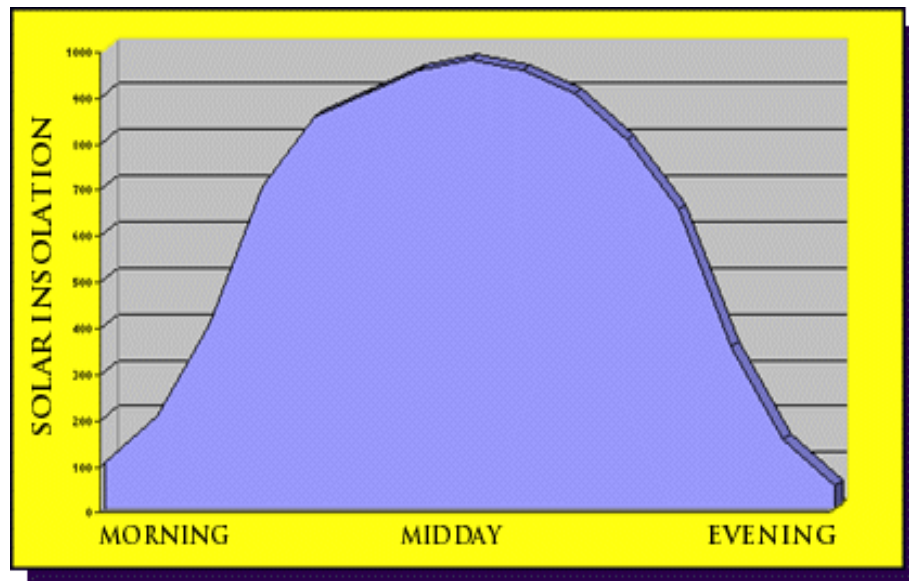


Figure 2.1: Solar insolation on a typical sunny day (Chukwuka, 2013).

The three parts of solar irradiance are also referred to as direct beam, diffuse, and ground-reflected irradiance.

Global irradiance is defined as the sum of these components. A variety of factors influence the amount of irradiance that falls on a surface, including the time of year, the angle of the surface cloud cover and the location of the sun in the sky.

These elements should be considered when designing the solar array. Figure 2.2 below shows how the solar energy that the sun emits toward the earth is properly broken down, showing how much energy is lost to the atmosphere, reflected off the surface, and returned to space.

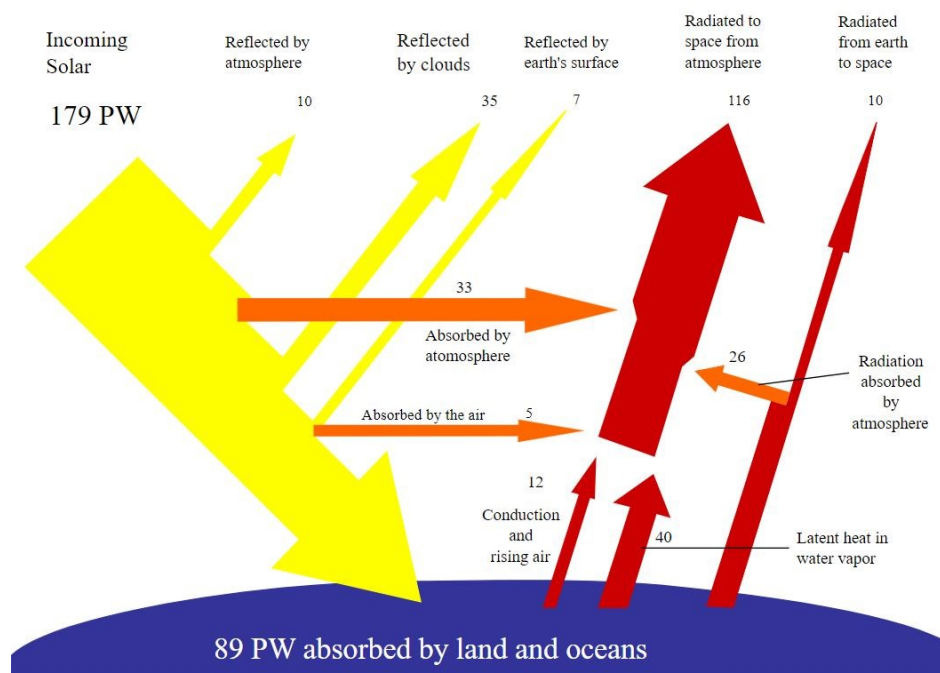


Figure 2.2: Breakdown of Solar energy (Sunrator, 2019).

2.2 Solar Panels

When French physicist Edmund Becquerel discovered that when certain materials were exposed to sunlight, they produced an electric current in 1839, solar energy was recognized for the first time. For his contributions to photovoltaic technology, Albert Einstein won the Nobel Prize in Physics in 1905. In 1954, Bell Laboratories created the first photovoltaic module, though it had no known uses at the time. A spacecraft's dependability and usability were improved in the 1960s thanks to the use of solar energy for power generation. Solar energy finally became widely used in the 1970s energy crisis (Kretchmer et al., 2017). Consequently, what precisely are photovoltaic (or solar) cells? A thin semiconductor wafer undergoes a specialized treatment to establish an electric field with a positive charge on one side and a negative charge on the other, which is essential for solar cells to function. In the figure 2.3 below, electrons from the atoms of the semiconductor material are ejected when light strikes a solar cell. Electrons can be captured as an electric current if the positive and negative sides of the cell are connected to electrical conductors to form an electrical circuit. (Kretchmer et al., 2017).

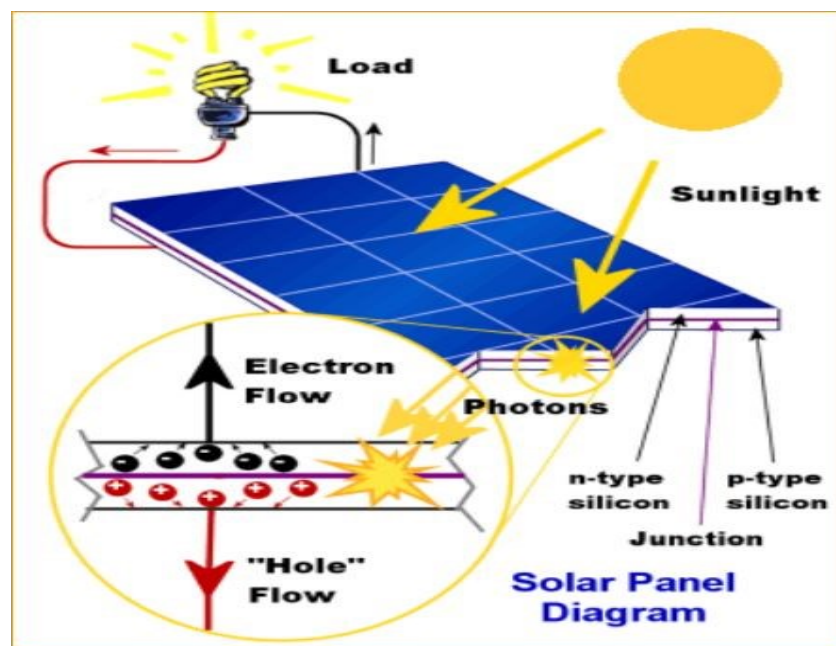


Figure 2.3: Solar panel diagram (Wisniewski, 2010).

The solar energy is captured and transformed into usable electrical energy by photovoltaics, also known as solar cells. They are constructed from silicon by joining two silicon semiconductors, one n-type and one p-type, to form an electron-rich layer and an electron-poor layer. In response to photons striking the cell, semiconductor atoms release their electrons, leaving behind positive charges. The diagram below (Figure 2.4), demonstrates how this produces an electromotive force that drives current to charge a battery or power a motor, as well as an electron flow that results from this. (Wisniewski, 2010).

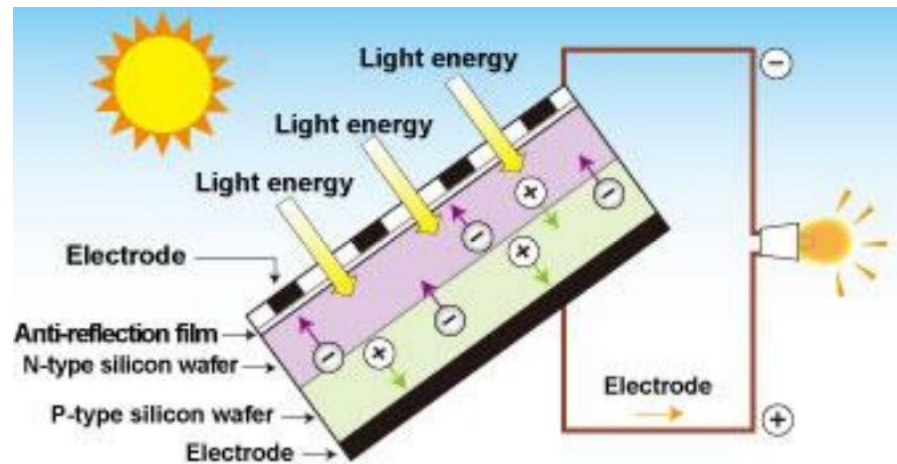


Figure 2.4: Solar panel operation diagram (Kretchmer et al., 2017)

Multiple modules make up an array, and multiple cells make up a module. Standard 12-volt electrical systems can use these arrays without a problem. Additionally, panels for personal use that have been treated can be produced. The operation and effectiveness of the solar module were investigated through several tests and experiments. A positive and a negative electrical lead are attached to the panel's back, allowing for the measurement of the current. With the aid of a solar analyzer and the software that works with it, voltage and current curves can be produced. Additionally, the leads for the positive and negative sides of the panel will be connected to the solar analyzer. Irradiance, date, temperature, and solar cell area are some of the variables that can be entered into the analyzer to improve the precision of the outcomes. The solar panel can be angled towards the sun for an analyzer scan to be performed, measuring the voltage and current generated by the photovoltaic process and evaluating the panel's total efficiency.

2.3 Electric vehicle (EV) Operation Description

To move, all vehicles need to rotate. This object faces four major obstacles that it must get past to move: rolling resistance, wind resistance, potential energy, and kinetic energy. As the vehicle moves forward, air molecules disperse to the sides, causing wind resistance. This explains why most vehicles have similar frontal shapes. Because air density varies with temperature, wind resistance varies throughout the day. The more wind resistance there is, the more energy is required to propel the vehicle forward. The deformation of the vehicle's tires on the road surface is the primary cause of rolling resistance. Resistance is always present because of the vehicle's mass and stationary tires. As the car accelerates, it also gains kinetic energy; when the propulsion stops, the energy is lost but makes up for it by allowing the car to travel further. It's critical to understand how the car uses its energy. Braking energy, for example, can be regenerated as electrical energy in electric vehicles via motor recuperation, reducing energy loss. To stop a moving vehicle with an internal combustion engine (ICE), the kinetic energy or potential must be converted into

another form. Braking causes the vehicle to come to a stop, producing heat in the process. Auxiliary consumption, also known as idle consumption, refers to the energy used to power a car's heating system, headlights, air conditioning, and ventilation. The battery powers heating in electric vehicles, whereas thermal energy loss in the motor and energy loss in vehicle powertrains power heating in internal combustion engines. This is the energy lost because of the gearbox, ball bearings, and differential drive characteristics. Because electric vehicles do not require a transmission, this energy loss is avoided. The motor has the ability to rotate the wheel directly. (Ndyamukama; 2017)

2.4 Solar Electric Vehicle and its Main Design Components

A solar car is an electric car that utilizes solar energy to charge its batteries and increase its range using photovoltaic cells built into the vehicle. (Wisniewski, 2010). The solar car is made up of an array of solar panels, a system for storing energy, and a system for powering an electric motor. In the figure 2.5 below, a schematic sketch is displayed. The energy storage system can be recharged through the photovoltaic (PV) array, and these two components can work together to power the motor and achieve the desired velocity for the vehicle. (Mills & Stumpges, 2013).

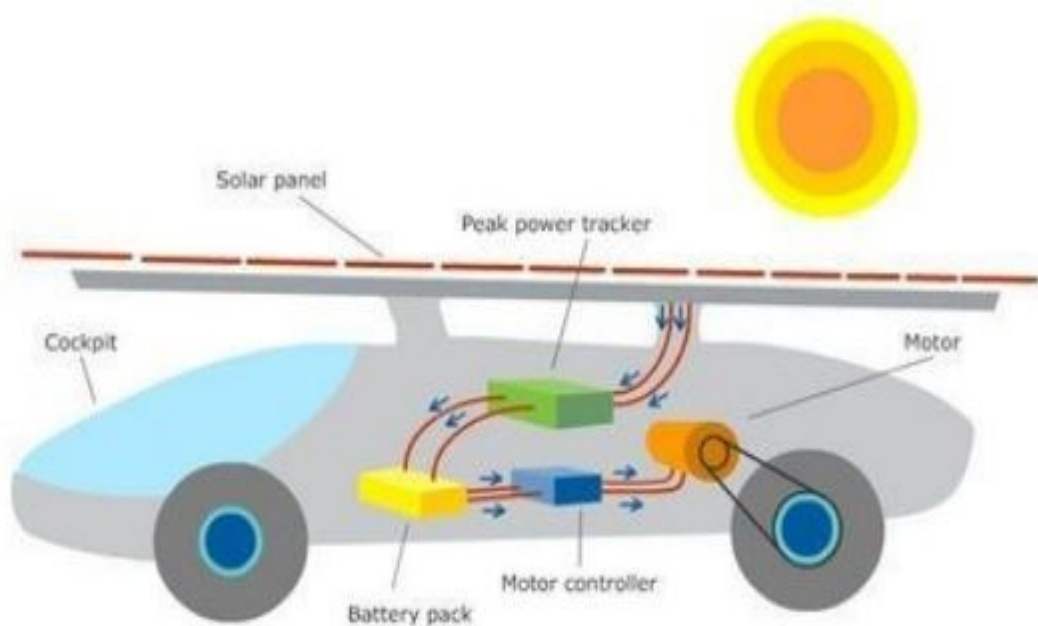


Figure 2.5: Solar Car design (Wisniewski, 2010).

2.4.1 Solar Array

Multiple individual solar cells are linked together in a variety of series and parallel configurations to increase the voltage or current output of a solar array. (Said et al., 2012). Thin film solar panels made of amorphous silicon, cadmium telluride (CdTe), and copper indium gallium selenide (CIS/CIGS) are available in

monocrystalline silicon, polycrystalline silicon, and all three types of thin film.—are the three categories into which solar panels are currently divided (Ahmad et al., 2010). The characteristics of various types of solar cells vary. Usually, it is advised to connect the PV panels in parallel to get around the shading effect.

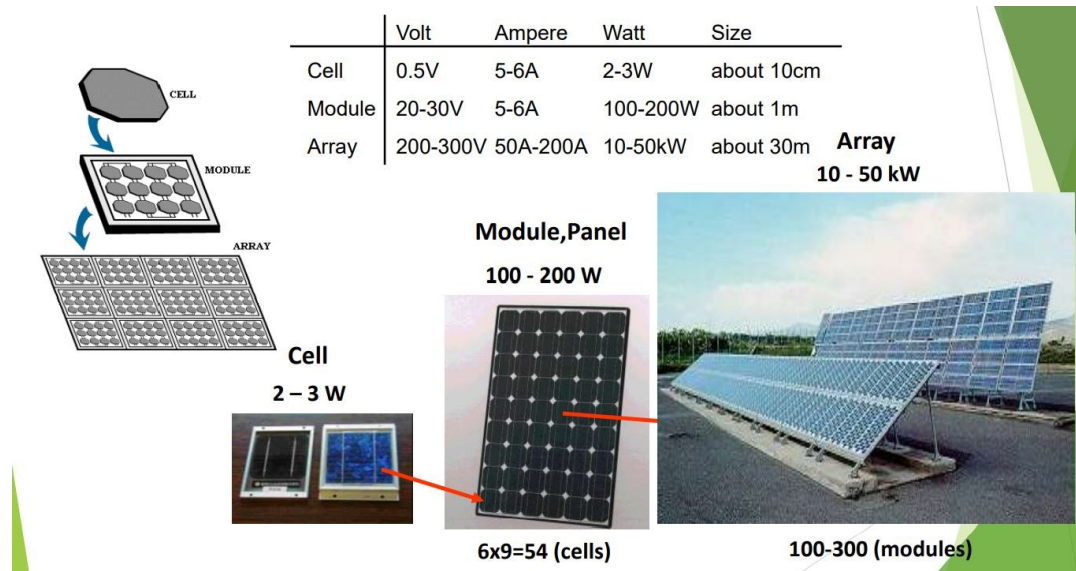


Figure 2.6: Hierarchy of Solar PV Array (Sunrator, 2019).

2.4.2 Maximum Power Point Tracker (MPPT)

Photovoltaic cells have a single operating point where their current and voltage can produce the most power. (Wisniewski, 2010). For photovoltaic cells, there is a single operating point where the maximum amount of power can be produced by the cell's current and voltage. As seen in figure 2.7 below, the MPPT is essentially a DC/DC converter that is installed between the solar array and the DC bus. The PV output voltage is set by the MPPT in order to get the most power out of the cell and deliver it to the load. (Wisniewski, 2010).

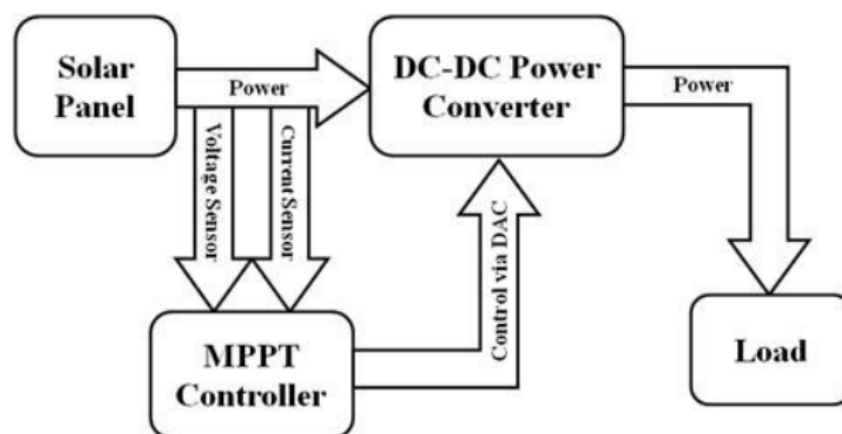


Figure 2.7: MPPT block diagram (Wisniewski, 2010)

The output power of a photovoltaic (PV) string has an inverse correlation with its operating voltage. As the voltage increases, the power output of the PV string increases steadily until it reaches a maximum, then decreases as the voltage approaches the open-circuit voltage. The PV string can always operate at its most productive position thanks to a tracker, regardless of battery voltage. The tracker output is $2.4\text{A} \times 100\text{V} = 240\text{W}$ if your battery voltage is 100V, and the optimal operating point for an array string is $2\text{A} \times 120\text{V} = 240\text{W}$. Tracker electronics inefficiencies cause a loss of 1-2 percent. MPPTs are divided into three categories: down (buck) converters, up (boost) converters, and dual (buck-boost) converters, which can convert in both directions but at a cost to efficiency.

2.4.2.1 Choosing the Most Powerful Power Point: The maximum power point can be determined in two ways.

1. Open circuit voltage (VOC) tracking: The tracker continuously monitors the VOC of the PV string and sets the operating voltage to, $V_{mp} = k \cdot V_{OC}$, where k is a constant. The procedure is straightforward and largely effective. This method is used by AERL trackers.
2. Power tracking: As the operating point is gradually changed, the tracker monitors changes in output power and modifies the operating point to increase output power.

2.4.3 System of Energy Storage

In solar cars, the battery is the most used energy storage system. However, ultra-capacitors are also used for short bursts of power. The ultracapacitor and battery pack are connected in parallel. It is possible to manage the energy in both steady and dynamic states to deliver the required current while driving in situations like normal, accelerating, decelerating, or braking by combining the two storage systems. 1) Power Source: A battery pack is a necessary part of any electric vehicle. Three purposes of the battery pack are to: (I) provide a backup energy source for use when the solar panel system is not producing enough power, (II) when necessary, supply direct current to the motor, and (III) reduce fluctuations in the current and voltage output from the PV system into the loads. (Alnunu et al., 2012). Performance, expense, and safety are carefully considered when choosing solar car batteries. When using any battery with a battery protection system (BPS), which includes battery isolation contactors, safety always comes first (Wisniewski, 2010). 2) Ultra Capacitors: These systems for short-term energy storage can store and releasing energy quickly and effectively. To put it simply, they are very effective in these applications because they can quickly supply a large amount of energy when power demand is greatest. Also, if a battery or fuel cell is unable to continuously provide or handle short bursts of power, ultra-capacitors can act as a backup source of energy. (Wu et al., 2011).

2.4.3.1 Battery Selection Options: A solar vehicle's battery is an essential component in its design and implementation. To power and move the vehicle, the solar panel must first charge the battery. The driver must feel secure in this setup. These are the three most crucial things to consider when purchasing a battery. These specifications are met by deep cycle lead acid and lithium-ion batteries. When choosing which battery to buy, these factors were considered, but the most crucial consideration was whether the battery would work with the car's motor. The motor type affected the final battery choice (Kretchmer et al., 2017).

2.4.3.1.1 Lead Acid: The lead acid battery was the first battery type considered. A solar-powered electric vehicle could use some specific types of lead acid batteries, but none of them are practical. For instance, the battery that typically kicks in an engine in a gasoline-powered car would not be appropriate for this thesis. Prior to being recharged by the alternator while driving, starter batteries have a finite amount of energy. Any electric vehicle needs a deep cycle battery. Long-lasting, dependable power is what deep cycle batteries are intended to offer. The ability to repeatedly discharge deep cycle batteries from full capacity to empty is one of their most crucial properties. Unlike starter batteries, which can only be fully discharged about ten times, deep cycle batteries can be fully discharged hundreds of times before losing their ability to hold a charge. Although it is very simple to charge deep cycle lead acid batteries with a solar panel, a charging controller is required to ensure the battery has a long lifespan and high performance. By charging the battery three times, the charging controller makes sure of this. The bulk charge is the initial stage. Before stopping when the voltage reaches just under 14 volts, the battery is charged to about 80% of its maximum voltage, amps, and capacity. The battery is gradually charged to almost 98 percent capacity during the second stage, absorption charge. The third and last stage, known as a "float charge," fully charges the battery without going overboard or boiling the acid. (Kretchmer et al., 2017). Because it can run a car and be recharged by a solar panel, a deep cycle lead acid battery is a good solution. Deep cycle lead acid batteries can be divided into two categories: sealed batteries and flooded batteries. Flooded batteries require routine maintenance to keep them functioning properly and prolong their lifespan. The battery is maintained in good condition by adding distilled water to each individual cell and using a hydrometer to gauge the specific gravity. To maintain the battery's effectiveness, the case must be taken off and changed about once a month (Kretchmer et al., 2017). Since a sealed battery is, as its name suggests, permanently sealed, this is not necessary. When considering a flooded battery, there is a safety concern because, even with the necessary safety measures, accidents are more likely whenever exposed acid is involved. Consequently, a flooded battery was dead. Safety comes first, so sealed batteries are preferred even though they are roughly twice as expensive as flooded batteries. Based on this knowledge, it was decided that a deep cycle sealed battery would be used in place of a lead acid battery.

2.4.3.1.2 Lithium Ion: Electric vehicles powered by the sun are best suited by lithium-ion batteries. Due to lithium's superior electrochemical potential and specific energy compared to all other metals, pound for pound, most lithium batteries can cycle well over 1000 times regardless of the cathode material. A simple controller is all that's needed to charge many lithium-ion battery chemistries, which were created specifically to be charged by solar panels. The only thing that can affect charge rate is the solar panel. The fact that lithium-ion batteries require little maintenance and only a basic battery management system (BMS) to ensure battery longevity is an additional advantage of using them.(Tinnemeyer, 2011). To determine which type of Lithium-ion battery to use, it was crucial to first consider the various options available. Cobalt Oxide (LCO), Nickel Cobalt Aluminium Oxide (NCA), Nickel Cobalt Manganese Oxide (NCM), Manganese Oxide (LMO), Titanate (LTO), and Iron Phosphate (LFP) are the most used lithium-ion battery types. The active materials used in lithium-ion batteries, known as cathodes, are named after the batteries. These cathode materials all benefit the battery in different ways. Cobalt Oxide, for instance, has poor thermal stability while Iron Phosphate provides the battery with excellent thermal stability. The initial step involved getting rid of Lithium-ion batteries that aren't suitable for use in electric vehicles. Lithium Cobalt Oxide is a better fit for laptop batteries, but Lithium Titanate and Lithium Nickel Cobalt Aluminium Oxide have more power than what is needed for a small device like a laptop. (Buchmann, 2009). Cost, performance, life span, and safety were the criteria used to compare the three remaining battery types as seen in the figure 2.8 below.



Figure 2.8: Lithium-Ion Battery Type Comparison (Kretchmer et al., 2017).

The cost and performance of the three battery types were found to be comparable during research into the various battery types, so the emphasis was instead placed on life span and safety. Because it was created to replace lead acid batteries, the iron phosphate battery earned the moniker superior. Because it was made to be used at high voltages for extended periods of time, it is by far the safest option since other batteries would malfunction in these circumstances.(Buchmann, 2009). The battery can be used for about 2000 cycles if it is properly used and stored. Compared to Manganese Oxide and Nickel Cobalt Manganese Oxide, this is very different. Iron phosphate offers the advantages of durability and safety in addition to having a good specific power and a relatively high specific energy. The distinction

between specific energy and specific power is the amount of energy stored in the battery per unit of mass or volume, respectively. The battery will be kept in a relatively small space, and the weight of the car is limited. The two essential things to be aware of are these. By doing this, the vehicle will be able to perform at its best without adding weight or taking up a lot of space. After considering all the pertinent factors, when it came to choosing a battery for a vehicle that would run on a lithium-ion battery, lithium iron phosphate (LiFePO₄) was found to be the best option.

2.4.3.1.3 Super Capacitor (SC): Ultra-capacitors are capacitors with much higher capacitance compared to regular capacitors but have low voltage limitations. Ultra-capacitors are a combination of rechargeable batteries and electrolytic capacitors. They can discharge and charge faster than batteries, can handle more discharge and charge cycles than rechargeable batteries, and store 10 to 100 times more energy per unit volume or mass than electrolytic capacitors. According to (Kumar et al., 2020); (Zhao et al., 2021); (Wang et al., 2016).

Devices with electrostatic double-layer capacitors (EDLCS) that are significantly higher than electrochemical pseudo capacitance use carbon electrodes or carbon derivatives as their electrode material. As a result, charge separation is possible at the interface between the electrode and the surface of the conductive electrolyte, where it occurs in a Helmholtz double layer. The separation of charges is only a few angstroms (0.3-0.8 nm), which is much smaller than the separation of charges in a typical capacitor.

Electrochemical pseudo capacitors are made using metal oxide or conducting polymer electrodes. These electrodes can be used in a variety of applications due to their high double-layer capacitance and electrochemical pseudo capacitance. Effects of faradic electron charge transfer in conjunction with redox processes include intercalation, electrosorption, and pseudo capacitance.

Composite capacitors Hybrid capacitors, like lithium-ion capacitors, employ electrodes with contrasting characteristics: one electrode has a predominance of electrostatic capacitance and the other one has a predominance of electrochemical capacitance, with the former being more common.

2.4.4 Electric Motor

The motor should be selected first because its needs determine the battery pack and PV array's output requirements (Menasce et al., 2013). In addition to having the necessary power and speed ratings, this motor also needs to be highly efficient, light in weight, and have sufficient starting and rated torques (Menasce et al., 2013). Most solar cars use three-phase brushless DC (BLDC) permanent magnet motors to convert electrical energy into mechanical torque, according to a review of the solar car literature (Mangu et al., 2010). The reason for using three-phase brushless DC (BLDC) permanent magnet motors in solar cars is due to their

favourable power-to-weight ratio, high efficiency, and ease of control. (Menasce et al., 2013). The BLDC motor is a mathematically similar alternating current electric motor that uses direct current electricity to excite it (Wisniewski, 2010). The axial flux's "pancake" shape BLDC motor uses a stationary wound stator, two magnetic rings, and a wheel to turn the vehicle. (Wisniewski, 2010). PWM is a common method for controlling the speed and torque of a BLDC motor by adjusting the electrical power delivered to it through a power electronics converter. By adjusting the duty cycle of the PWM signal, the average voltage applied to the motor can be controlled, leading to control of its speed and torque. (Mangu et al., 2010). This means that when the brake is used, the motor switches its function from driving the vehicle to generating power and sending it back to the storage system via the motor controller. (Mills & Stumpges, 2013). Because it uses the strong braking forces to generate electrical energy that can be used to recharge the batteries, this technique is known as regenerative braking (Mills & Stumpges, 2013). Despite the small amount of energy returned to the storage system, every little bit helps to raise the vehicle's efficiency.

Electric motors are the main structural element of electric vehicles. They cause the vehicle to accelerate by converting electrical energy into mechanical energy. The vehicle is typically made up of two battery packs with distinct voltages. For better balance, the main battery, which is heavier and has a higher voltage, is typically mounted at the bottom of the vehicle. Either an AC charge or a DC charge provides it with energy. It is frequently charged by AC, which is changed to DC by the rectifier, which is connected to a higher voltage battery. Three electric converters comprise electric vehicles. Direct current (DC) is transformed into the alternating current (AC), also referred to as the inverter, by the DC-AC converter, which is also used with electric motors. In an electric vehicle (EV), there is a high voltage battery which is used to power various electrical components in the car such as the dashboard, lights, and alarm system. Along with this high voltage battery, there is also a 12 V low voltage battery that is commonly found in conventional cars and is used for the car's low voltage consumers. The DC-DC converter is necessary to convert the direct current from the high voltage battery to the alternating current required to recharge the low voltage battery. The main battery pack is also connected to the heating and air conditioning systems, which are powered by the main battery (Ndyamukama, 2017). The central drive powertrain, which is shown in figure 2.9 below, is the most widely used technology for EVs and conventional vehicles.

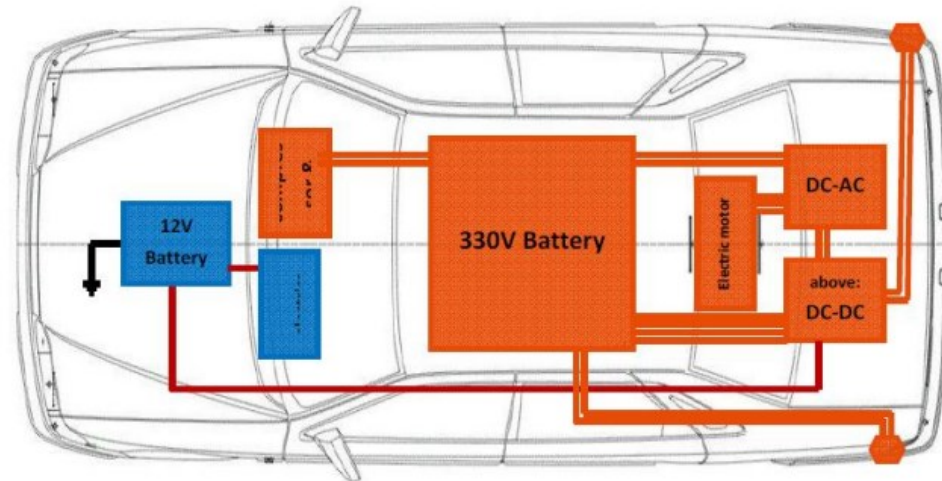


Figure 2.9: View from the top of an electric car(Ndyamukama;, 2017).

2.5 Types of Electric Vehicles

Electric vehicles come in four different varieties: BEVs (battery powered), HEVs, PHEVs and fuel cell powered vehicles.

2.5.1 Battery electric vehicle

BEVs are also referred to as "undefined vehicles" because they are entirely electric-powered and do not have a gas tank to store extra fuel. BEVs don't release any harmful gases into the environment and are controlled by large batteries (Li et al., 2017). A connection allows the battery to be recharged from the network or another external power source (Schuller et al., 2014). Also, not very heavy is the car itself. A high-force footing engine is a necessary but inefficient requirement for BEVs. When it's necessary to stop, pause, and run, BEVs are the right choice. The two primary drawbacks of BEVs are recharging times and battery executives. BEVs include vehicles like the Tesla Model S.

2.5.2 Hybrid electric vehicles (HEV)

In comparison, EVs have limited range and take longer to refuel due to their dependence on electrical charging. However, they offer advantages in terms of fuel efficiency, reduced emissions, and decreased dependence on fossil fuels. According to (M. Sabri et al., 2016), (Taylor, 2008), and (Poullikkas, 2015), the main drawbacks of ICE are its high fuel costs and related pollution; (Sandy Thomas, 2009). This is because the fuel efficiency parameters of the engine do not match the operational parameters. K.E dissipation occurs when a vehicle is operating in an urban environment. Operations that stop and start have poor hydraulic efficiency. Battery-powered electric vehicles (EVs) are extremely energy-efficient and environmentally friendly. This combination is popular because it combines the benefits of traditional internal combustion engines with modern power electronics, resulting in a highly efficient and effective vehicle.

Generally speaking, a hybrid vehicle is an electric car that also has two or more other power sources, like gasoline or diesel, and energy converters (Battery-electric motor system). Electric power is added to HEVs to transform them into hybrid electric vehicles. A bidirectional power source and a converter are typically used in a hybrid drive train to recover some of the braking energy, which is heat transfer in ICE vehicles. Transmission that goes both ways is an alternative.

2.5.2.1 Series hybrid Electric vehicles: In a series hybrid drive train, a single electric motor, and the vehicle it drives are powered by two different energy sources. The series of the hybrid drive system is shown in Figure 2.10 below. The unidirectional power source on the IC engine is the generator and generator output to power converter. A battery, solar panel, or ultra-capacitor are examples of devices that can be used in both directions. The term "bidirectional power sources" is also used to describe them. connecting the traction electric motor and the power converter. Both a generator and a motor can be used to power this motor in forward and backward motion. (Emadi et al., 2003).

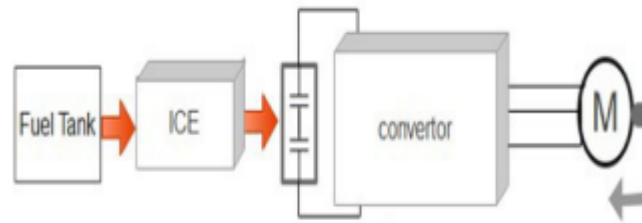


Figure 2.10: Series hybrid electric vehicle schematic diagram(Emadi et al., 2003).

2.5.2.2 Parallel hybrid Electric drive trains: As shown in figure 2.11 below, vehicles with equal hybrid drive systems combine internal combustion engines and electric motors to produce the force necessary to move the wheels.(Sperling, 1995); (Sandalow, 2009); (Armaroli & V Balzani, 2011).

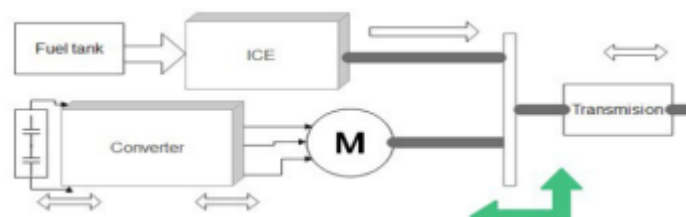


Figure 2.11: Parallel hybrid electric vehicle schematic diagram (Emadi et al., 2003).

2.5.2.3 Series- Parallel Hybrid Electric vehicle: The integration of both parallel and series HEV features into the structure is shown in Figure 2.12 below. The need for an electric machine and an auxiliary planetary gear unit complicates the control of this structure.

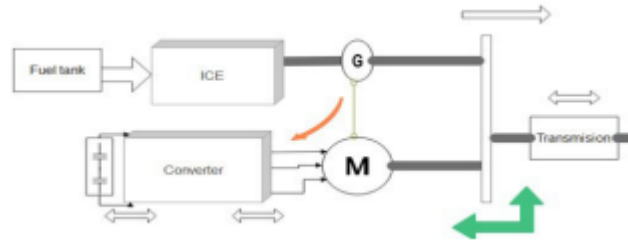


Figure 2.12: Series- Parallel hybrid electric vehicle schematic diagram(Emadi et al., 2003).

2.5.3 sources of energy for hybrid electric vehicles

2.5.3.1. Fuel cell: Using chemical reactions, a fuel cell generates energy. Two electrodes make up a fuel cell: the anode and the cathode. Electrodes are the places where electricity is produced (Kirubakaran et al., 2009). In a fuel cell, where charged particles are transferred from one electrode to the other using an electrolyte, the process at the electrode can be sped up using a catalyst. hydrogen is a fuel. Oxygen is required by fuel cells, however. Water is a non-polluting by product of most of the oxygen and hydrogen used in the generation of electricity ((Mahato et al., 2015); (Larminie & Dicks, 2013); (Aksu & Halicioglu, 2018)).

2.5.3.2 Regenerative braking system: A kinetic energy recovery system, or RBS, lowers the speed of a moving vehicle and increases fuel efficiency by converting the kinetic energy of moving objects into potential energy or stored energy.

2.5.3.3. Photovoltaic systems: Solar energy is used to create electricity by PV (Photovoltaic) systems, which are made up of solar panels, inverters, and other mechanical and electrical parts.(Wilson et al., 2020). PV systems come in a variety of sizes, from modest portable or rooftop units to sizable utility-scale power plants. Even though they can function independently, off-grid photovoltaic systems (Uddin et al., 2018).

2.5.3.4. Super Capacitor or ultra-capacitor SC (super capacitor): Ultra-capacitors provide a solution by combining the high energy storage of rechargeable batteries with the fast discharge and charge rate of electrolytic capacitors. They have high capacitance values, can withstand multiple discharge, and charge cycles, and store more energy per unit volume or mass compared to electrolytic capacitors, making them useful for a variety of applications. Ultra-capacitors have advantages over other energy storage devices, such as being able to discharge and accept charge much quicker than batteries, have a higher energy storage capacity per unit volume or mass compared to electrolytic capacitors, and can endure more discharge and charge cycles compared to rechargeable batteries. (Scibioh & Viswanathan, 2020); (Zhao et al., 2021); (Wang et al., 2016).

2.6 Brakes

Brakes are mechanical devices used to control motion by absorbing kinetic energy from a moving system. They are essential in automobiles because they are used for stopping and controlling speed. Automobiles typically use a friction braking system, which is comprised of mechanical, hydraulic, and electronic components. Kinetic energy is transformed into thermal energy through friction when the brakes are applied by the shoes that press against the brake drums or rotor. Brakes therefore act as a switch for different types of energy. A simple automobile braking system includes the following major components: a pedal, booster, master cylinder, combination valve, lines for the passage of brake fluid, emergency brakes, disc brakes, and drum brakes. The automobile friction type braking system is either a disc

system or a drum system, and the system is selected based on the task at hand. A detailed illustration is made in figure 2.13 below.

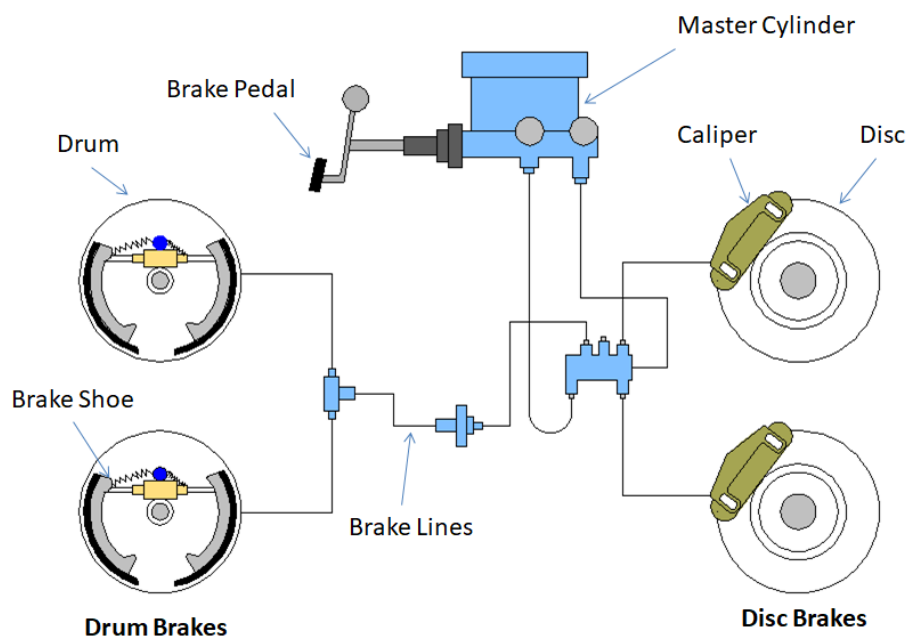


Figure 2.13: Automotive braking system (mechanicalbooster.com, 2018).

2.6.1 Anti-lock braking system

According to research, abrupt braking makes a car unbalanced and leads to collisions because the wheels become immobile when the conventional braking system locks them (Kayisoglu et al., 2019). To prevent the brakes from locking up while braking, the anti-lock braking system (ABS) was developed. The ABS is a braking system that guarantees complete steering wheel control by keeping the wheels from locking up in sudden braking situations in all road conditions and at all speeds, allowing the driver to exit the vehicle with a straightforward maneuver by turning the steering wheel lightly while the vehicle is skidding. As seen in figure 2.14, the Brake Control Module, an electronic control device, regulates how many revolutions each wheel makes when ABS is applied to the brakes. It comes to a halt by sending commands to the wheels to activate and deactivate brake callipers at approximately twenty times per second.

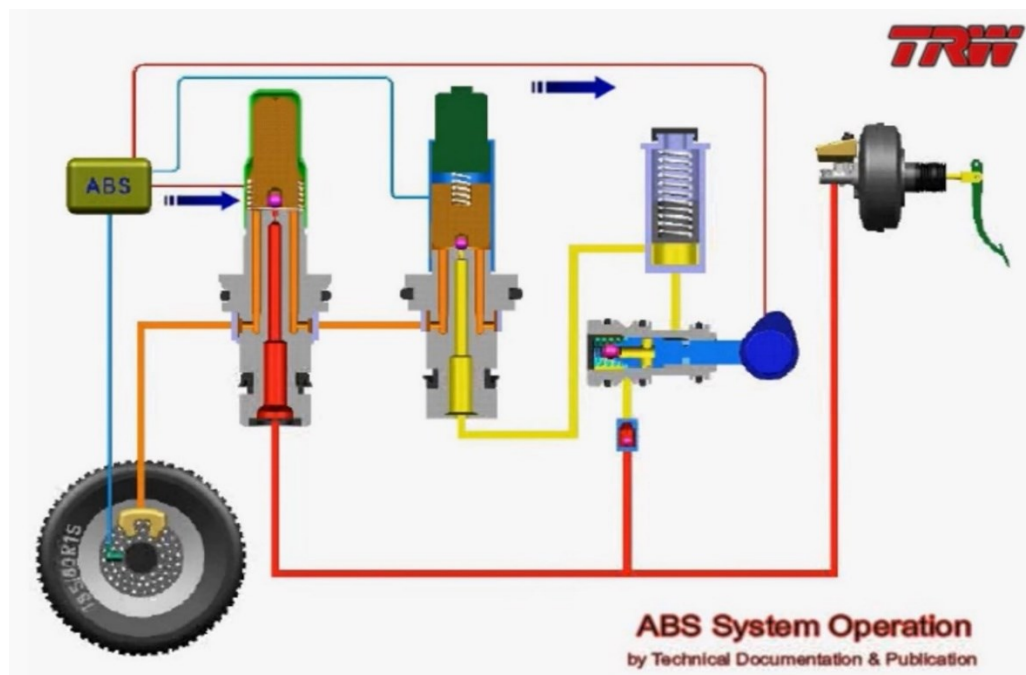


Figure 2.14: ABS operation (Alqahtani, 2016).

The Hydraulic Control Unit adjusts the brake cylinder pressure of each wheel using inlet and outlet solenoid valves in response to commands from the engine control unit (ECU). All electronic and electrical tasks as well as the system's control operations are carried out by the ECU. It determines the vehicle's wheel speed using signals from the wheel speed sensors.

Wheel Speed Sensors that use a magnetic field to measure the speed and direction of rotation of the wheels without touching them.

Deceleration sensors detect the vehicle's deceleration rate and send the signal to the ECU to determine the road surface conditions and make the necessary control measurements. The deceleration speed sensor is in the luggage compartment of passenger cars and in the engine compartment of other vehicles.

The valves perform their functions in three different positions. In the first position, the valve is fully open, allowing the pistons to provide full power to the callipers. In the second position, the valve line is severed, limiting the flow of hydraulic fluid to the piston, and resulting in no power transmission. In the third position, the valves are half open, allowing a small amount of hydraulic fluid to flow and ensuring a controlled braking force.

The hydraulic pump, which is connected to the valves and generates hydraulic pressure in the lines.

The ABS Control Module is a microprocessor that evaluates the information from the wheel speed sensors and sends commands to the actuators as needed. It is located beneath the hydraulic unit and, if faulty, disables the ABS and all connected systems.

Modern technology uses the anti-lock braking system (ABS) and its techniques. (Bhasin, 2019). The anti-lock braking system, a safety feature in automobiles, regulates wheel slip to maximize friction application and maintain steering stability while braking. The ABS system consists of essential components including valves, an electronic Control Unit (ECU), and wheel speed sensors (Sensor ring & Sensor pickup). The callipers on the rotating wheel must be locked and released by hydraulic fluid flowing through the brake lines, which is controlled by valves. All ABS data and signal functions are handled by the electronic control unit. It receives, decodes, and employs voltage pulses generated by each wheel speed sensor to determine changes in wheel speed. In order to achieve the best braking performance, the ECU cycles the ABS modulator valves if it determines that the perceived wheels' pulse rates indicate an impending lock-up. The sensor ring and sensor pickup are the two main components of the wheel speed sensor. The sensor ring has notched teeth, the number of which varies according to system style. When the sensor ring's teeth cut across the wire coil/magnet assembly's magnetic field, electrical pulses are produced by the sensor pickup's wire coil/magnet assembly. The closed-loop ABS has several inputs and outputs. Wheel speed sensors provide the inputs, and brake system pressure control obtained through ECU commands provides the outputs. The ECU computes the acceleration or deceleration of each individual wheel by comparing the signals from all four wheels' sensors. As a result, the amount of brake pressure applied to one or more wheels can be altered as required.

The system proffers the following advantages over the conventional braking system.

1. It prevents the wheels from completely locking, eliminating the possibility of the vehicle skidding.
2. The likelihood of a collision is reduced because the driver has more control over the braking process.
3. The ABS system provides more precise steering control.

With the following drawbacks:

1. Purchase and installation costs are exorbitant.
2. Higher maintenance costs compared to vehicles with traditional braking systems.
3. Expensive repairs and high operating costs for vehicles that use ABS.

The study also considers other systems being developed to improve the functionality of ABS, such as Automatic Traction Control, which uses an identical component to ABS but operates at a slower speed. The brake is applied 10–14 times per second to slow the wheels and regain traction after measuring the speed of each wheel to predict when one or more will become loose and spin.

2.6.2 Braking system in electric vehicles

Energy recovery systems have been developed to mitigate the energy loss during braking in electric vehicles. These systems recover the kinetic energy that is

lost during braking and convert it into electrical energy that can be stored in the vehicle's battery. This helps to improve the overall efficiency of the vehicle and extend its range. In the article by Rama (2019), it was discussed that regenerative braking system can convert the car's mechanical energy and the heat energy that is usually lost during braking into electrical energy. This system aims to reduce the waste of energy in conventional braking methods. Then, by sending all of the accumulated momentum or kinetic energy to the generator, the vehicle is brought to a safe, gradual stop. The flow of energy in braking systems is depicted in a flowchart in figure 2.15.

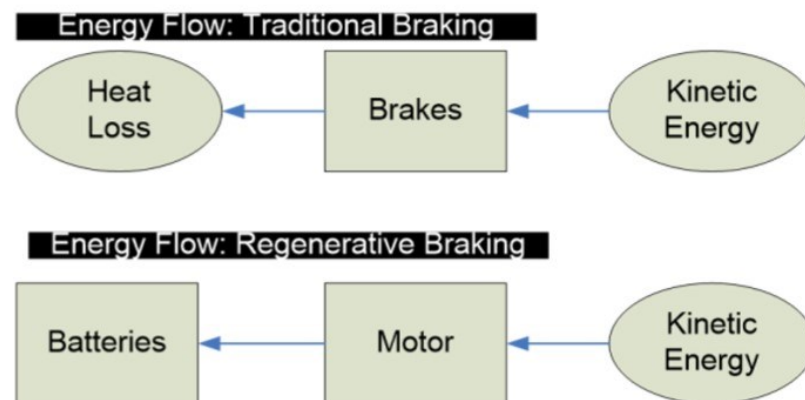


Figure 2.15: Energy flow in braking systems (Rama, 2019).

Regenerative brake controllers, which are electronic devices, supervise this control and decide when and how quickly to apply the brakes. The brake controller uses braking to direct the motor's electricity into the batteries or capacitors. Make sure the batteries receive the appropriate amount of power and that the system's electricity intake does not exceed the batteries' capacity. Figure 2.16 below shows a diagram of a powertrain.

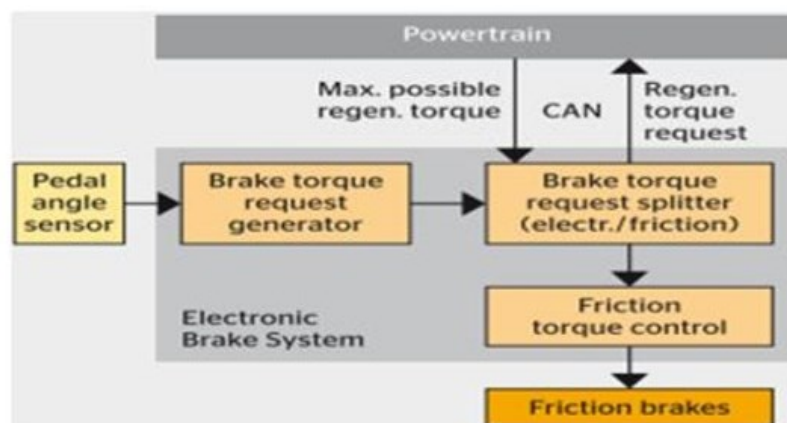


Figure 2.16: Brake torque blending overview (Rama, 2019)

The regenerative braking system is therefore believed to have the following benefits.

1. Conserving energy
2. Reduced wear on vehicle brakes, resulting in a longer working period.
3. Fuel efficiency has been improved.

However, it appears to have the following limitations.

1. the necessity of closely balancing the supply and generated electricity
2. When the batteries are fully charged, regenerative braking is prohibited by the brake controllers because adding another charge from regenerative braking would raise the voltage of a fully charged battery above the permitted limit.
3. Increasing the vehicle's total weight by 25-30 kg

The following still applies when conventional friction-based braking is combined with regenerative braking:

1. The friction brake is still required to bring the vehicle to a complete stop because regenerative braking is less effective at lower speeds.
2. The rotor needs to be physically locked in order to stop cars from rolling down hills.
3. If the regenerative brake fails, the friction-based brake serves as a backup.

Many road vehicles with regenerative braking typically only have power on a few wheels, and the power only applies to those wheels; friction-based brakes are used on the other wheels to provide controlled braking in challenging conditions, like slick roads.

To increase energy recovery effectiveness and take braking safety and stability into account, an article on a control strategy for a regenerative braking system in electric vehicles while traveling downhill was published by. In this study, changes in braking force distribution and stability, as well as the effects of slope on regenerative braking recovery and safety, are all examined. Based on the outcomes of simulations and downhill slopes, mechanical analysis is suggested. The vehicle under consideration is an electric single-shaft car with a front-wheel-driven, dual-stage braking system. In contrast to the second type of braking system, which uses electricity and is primarily made up of a battery, motor, and transmission system, the first type of braking system is hydraulic. The components in an electric vehicle, including the electronic control unit, battery management system, motor and brake controllers, and CAN protocol, work together to control its operation. During the braking process, the hydraulic actuator and generator act as the mechanical and electric braking components. The study found that the regenerative braking control strategy effectively recaptures energy and improves braking stability, as shown in the graph of braking distribution coefficients in Figure 2.17.

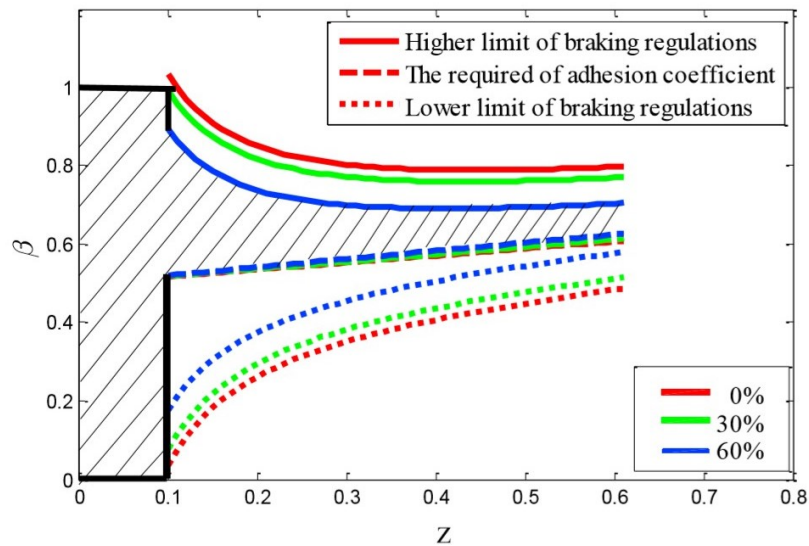


Figure 2.17: Braking distribution coefficients' range(Zhang & Cai, 2018)

According to (Basrah, 2017), an ABS is a component of active safety systems that assists drivers in coming to a safe stop during panic braking while maintaining the vehicle's stability and steerability. Although the RBS is disabled in favor of the ABS at a safe (low) deceleration threshold, this is not always the case. Because of this safety margin, much less energy is recovered than would be possible if both RBS and ABS were permitted to operate concurrently. The integration of RBS and friction brakes may improve a vehicle's energy economy by allowing for more frequent energy recuperation activations, which is especially important when deceleration demands are high. The main objective of this doctoral thesis is to design and implement new torque blending strategies for wheel slip control systems for various vehicle topologies using various EM configurations, including four, two, and one Electric Machines EM. The combination of the two brake actuators will improve braking performance as well as the vehicle's overall energy efficiency in the future. ABS can also be enabled by pure EM in some cases when the regenerative brake torque is sufficient.

Regenerative braking systems greatly enhance fuel efficiency and raise the appeal of the vehicle. There are many ways to recover energy from braking, including).

a. The electric motor, which serves as both a motor and a generator, is the main moving part or regenerative braking system in the vehicle.

b. Utilizing hydraulics and electrical/electronic components, a new system called Hydrostatic Regenerative Braking (HRB) is introduced to increase vehicle fuel efficiency.

c. The air tank could be filled while braking using the energy produced by the regenerative braking system. by capturing kinetic energy, which is required for braking, compressing the air, and then using the compressed air to drive the vehicle.

d. Kinetic energy is converted to potential energy in a nitinol spring in a regenerative braking system. The wheels are powered by the stored potential energy when the system needs to accelerate.

Due to its simplicity, low noise, light weight, and lack of leakage, the electric regenerative system was preferred over the hydraulic regenerative system. For fully electric vehicles with an electric motor, regenerative braking works better. This electric motor has some intriguing characteristics, such as the ability to transform electrical energy into mechanical energy when rotating in one direction while transforming into an electric generator when rotating in the opposite direction. Car batteries can be charged using this energy, among other things. Momentum becomes crucial in keeping the car moving after it reaches a certain speed. Energy from the battery, which is charged by the electric motor's reverse motion, is required to start the vehicle from a complete stop. electric motor with kinetic brake energy that runs on batteries.

This outcome is shown in Figures 2.18, 2.19, and 2.20. The electricity produced by the motor must be directed into a circuit to reach the battery. A regenerative braking system that can transform kinetic energy into electricity is shown in Figure 2.21. The battery is then charged using this electricity.

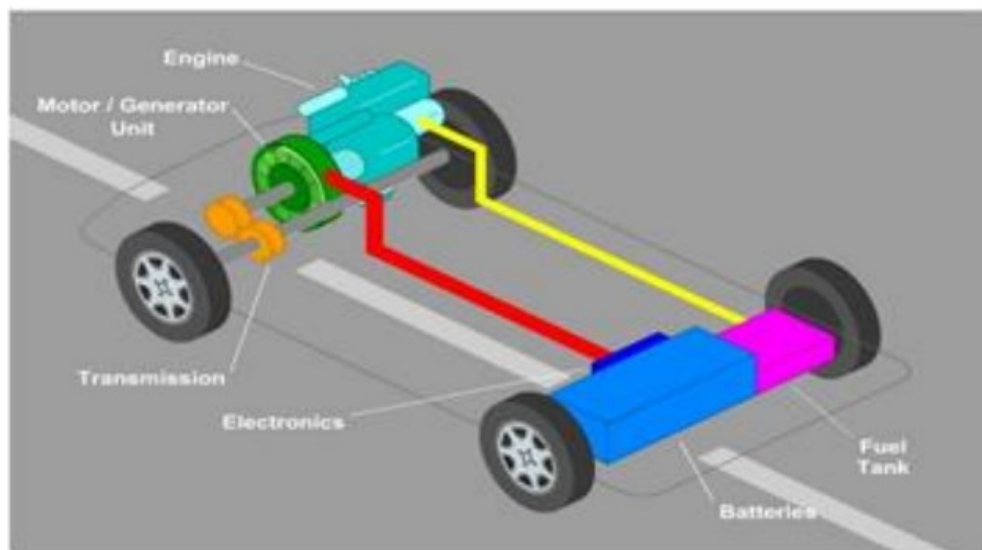


Figure 2.18: IC engines and electric regeneration systems together(Mandal et al., 2017).

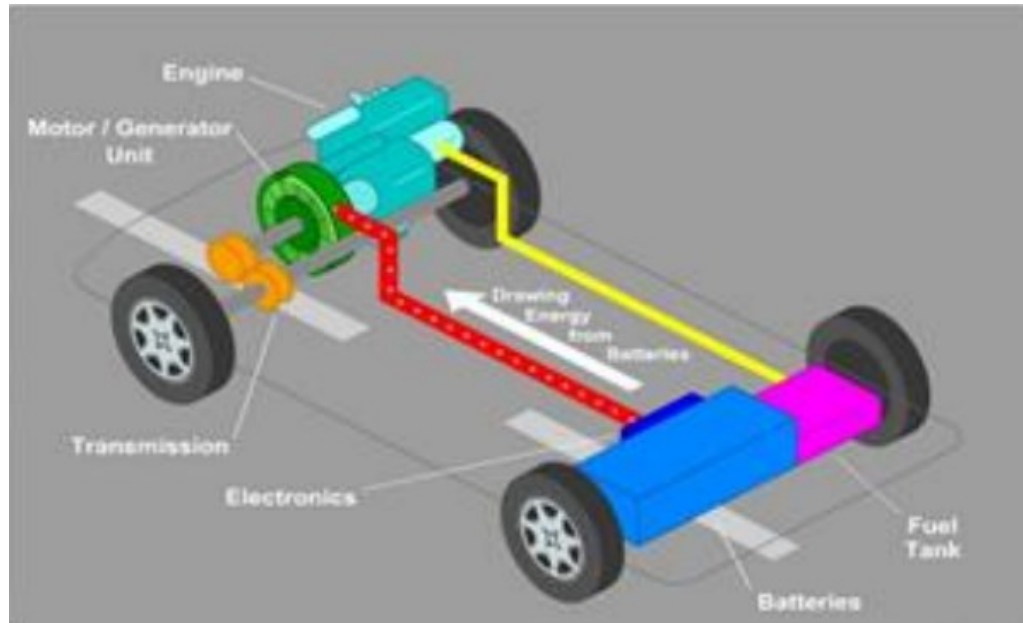


Figure 2.19: Energy usage from the battery(Mandal et al., 2017).

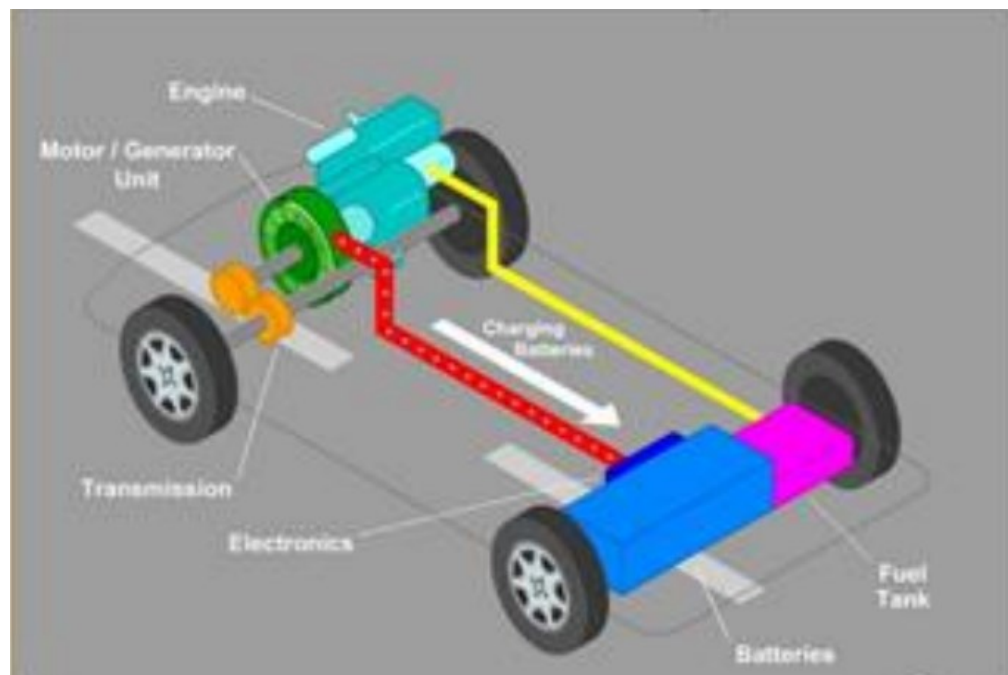


Figure 2.20: when the brake is applied, the battery charges(Mandal et al., 2017).

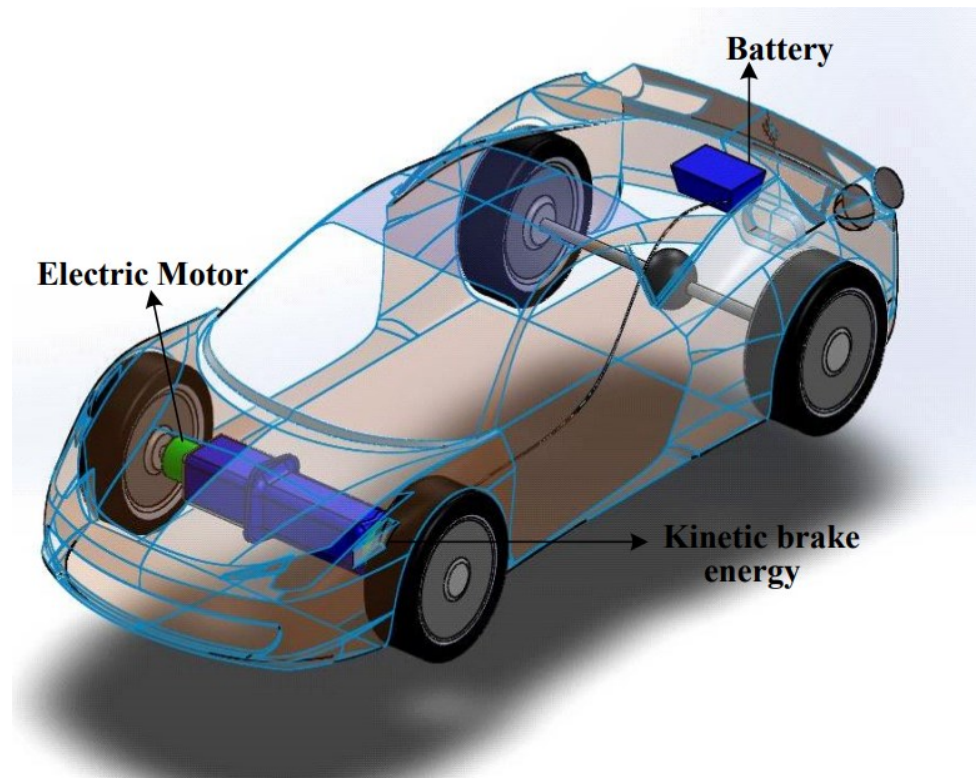


Figure 2.21: The generator, which is the electric motor in reverse direction, stores the energy in the vehicle's battery.(Mandal et al., 2017).

2.7 Related Research

Using design software, Al-Hussein Bin Talal University (AHU)/Maan-Jordan designed and modelled a 20-kW solar on grid power charging unit for electric vehicles. According to (Al-rawashdeh, 2019). Two scenarios were taken into consideration: one with five vehicles operating between 8 am and 12 pm and five operating between 12 pm and 4 pm, with a time of charge of four hours for each scenario, and the other with eight operating between 8 am and 12 pm with a charge time of four hours for each scenario. They concluded that the system is effective and helpful for those who use electric vehicles at the university. It was reported that the designed solar charging unit decreased CO₂ emissions from power generation .

Thesis by (Fouad, 2014) employed a different similar design in which PV sources and the grid were combined to supply EV load. On the other hand, the PV is renowned for being sporadic and being strongly influenced by geographical and meteorological factors. To address the inconsistent output of photovoltaic (PV) systems, a battery storage system was integrated with PV in a grid-tied system to ensure steady operation of the hybrid charging station. The thesis proposes and implements an efficient hierarchical energy management strategy to maximize the use of on-site PV energy, accommodate the fluctuating demands of EVs, and reduce

the strain on the grid. The goal is to develop a hybrid-source charging station that is cost-effective, efficient, and reliable to meet the needs of EV charging in various conditions. The strategy increased all three metrics: overall performance, dependability, and cost. The interleaved conversion stage of the hybrid charging system's overall performance, as well as the coordinated control mechanism's efficient design and corresponding energy management strategy, depended on it.

Additionally, a solar-powered charging station for cities was developed by (Raghavan, 2018). The most well-liked commercial EVs on the market were considered when developing simplified EV load models. The designed solar-powered charging station, which was chosen specifically for urban cities in Ontario, was used to test the developed EV load models. The architecture of the piece was selected with installation and operation costs in mind. By adjusting the power ratio and computing the annual energy yield for various types of orientation while considering all EV load models, optimization in the design of a solar-powered charging station was presented. Following that, a Net Zero Photovoltaic (PV) charging station was created, tested with a few different load models, and each design was subjected to an energy economic analysis.

Most of the earlier studies that have been looked at deal with grid-connected solar power systems that require charging stations. (Ndyamukama; 2017) This research is much more closely related to the integration of solar systems for EV. It investigated a solar-powered system for an EV to use solar energy instead of electricity from the grid to move the car. The location and weather forecast were used by the system to predict when solar panels would be produced. To meet the energy needs of passenger vehicles in some areas, solar energy was used. If the solar energy wasn't enough, the system was compelled to buy electricity from the grid. The system design's results showed that solar power usage was rising while grid energy use was falling. Testing of the system showed that as solar panel efficiency rises, so will the use of solar energy. In conclusion, the system's design lowers overall electricity costs while improving the efficiency of the solar-panel system.

Another study by (Mohan et al., 2019) examined whether solar-powered plug-in electric vehicles require little maintenance. The main drawback of electric vehicles, which is their short driving range, was discussed and addressed. The battery of the vehicle can be charged while it is moving by installing a solar PV module. They avoided using mechanical parts like the gearbox and differential in their work. In their opinion, driving is made possible by direct drive to wheels.

In the works of (Benboubker, 2020), It was recommended to use a low-speed solar-powered electric vehicle for the analysis, design, implementation, and testing of an electric vehicle powered by a mounted PV solar panel. They first calculated the power output necessary by performing a simple mechanical analysis of the motion of the car on an incline to determine the specifications of the necessary components, which included the electric motors, batteries, solar panel, and charge controller. They also used aerodynamic drag to support the body design of our vehicle. The chassis'

structural analysis and 3D design were then carried out using the metrics of displacement and von Mises stresses. They also provided some safety advice, the most important of which is to consider conversion rather than new construction.

By significantly improving the design for the fabrication thesis (Kretchmer et al., 2017). They produced a vehicle that meets the engineering requirements for an international competition. Designing and building a dependable electric vehicle powered by solar energy was the thesis's main goal. The goal of the thesis report was to create a comprehensive first iteration design with plans for fabrication.

However, some students disassembled, altered, and produced an ICE vehicle into a fully electric vehicle (Nawaz et al., 2017). A strong brushless DC motor was installed in the back and connected to the driveshaft using a chain and sprocket system as the first stage of the modification. Battery-operated rechargeable motor (4 lead-acid batteries, 12V each). By coupling these lead-acid batteries to the power grid (110V/220V), they can be charged externally. Their objective was to lessen the reliance of the vehicle on external power sources by using effective Solar Panels as a secondary source of power to charge the batteries. The car could reach a top speed of 60 km/h, which is a steady and secure speed, according to their test results.

Another method to include a secure energy source is regenerative braking. (Mandal et al., 2017) tried to recover energy from the vehicle's braking load. In their research, a model electric regenerative system was created, and its performance was experimentally tested. The prototype system was driven by a 12V motor that could recharge a 2.4V battery. The experiment measured the amount of time needed to store 0.84W in the battery using a variable load. The results showed that the battery was recharged by 0.80C after 8 seconds of rotation with a maximum load of 648g and by 0.15C after 1.5 seconds of rotation with a minimum load of 72g. It was discovered that the amount of energy stored in the battery increased along with the braking load. In some cases, this energy can be added to the primary power source and used to power auxiliary components like fans and lights. In a nutshell, the thesis has made the completely wasted energy that is produced during braking visible and paved the way for it to be used productively, possibly providing extra energy for solar-powered cars.

Some modifications were made by (Selvan et al., 2018). In their design, they incorporated a safety system and a vehicle monitoring system. The vehicle monitoring system has several sensors that can pick up important information like engine temperature, energy level, and battery chamber temperature. Accelerometers and speed sensors also pick up unusual vibrations in vulnerable places and overspeeding. This information is sensed and stored in the cloud. This enables the remote observation of driver and vehicle behavior.

The study, according to (Elmenschawy et al., 2016), examined how energy management technologies, such as photovoltaic and energy storage systems, affect the potential of solar vehicles. The objective was to monitor and optimize the

electrical power flow between the energy storage devices and PV. To achieve this, the thesis chose a 1035 W monocrystalline PV module, a 5-kWh lithium-ion battery, a 2 kW in-wheel axial flux permanent magnet brushless DC motor, and silicon carbide components in power converters. A secondary energy storage system that makes use of an ultra-quick capacitor's charging and discharging abilities. By creating Buck-Boost converters, the output voltage of three different sources—photovoltaic panels, batteries, and ultracapacitors—was controlled. Simulations and tests were employed to validate the proposed design.

Finally, driving a solar-powered electric vehicle is practical. To ensure that once the system was installed and ready to supply these vehicles, energy generation would not result in any CO₂ emissions, (Valero et al., 2013) investigated the viability of using solar photovoltaic modules to recharge various electric vehicles. The cost-benefit analysis of using a photovoltaic system versus buying electricity from the distributor was also included in the study. Finally, solar photovoltaic systems are regarded as more affordable for charging a pure electric vehicle (EV).

CHAPTER III

Methodology

The proposed design in this thesis is the efficient energy conversion system for an electric vehicle. The design will incorporate the integration of solar energy with braking system energy for a longer range of velocity. This electric vehicle can also be referred to as a solar electric vehicle.

The objective is to create an energy management system for a solar electric vehicle to enhance its efficiency. This will be achieved by utilizing solar PV energy for extended range and designing an efficient braking system to maintain a sustainable energy supply while the vehicle is in motion. Additionally, the system will store energy in the battery. This chapter provides information about the research design, having the following objectives to resolve.

- I. The current research work is to study the travel behavior of passenger vehicles in Cyprus by conducting a survey using Google Forms E-Questionnaire. I will then create a load profile based on the daily energy requirements of the passenger vehicles.
- II. Next, I will determine the energy production capability of the solar panels on the electric vehicle in the chosen location. Lastly, I will estimate the amount of energy generated to fulfill the energy demands of the passenger vehicles.
- III. The design of the solar energy is based on the irradiance and temperature at the location.
- IV. Afterwards an effective braking system is designed to add to the solar energy designed.
- V. The integration of both energies requires a storage system which is designed using Simulink.

3.1 Architectural model of the study

The design structure of this study is illustrated below. There may be some changes towards the end of the design, but the architectural design is a guide into the achievement of the thesis's objectives.

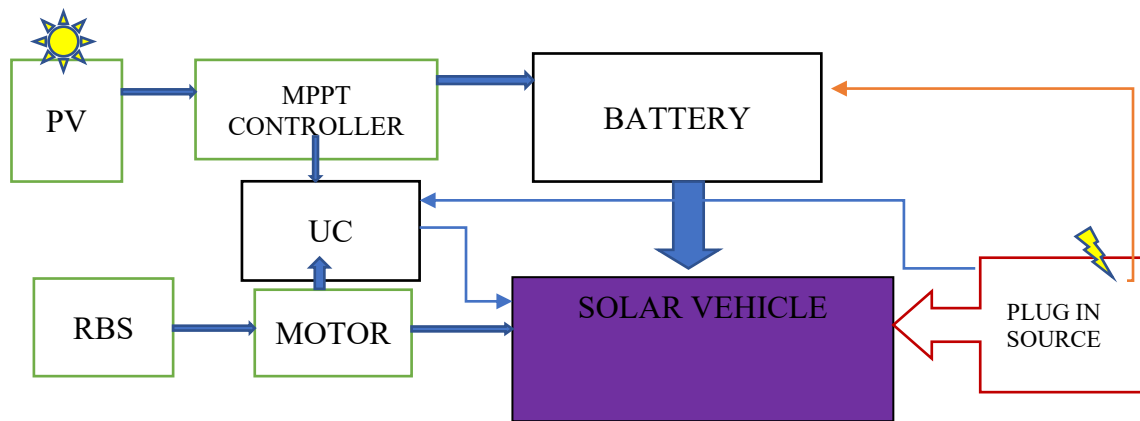


Figure 3.1: Block Diagram design of the SEV

3.2 Northern Cyprus Climate Analysis

Cyprus is an island republic in the eastern Mediterranean Sea, south of the Anatolian Peninsula, officially known as the Republic of Cyprus. Although geographically located in Western Asia, it is culturally and politically more closely associated with Southeast Europe. This island, located south of Turkey, east of Greece, and west of Syria, is the third largest and third most populous in the Mediterranean. The island is home to Nicosia/Nicosia, the nation's largest city and capital.

Cyprus has an intense Mediterranean climate, with long, dry summers lasting from mid-May to mid-October and mild winters lasting from December to February, separated by brief autumn and spring seasons. The summer season is distinguished by high temperatures and clear skies, but the pleasant climate of coastal districts is aided by a gentle breeze from the ocean.

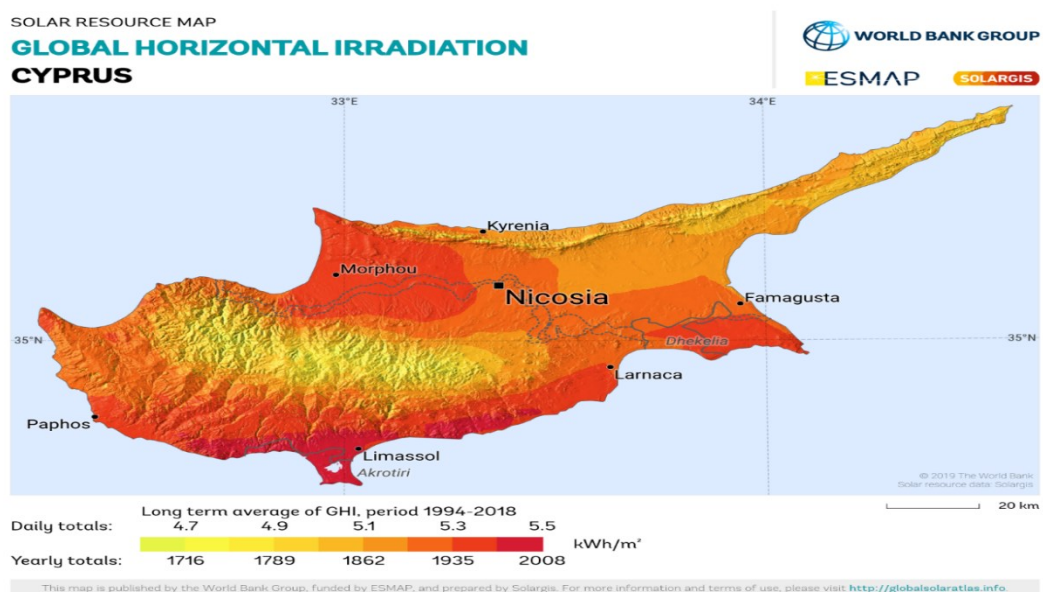


Figure 3.2: Global horizontal irradiation GHI of Cyprus Island (Group, 2021).

The summer season (June-September) has longer days than the winter season (December-February), as illustrated in the graph below. The longest days of the year occur in June and can last up to 14 hours and 30 minutes. Winter, on the other hand, has the longest period of darkness. In December, Nicosia's nights last approximately 15 hours, with days beginning approximately 2 hours later (Group, 2021).

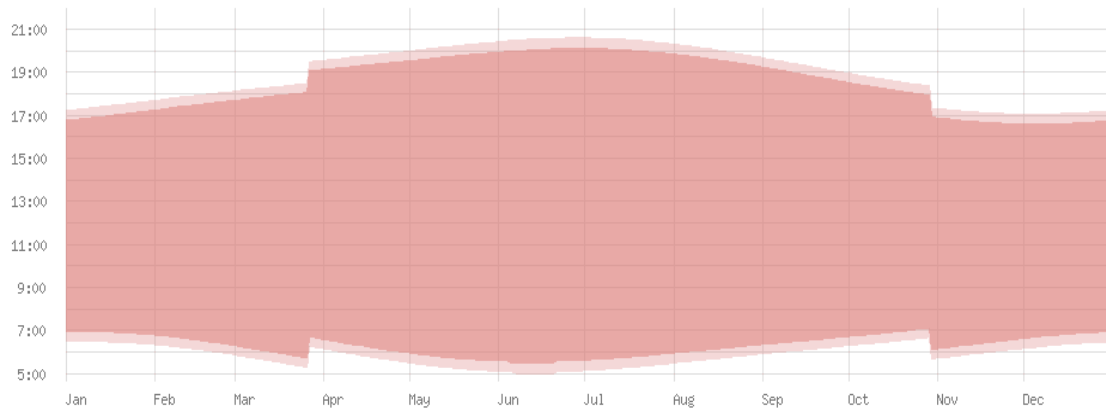


Figure 3.3: Day Light Graph in Cyprus (weather-and-climate.com, 2022).

July has the most sunshine of the year, with an average of 397 hours of sunlight. January, on the other hand, has the least amount of sunlight with an average of 171 hours.

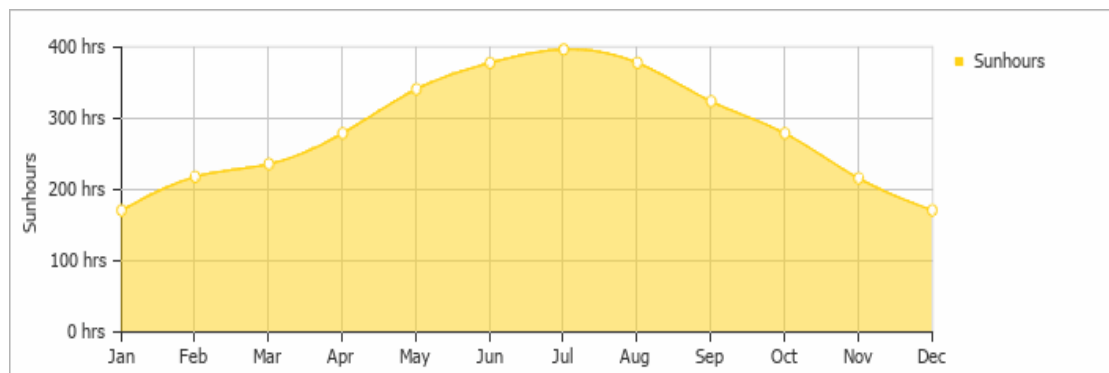


Figure 3.4: Sun hours graph of Cyprus island (weather-and-climate.com, 2022).

The graph displays that Nicosia experiences its highest temperature in August, with an average temperature of 25.6°C (78°F), while January is the coldest, with an average temperature of 11.15°C (52°F).

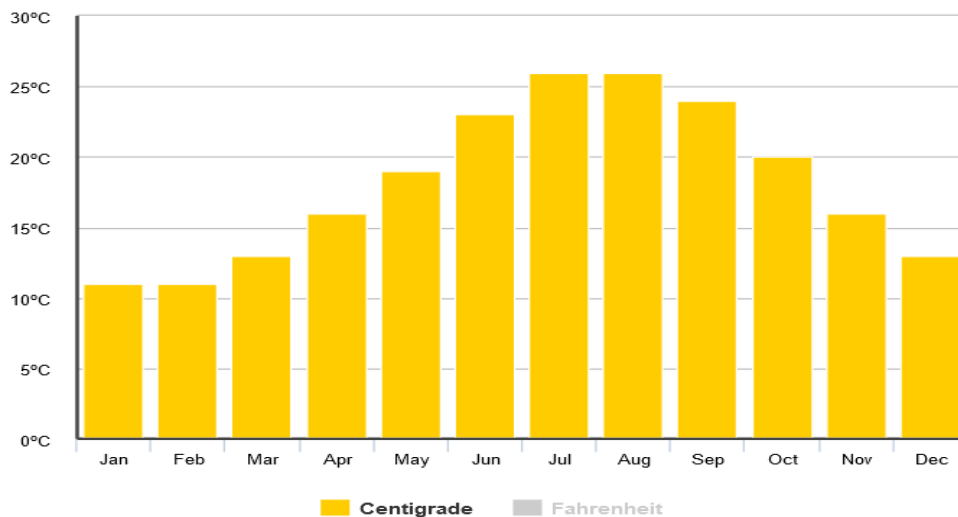


Figure 3.5: Monthly Average temperatures

Over the years, Cyprus weather is defined by the figure 3.6 below,

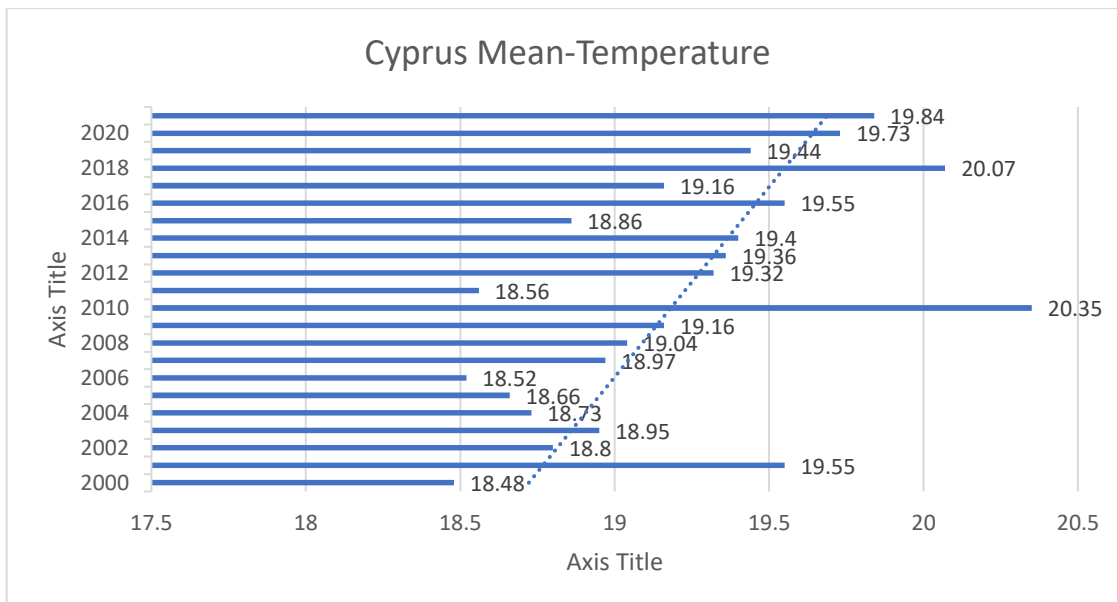


Figure 3.6: Historical Mean temperature of Cyprus for 20 years (weather-and-climate.com, 2022)

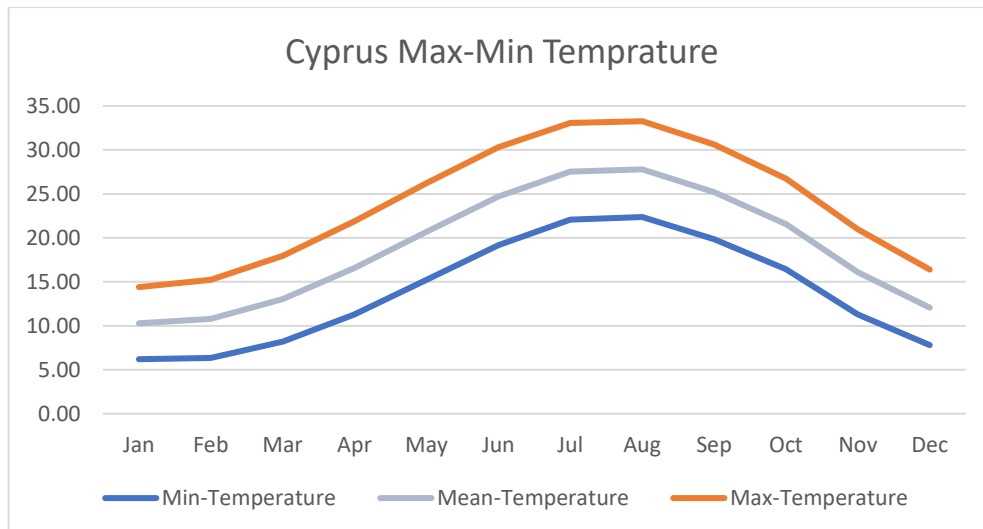


Figure 3.7: Cyprus Maximum-Minimum Temperatures (weather-and-climate.com, 2022)

The Sun emits energy in the form of solar radiation, which travels through space as electromagnetic waves. This energy, produced through nuclear fusion in the Sun, plays a major role in atmospheric processes and is 10,000 times greater in power compared to the energy consumed by humans. One form of solar radiation is short wave radiation, which weakens as it passes through the Earth's atmosphere due to reflection, absorption, and diffusion by various substances like ozone, water vapor, and particles. Eventually, the radiation reaches the Earth's surface and either reflects or is absorbed, causing the atmosphere to heat up due to the emission of long-wave radiation from the surface. The wavelength and frequency of the electromagnetic waves are crucial factors to consider in determining their energy, visibility, and penetrative strength. (weather-and-climate.com, 2022).

The electromagnetic waves produced by the Sun have a range of wavelengths and are collectively referred to as the "electromagnetic spectrum." This spectrum encompasses all visible light. The exact distribution of solar radiation across different parts of the spectrum is approximate.

- Infrared -49%
- Visible light -43%
- UV radiation at 7%

This section investigates the measurement of the total amount of shortwave solar energy that reaches the Earth's surface daily over a large area. The factors that are considered include the length of the day, the height of the Sun above the horizon, and the absorption of the energy by clouds and other components of the atmosphere. Shortwave radiation includes both visible light and ultraviolet radiation. Due to seasonal variations, the average daily incident of shortwave solar radiation changes greatly throughout the year.

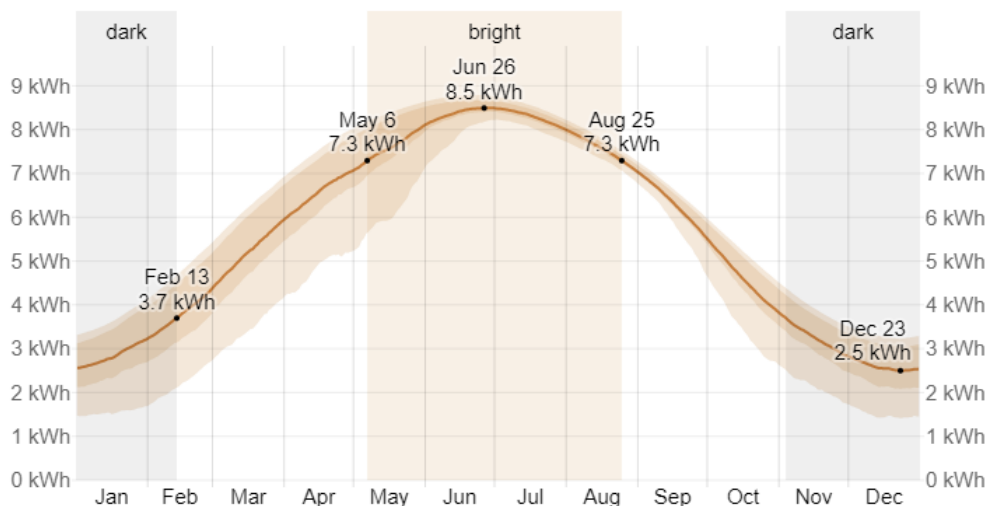


Figure 3.8: Shortwave energy radiation graph in Cyprus

The period with the highest intensity of shortwave solar energy lasts for 3.6 months, from May 6 to August 25, during which the average daily incident of shortwave energy per square meter is above 7.3 kWh. From November 4 to February 13, it is winter and the average daily incident of shortwave energy per square meter is less than 3.7 kWh. The darkest month in Cyprus is December, with an average of 2.6 kWh per square meter.

3.3 Travel Survey within North Cyprus

The objective of this survey is to find the distance covered by drivers within north Cyprus to determine the energy demand required to be designed in the solar electric vehicle. This will help this study have a case study or in other words a research focus for the design of the SEV. Therefore, to gather the data needed for the design model, it is more effective to study the travel patterns of drivers. This data can be collected through an electronic questionnaire using Google Forms. The questionnaire will ask specific questions to accurately gather information related to travel research. Questions such as age, occupation on personal level are asked. also, date of travel, purpose of travel, distance travelled, and form of transportation were asked to narrow the collective data for objective of this survey.

These data are collected for the two important seasons in North Cyprus, the winter and summer season as energy demand for both seasons are the consideration of this study.

It should be noted that this data collection is just basic in the sense that they are not elaborate data collection for a long period of time, but data collection for a daily purpose activity such as going to work, getting groceries or daily travel to school.

The data collected are explained in the tables below.

The form of transportation has to do with what means an individual travelled from one location to another within the region of study (North Cyprus). This also shows the habit of movement of individuals within north Cyprus. Table below shows the listed forms of transportation used for data collection in the goggle forms e-questionnaire.

Table 3.1: Survey transportation mode

S/N	TRANSPORTATION MODE	EXPLANATION
1	Private salon or SUV	For individuals with their private vehicles
2	Bus or coach	Mainly for University students or staffs in north Cyprus due to the university economic setup of the region
3	Taxi	For individuals who probably take a public vehicle to work
4	Ferry	Perhaps for individuals coming from Mersin in turkey or neighbouring islands into north Cyprus
5	Public transport	These are paid for buses commonly used aside the taxi used for public transportation
6	Cycling	Certain individuals may prefer cycling in their travels for health or other reasons form one place to another
7	Walking	And some individual's travels may be a short distance journey trekkable within their human strength limits.

All these forms of transportation are consideration in gathering the travel survey data.

Whereas there is length coverage for these forms of transportation within the region of focus. The following distance ranges are set in the questionnaire.

- Distance range from 0 to 1 km.
- Distance range from 1 to 5 km.
- Distance range from 5 to 10 km.
- Distance range from 10 to 15 km.
- Distance range from 15 to 20 km.
- Distance range of more than 20 km.

Considering these distances, this are likely distance to be covered during travel within Nicosia. A distance covered from City Center to NEU site is about 12.37Km on the driving route.

For the travel, the following purpose are listed in the table below to match up the reason for the distance covered with the choice of transportation mode. As earlier said, the questions are based on a one-time travel or a frequent travel in an individual's itinerary.

Table 3.2 Travel purpose list

PURPOSES
A. Trip to/ from work
B. Business Trip
C. Business trip on leave
D. Grocery Shopping
E. Other Shopping
F. Errands
G. Transporting another person
H. Trip to/ from school or other educational institution
I. Visiting friends, acquaintances, or relatives
J. Exercise, Outdoor activities
K. Social outings
L. Trip related to Hobbies or other free times
M. Driving around without specific destination
N. Other leisure trip

The aim of this survey is to determine if there are any constraints related to the length and duration of the journey when an individual travels, to establish the limitations of the study. The overall survey result of the questionnaire is as follows in the following figures.

According to the survey shown in the figure 3.9 below, there are 33 candidates in total in a short span of 3 months data collection. The basis is to have a quick case study and not a broad study data collection.

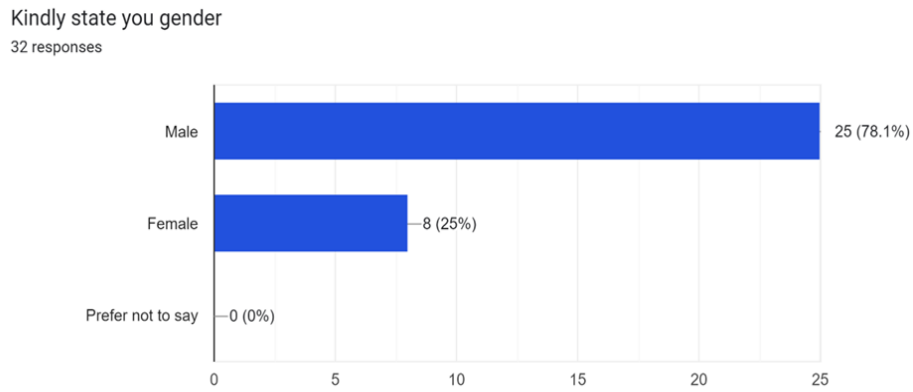


Figure 3.9 Survey Gender Chart

Based on location, most correspondents are based in Nicosia. This has narrowed the survey study to focus on the Nicosia region. Figure 3.10 below depicts the statistics of correspondent's location.

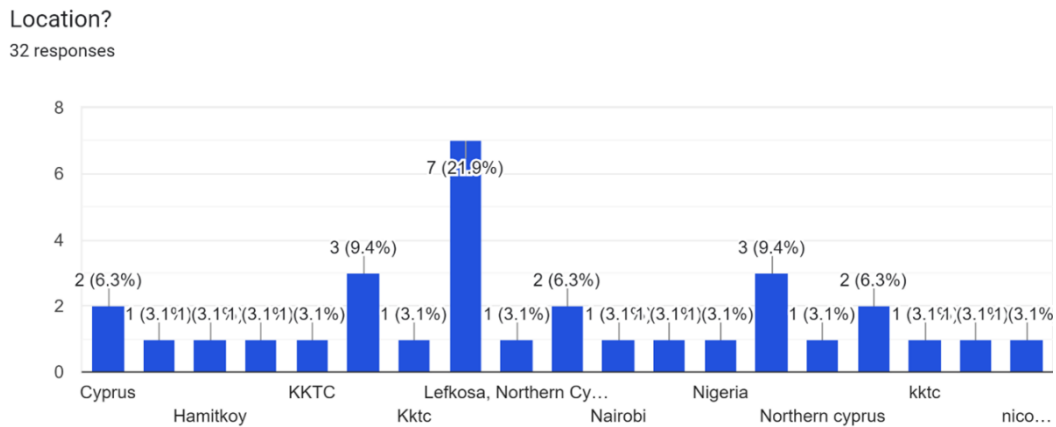


Figure 3.10 Correspondence Location Statistics

Moreso the work nature of correspondence matters as to determine the purpose of journey. The work nature of individuals is a major as it is a condition of the migration no of individuals from one part of the island to another. The figure 3.11 below shows a chart o the correspondence work nature. Majority of correspondence are students. In further research study, I will employ more time in getting more correspondence to provide more data. Either way, on the island, students are common with renting private salon vehicles to travel from one destination to another on different purposes.

Occupation?

32 responses

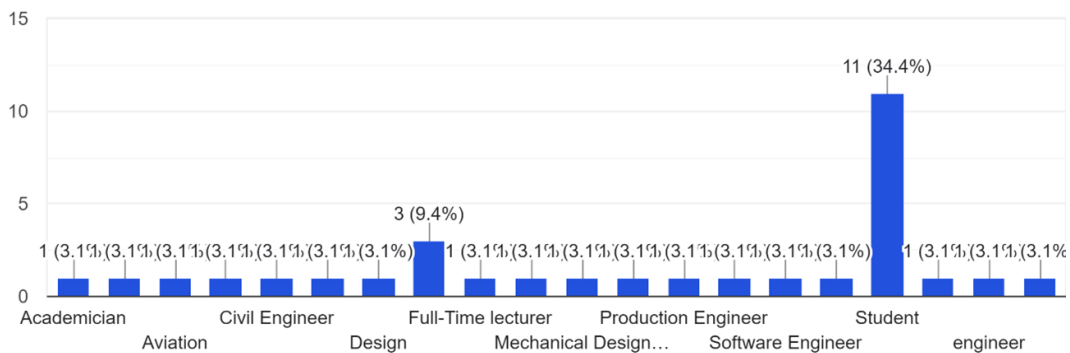


Figure 3.11 Correspondence work nature

Analysis of Survey for winter and summer seasons

After the collation of data, the time, purpose, length of travel and the mode of transportation are being analysed to better understand the demanded energy needed based for the correspondent individuals in this survey. It is already acknowledged that the majority correspondence is resided within Nicosia and mostly movement is restricted within Nicosia.

Starting with the time of departure for travel, the chart figure 3.12 below illustrate the results from the survey gathered in the e-questionnaire.

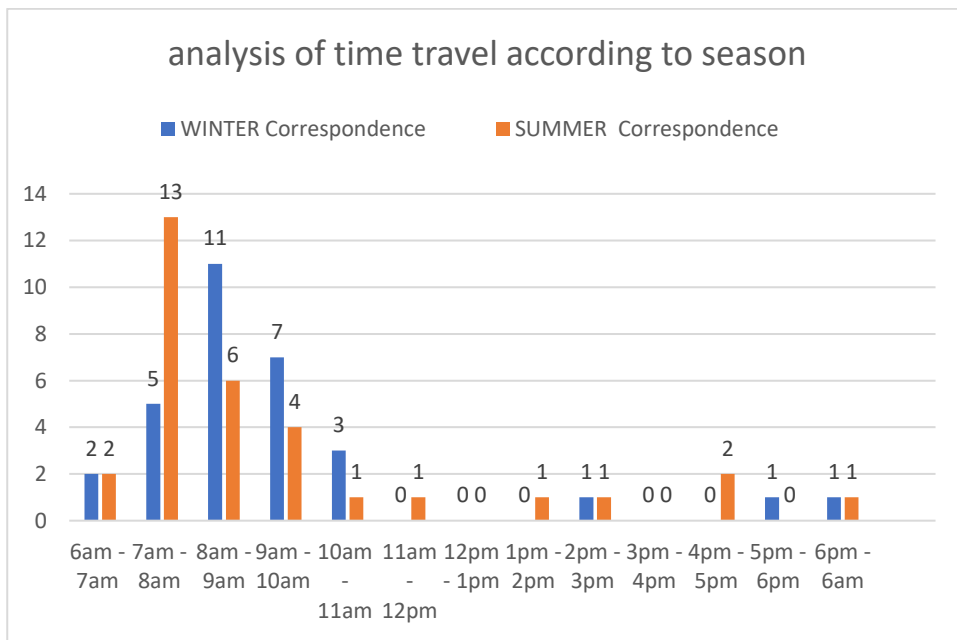


Figure 3.12 Timeline Factor of the survey

Based on the chart above, there are more movements during the summer than in winter. and time of travel are earlier than for winter. Most of the movement in the

afternoon and evening are related to non-official purposes such as getting groceries and visitations while morning movements are related to work and school. Which means in the design of a SEV, it is a good idea that the cars would be have enough time to recharge for travels in the evening, after most of the correspondence are done with work or school as seen in the chart for both summer and winter. This study aims to determine the optimal time when the journey is less busy, and the conditions are suitable for the solar PV panel to generate and store energy in a battery for future use.

Further analysis is on the length of travel, which is reviewed in figures below. It should be noted that the purpose of travel determines the length of travel. The average distance travelled within the case study region is 7.5km. This is reviewed in the purpose of travel which is mainly work and schooling within the time frame of 8am in the morning and returned home 6pm in the evenings. The comparison between the figures for summer and winter reviewed that most movements within the range of 1km – 5km are based on walking, cycling and quick purpose events as the temperature in this season are quite conducive than the winter season where we have more distance covered based on usage of a vehicle.

The purpose of travel is the main data that affects the outcome of this survey. For whatever reason individuals travels determines the distance covered and the opportunity for the aim of this study is achieved, which is for the vehicle to be able to recharge itself via solar. It's important to note that a significant number of responses in the survey are from individuals who travel for work and educational purposes. This is important to consider when analysing the data obtained from the survey. The diagrams below depict the result of the survey.

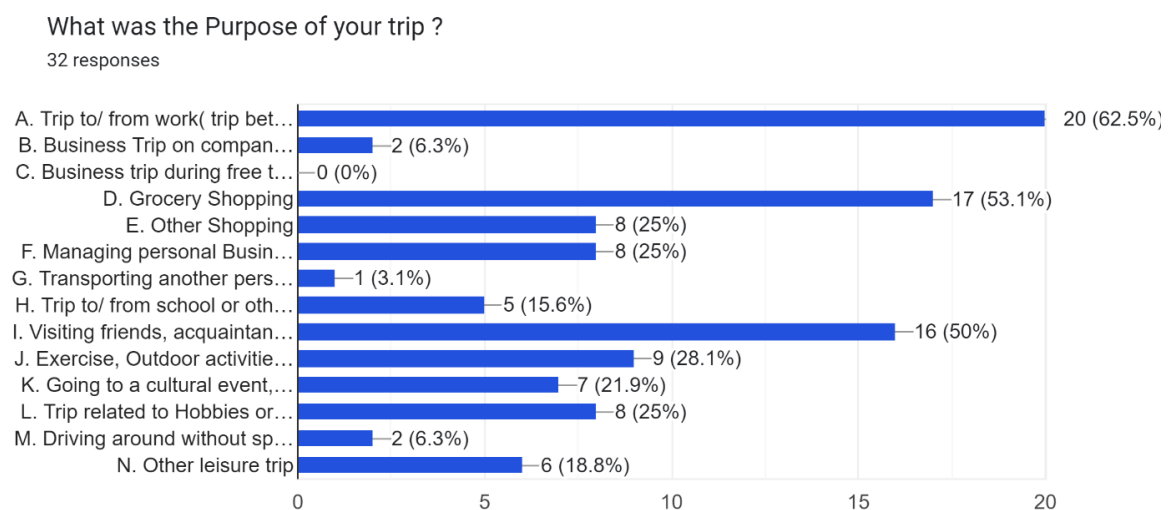


Figure 3.13: Purpose of trip during Summer

What was the Purpose of your trip ?

30 responses

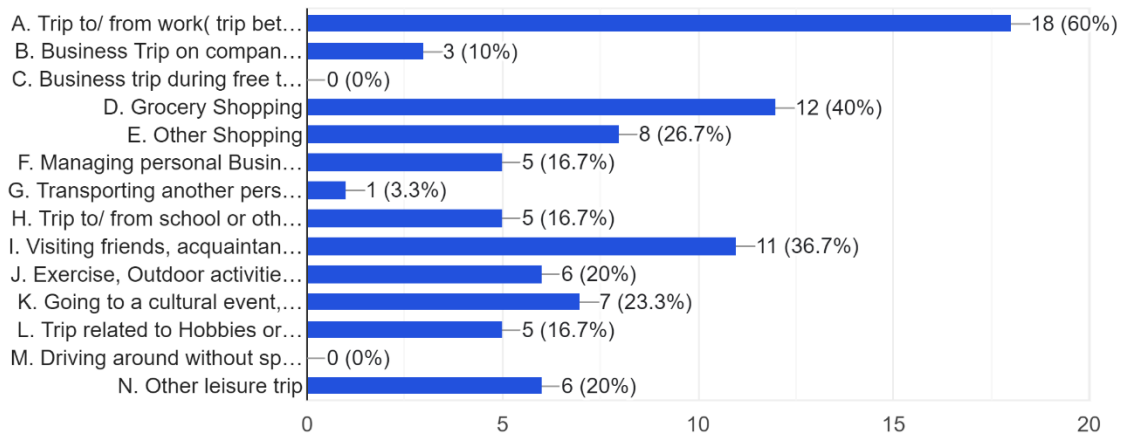


Figure 3.14: Purpose of Trip during Winter

Travel purposes are limited during winter but are more during the summertime. This is a great opportunity for the use of solar energy for the design of the sev.

It is important to note if individuals use their private vehicles more during the summer or winter season. From the survey it is observed that many individuals preferred to use their personal vehicles more in the summer than winter. Whereas in the winter, buses, public vehicles are more preferred.

This data is necessary to determine the load profile for the sev. This makes the approach of sev recharging during the summer possible as private vehicles are charged while parked based the time frame of correspondence in this survey analysis.

What was the distance of this trip?

32 responses

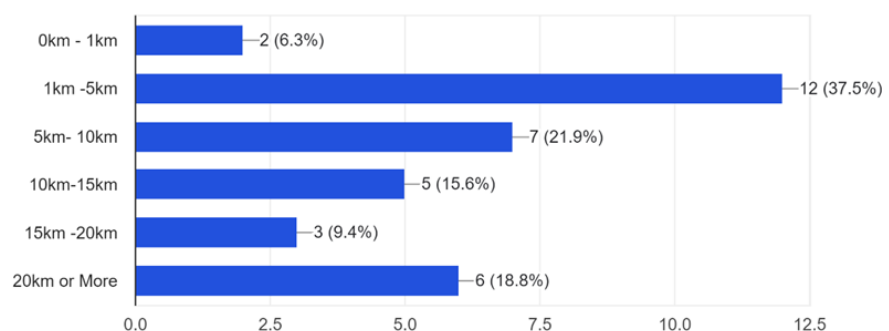


Figure 3.15: Distance travelled during Summer.

What was the distance of this trip?

30 responses

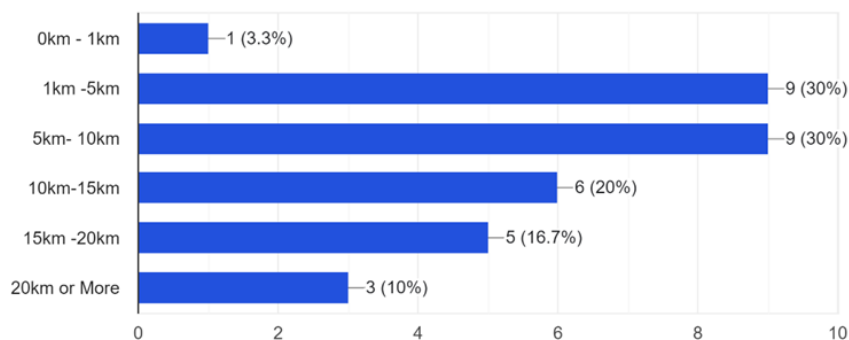


Figure 3.16: Distance travelled during Winter.

The analysis of the mode of transportation is as depicted in the figures 3.17 and 3.18 below for both summer and winter season.

What form of transportation do you take from a Point A to a Point B

32 responses

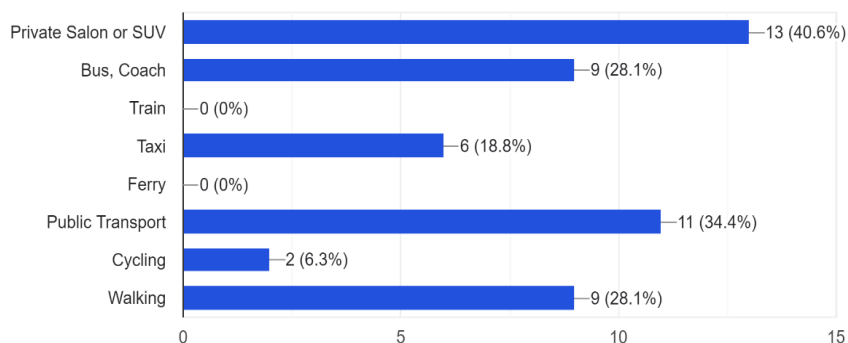


Figure 3.17: Mode of transportation during Summer

What form of transportation do you take from a Point A to a Point B

31 responses

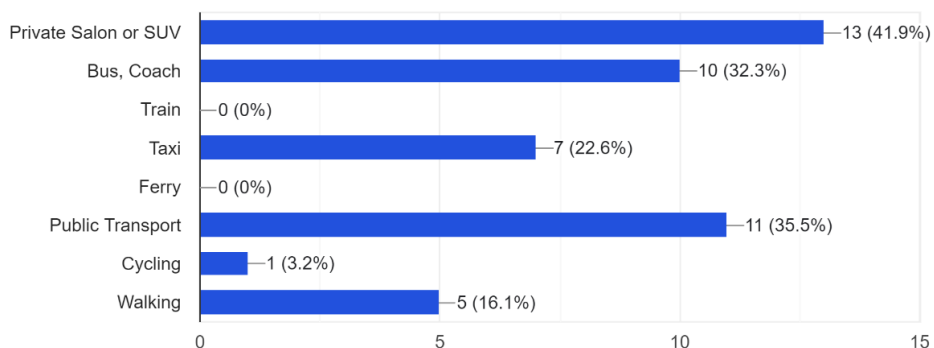


Figure 3.18: Mode of transportation during Winter

As analysed in the previous data collections, more travels are recorded in summer than winter. Also, the use of private vehicles is dominant in summer than in winter, with more public transport used in winter than in summer. Less cycling and walking are also in winter than summer. This assigns the possibility of the objective of this study to have a sev that can utilize solar energy especially with private vehicles as more solar radiation are more in summer than winter.

3.3.1 The load profiles.

In summary to survey, the average distance travelled is 7.5km within Nicosia region which is presently the area of study for the aquation of solar energy data, the total distance covered withing Nicosia according to correspondence is 15km range (resource app: <https://www.distance.to/>),which Gonyeli to Hamitkoy being the longest.

Most correspondence are travelled for the main purpose of work and studies which makes this study design primarily for individuals with same purpose. the time frame starts from 7am in summer with about two hours movement to area of destination and a return trip of about 3-4 hours considering traffic within Nicosia. in addition, an energy usage of 1 hour for any further movement within the day, this brings total usage of vehicle to a 7-hour vehicle usage at an average distance of 7.5km daily for mode of transportation such as the private salon or SUV. The busiest times are between 7am to 9am and between 4pm to 5:30pm in the evening when correspondence is back from work.

The energy demand of the individuals in the survey is used as the basis for creating the load profile in this study. Considering the common location, which is Nicosia, with a total distance coverage of 15km travel length. The electric vehicle data considered is the solar electric vehicle lightyear 0, it is the first solar electric vehicle in production in the world started in summer of 2022. It is known with an energy consumption of 10.5kWh/100km. Therefore, based on this calculation, the required energy per day for the total distance travelled within 15km radius in Nicosia is 1.58kWh.

This data is better illustrated for summer and winter in the figures 3.19 and 3.20 below. The timeline is measured with the distance travelled. It is further analysed that 1km radius have an energy usage of 0.105kWh.

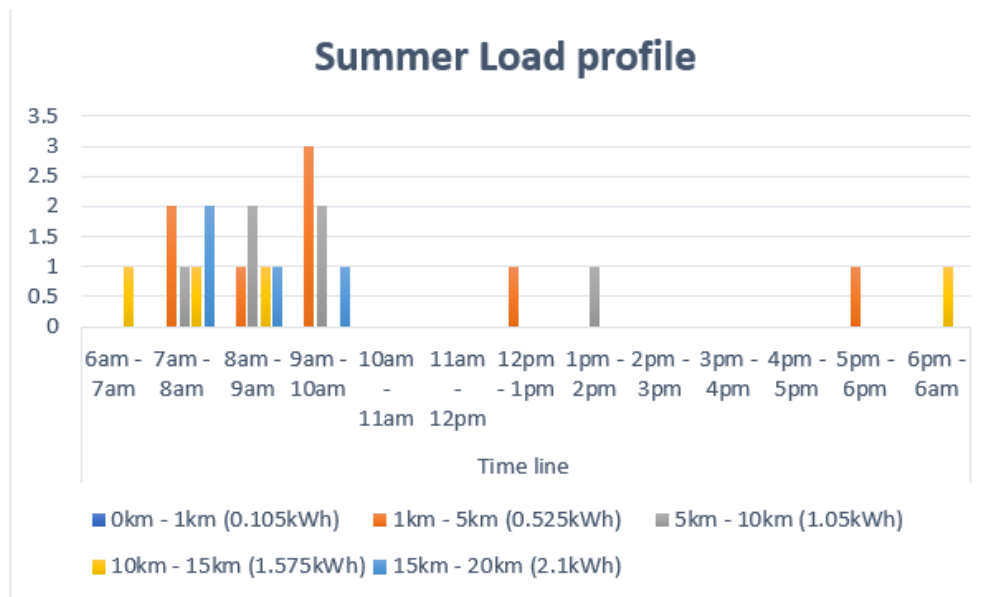


Figure 3.19: Summer Load Profile

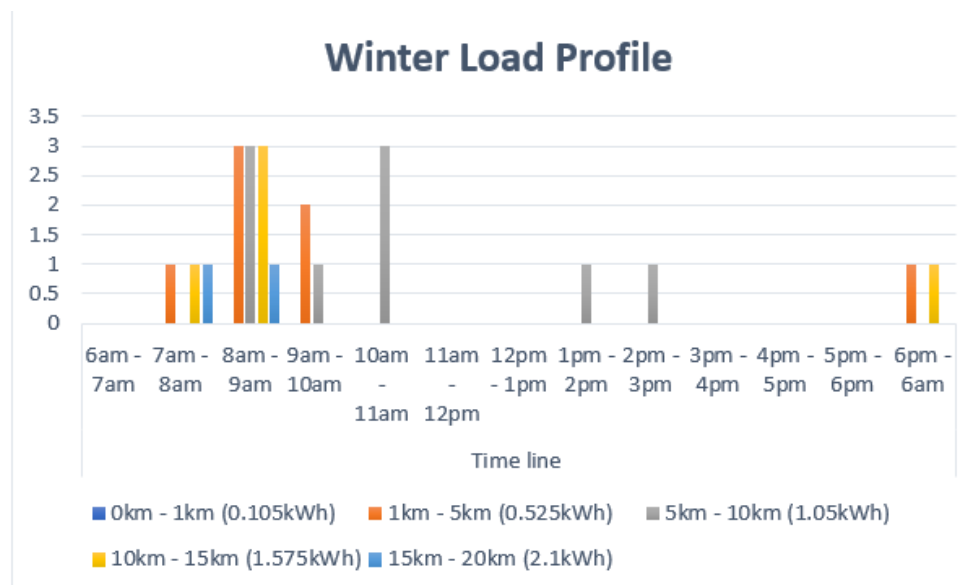


Figure 3.20: Winter Load Profile

It should be noted that with the survey carried out, the data is inaccurate to determine what travel distance occur more in Nicosia in winter and summer as the survey is only limited to a few people.

3.4 Solar powered vehicle design

The exterior design of the vehicle features a solar module mounted on the horizontal surfaces of the hood, roof, and trunk. This module generates solar energy and charges the car battery through a charge controller. The battery is fully charged before being connected to the solar module, ensuring that it stays charged at all times. This is illustrated in the figure 3.21 below.

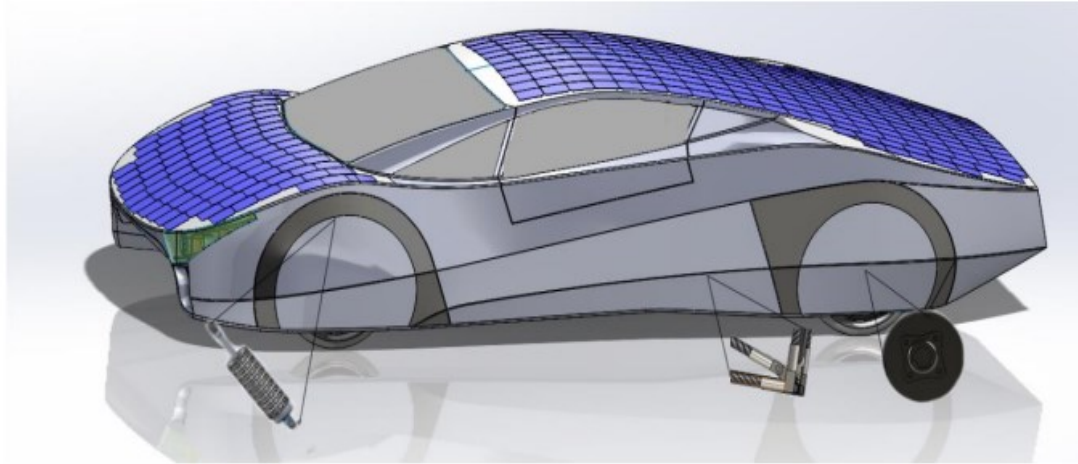


Figure 3.21: Vehicle design illustration with solar panels

The electric vehicle's solar panel captures sunlight and converts it into electricity. The power tracker takes the power from the solar panel and transforms it into a form usable by the main battery. The power tracker changes the solar PV voltage to match the system voltage before sending the energy to the battery for storage. The motor uses the stored energy to power the wheels and the motor controller regulates the energy flow to match the driver's throttle input. This working principle is illustrated in the figure below.

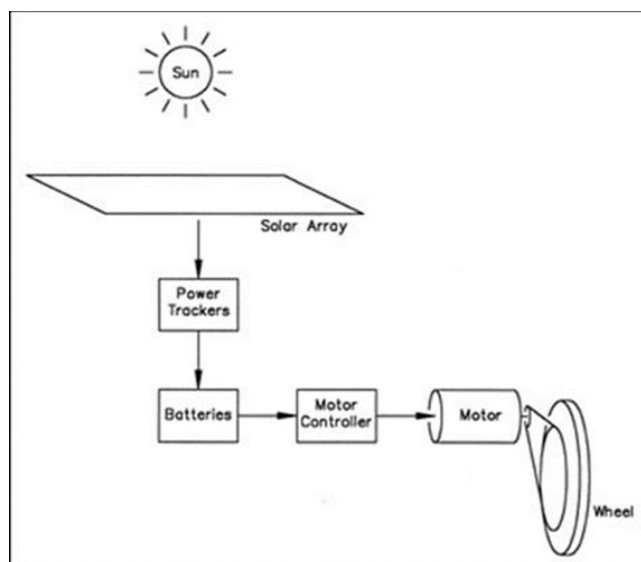


Figure 3.22: Working principle (Raghavendra. 2013)

3.4.1 Design specifications of vehicle model

This study focuses on the Tesla Model S electric vehicle and its mechanical specifications. The hood, roof, and trunk were identified as suitable locations to install solar PV panels in a horizontal position, with a total available area of 4.5 square meters.

The Lightyear0 is considered for the electrical specifications of this study. The vehicle model shares the objective of this study, hence the reason for the study. The absence of certain technical data has put the study at a disadvantage, which opens the opportunity of using tesla model S for the mechanical specification.

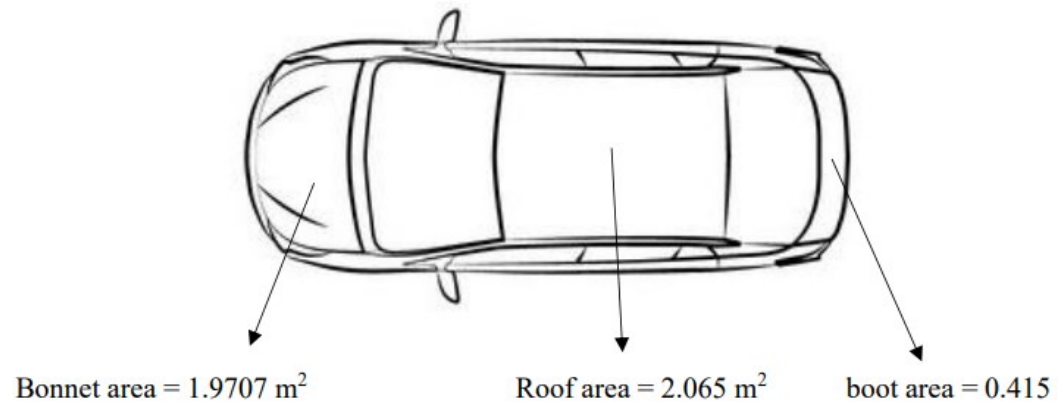


Figure 3.23: Tesla model S body specifications (Outlines Thesis. 2017)

This study uses the Tesla Model S, and the following technical data is available for it.

Table 3.3: Mechanical specification for the design study (Tesla Model S)

S/NO	DATA	VALUE
1	Tire radius front and rear	0.27m
2	Length	4970mm
3	Width	2187mm
4	Height	1445mm
5	Empty weight	2129kg
6	Cd	0.208
7	Frontal area	1.9707m ²
8	Boot area	0.415m ²
9	Roof area	2.065m ²

For the electrical specifications which influences the energy management result of this study design, the technical specifications of lightyear0 is shown in the table below.

Table 3.4: Technical specification for the design study (Lightyear0)

S/N0	DATA	VALUE
1.	NEDC range	625km
2.	Max. Power	130kW
3.	Max. Torque	1720Nm
4.	Max. Speed	160km/h
5.	Average consumption	10.5kWh/100km
6.	Battery type	Lithium ion
7.	Battery capacity	60kWh
8.	Cd value	0.175
9.	Charging Speed	3.7 kW, Home ,32 km/h 22 kW, Work ,200 km/h 50kW, public,520 km/h

3.4.2 Mathematical Modelling of the Solar Electric Vehicle for Power and Energy required.

In the figure below, the forces exerted on the SEV are illustrated in the diagram. With an 'assumed' average constant velocity of 5.56m/s going at a tilt angle θ

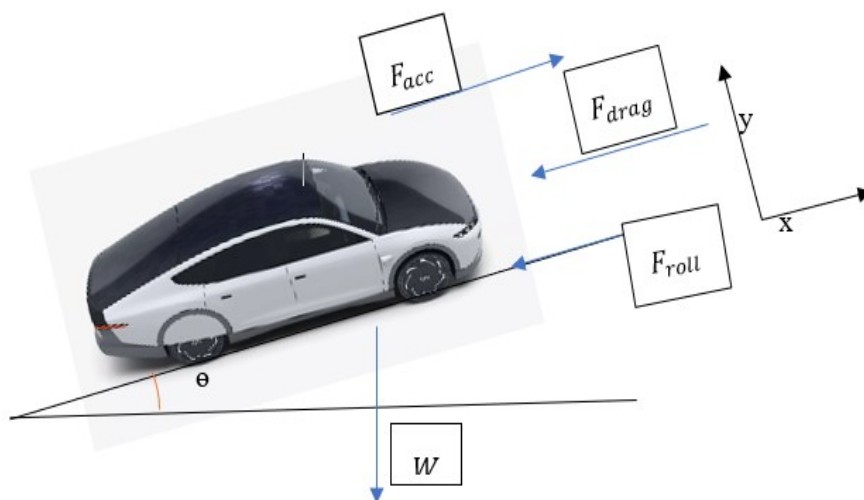


Figure 3.24: forces acting on SEV on an inclined plane

At equilibrium the sum of the forces is zero that is;

$$\sum F_x = 0 \quad (1)$$

Therefore, along the x-axis, the net force F_{total} , is;

$$F_{total} = F_{acc} - F_{drag} - F_{roll} - F_W \quad (2)$$

F_{acc} - Acceleration force which is 0 since the velocity is constant

F_{drag} - Drag force, also referred to as the aerodynamic the force of air resistance that opposes the movement of the vehicle.

F_{roll} - The rolling resistance force that opposes motion due to the deformation of the tires.

F_W - The Slope force due to the total weight of the vehicle.

Therefore, calculating the drag force ,

$$\text{We know that; } F_{drag} = \frac{1}{2} \rho_{air} A C_d V_r^2 \quad (3)$$

ρ_{air} (kg/m^3) – Density of air at specified altitude

A (m^2) – Front area of the vehicle

C_d – coefficient of air drag (I am using lightyear 0 specification)

V_r - velocity of the vehicle relative to that of the wind.

The air density varies based on the temperature, altitude, and weather conditions in the region. According to the Pvsyst application , the altitude of Nicosia is 150m, with an average air velocity of 3.7m/s. Using aerospaceweb.org, the air density of Nicosia is $1.2075kg/m^3$. Figure 3.25 below shows the Pvsyst software topographical view of Nicosia with the altitude.

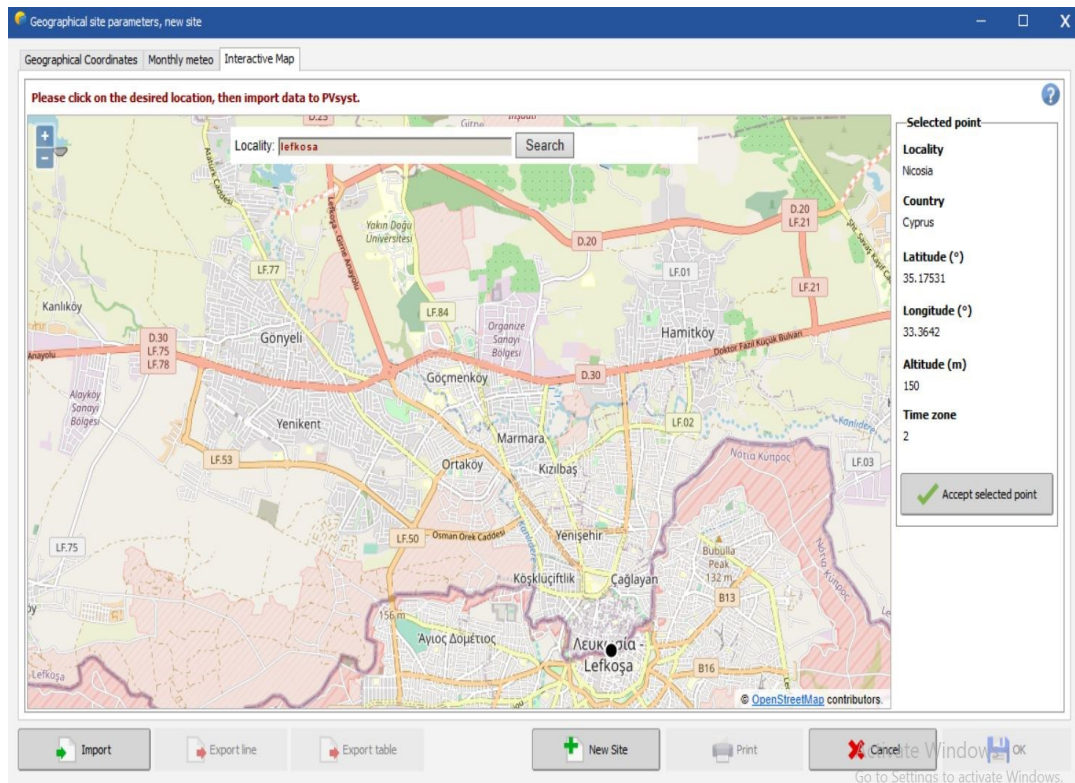


Figure 3.25: Geographical view of Nicosia.(Pvsyst , 2022).

Based on data, I will be using technical specifications of lightyear0 and mechanical body specifications of tesla model S for all calculations and analysis in this study. The tesla model S has frontal area of $1.9707m^2$ and lightyear0 coefficient of air drag is 0.175. Therefore, the drag force ;

$$F_{drag} = \frac{1.2075 \times 1.9707 \times 0.175 \times (5.56 - 3.7)^2}{2} = 1.44N$$

Calculating the slope force F_W ,

$$F_W = M_v g \sin\theta \quad (4)$$

Since most of the time, the SEV operates on flat surface with $\theta = 0$, $F_W = 0$.

M_v (kg) - total mass of the vehicle

g (m/s^2) – gravitational constant

θ (rad) – road slope angle

Assuming the surface is tilted at an angle of $\theta = 10^\circ$, with a radian equivalent of 0.17rad.

Approximately the total mass of the SEV is as estimated below.

$$M_v = M(\text{body}) + M(\text{driver}) + M(\text{battery}) + M(\text{PV_cells}) + M(\text{motors}) + M(\text{wheels})$$

$$M_v = 500kg + 60kg + 350kg + 20kg + 20kg + 50kg = 1000kg$$

Therefore, F_W at tilted angle is ;

$$F_W = (1000)(9.81) \sin(0.17) = 1660N$$

Calculating the rolling force F_{roll}

$$F_{roll} = C_r W \cos\theta = C_r M_v g \cos\theta \quad (5)$$

C_r – Coefficient of road rolling friction

$W(N)$ – Total weight of vehicle

θ (rad) – road slope angle

To determine C_r – at low speeds, the rolling friction varies linearly with speed such that.

$$C_r = 0.012 \left\{ 1 + \frac{v}{100} \right\} \quad (6)$$

V^r is in mph , therefore $5.56\text{m/s} \equiv 11.8\text{mph}$

$$C_r = 0.012 \left\{ 1 + \frac{11.8}{100} \right\} = 0.013$$

$$F_{roll} = 0.013(1000)(9.81) \cos(0.17) = 126N$$

Hence the power required by the SEV is.

$$F_{total} = F_{acc} - F_{drag} - F_{roll} - F_W$$

$$F_{total} = 0 - 1.44 - 126 - 1660 = 1787.4N \text{ (along negative } x \text{ - axis)}$$

But at a flat surface, without the vehicle going up a hill,

$$F_{total} = 0 - 1.44 - 126 - 0 = 127.44N \text{ (along negative } x \text{ - axis)}$$

$$\text{Power} = \text{Power} = F_{total} \times v = 127.44 \times 5.56 = 708.57 \cong 709W$$

In the diagram below is an inaccurate input data simulation of the forces acting on the SEV. In the next chapter , an accurate input data will be used for output of the forces acting on the SEV based on the modelling in this chapter .

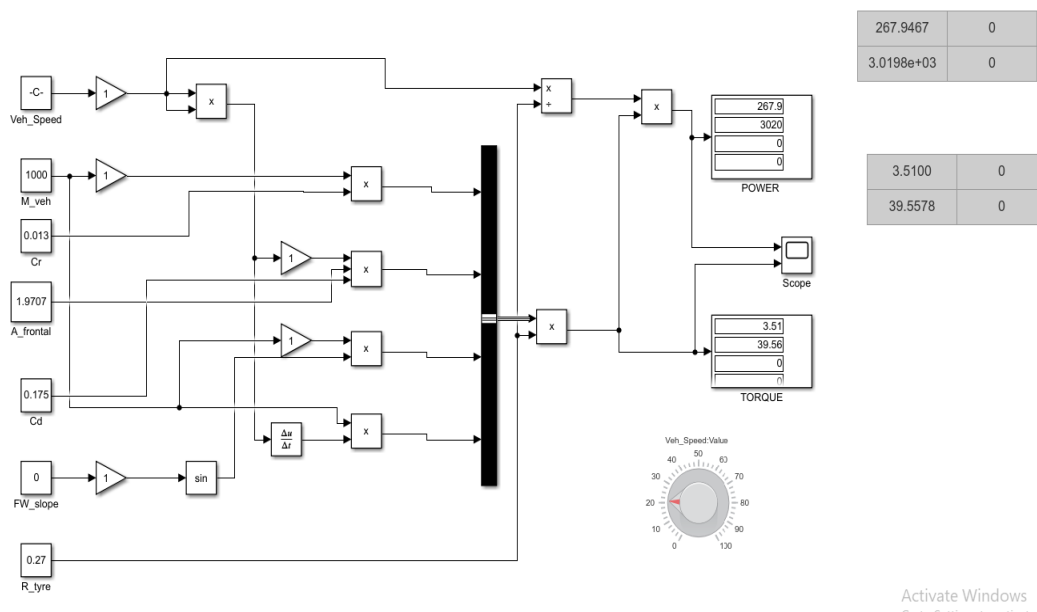


Figure 3.26 Simulink model of forces acting on SEV.

And the energy needed, based on the required hourly need from questionnaire survey which is a average travel of 7 hours daily

$$E = Power\Delta t = 709 \times 7 = 4960Wh \approx 4.96kWh$$

3.4.3 Mathematical Modelling of the SEV for the Electric Motor

Since the SEV operates mostly on flat surface, with energy required as 4.96kWh. Presumably, the power output of the electric motor should be.

$$P_{out} = 5kW$$

Each motor will be 2.5kW with an efficiency of 90% (assumably),

$$P_{in} = \frac{5}{0.9} = 5.56kW$$

$$E_{in} = 5.56 \times \frac{7h}{day} = 38.92kWh$$

3.4.4 Mathematical Modelling of the SEV for the Battery Capacity

From the input of the motors, there is a supply of 5.56kW sustainable for 7 hours. Therefore, it can also be calculated that.

$$E_{out} = 5.56 \times \frac{7h}{day} = 38.92kWh$$

Assuming the allowable battery autonomy is 4 hours, with depth of discharge as 80%. The minimum battery capacity is calculated as

$$C = \left(\frac{4}{24} \text{ day}\right) (38.92) \left(\frac{1}{0.08}\right) = 81\text{kWh}$$

Converting to Ah, with a voltage of 12v

$$C = \frac{81000}{12} = 6750\text{Ah}$$

This shows the SEV at a velocity of 5.56m/s will supply energy by itself with a battery capacity of 81kWh, 6750Ah for 4 days and few hours without recharging.

The power is 709W, with a voltage of 12 gives 59.1A, and to get the number of days of continuous usage, we divide 6750Ah by 59.1A, you get 114hours of battery usage.

3.4.5 Mathematical Modelling of the SEV from the Solar Panel

This model is intended to determine the peak power of the solar panel. But first considering the Monthly and daily solar irradiation in Nicosia . The most recent data for the year 2022 was gotten from solacast TMY Met, using Pvsyst software. From the figure below . The data illustrated in the figure shows the monthly energy radiation in Nicosia and the second shows the average daily energy.



PVsyst V7.3.1

Geographical Site		Situation												
Nicosia		Latitude	35.18 °N											
Cyprus		Longitude	33.36 °E											
		Altitude	150 m											
		Time zone	UTC+2											
Monthly Meteo Values														
Source	Solcast TMY													
	Jan.	Feb.	Mar.	Apr.	May	June	July	Aug.	Sep.	Oct.	Nov.	Dec.	Year	
Horizontal global	75.5	87.7	137.8	174.3	192.8	229.2	240.1	216.0	168.2	128.0	86.5	71.2	1807.3	kWh/m ²
Horizontal diffuse	28.2	29.4	42.2	55.6	59.4	57.2	53.2	57.3	48.4	38.6	27.6	27.1	524.3	kWh/m ²
Extraterrestrial	157.8	183.3	255.8	299.2	344.1	346.4	351.6	324.0	268.2	221.6	164.6	144.6	3061.3	kWh/m ²
Clearness Index	0.478	0.479	0.539	0.583	0.560	0.661	0.683	0.667	0.627	0.578	0.526	0.492	0.590	ratio
Ambient Temper.	14.7	14.7	15.2	17.8	20.8	25.4	27.4	29.2	27.5	22.9	16.9	16.7	20.8	°C
Wind Velocity	4.0	4.6	4.0	3.6	3.2	3.1	4.3	3.7	3.4	2.8	3.5	3.7	3.7	m/s

Figure 3.27: monthly irradiation in Nicosia (Pvsyst, 2022).



PVsyst V7.3.1

Geographical Site		Situation	
Nicosia		Latitude	35.18 °N
Cyprus		Longitude	33.36 °E
		Altitude	150 m
		Time zone	UTC+2

Monthly Meteo Values														
Source	Solcast TMY													
	Jan.	Feb.	Mar.	Apr.	May	June	July	Aug.	Sep.	Oct.	Nov.	Dec.	Year	
Horizontal global	2.43	3.13	4.44	5.81	6.22	7.64	7.74	6.97	5.61	4.13	2.88	2.30	4.95	kWh/m ² /day
Horizontal diffuse	0.91	1.05	1.36	1.85	1.92	1.91	1.71	1.85	1.61	1.25	0.92	0.87	1.44	kWh/m ² /day
Extraterrestrial	5.09	6.55	8.25	9.97	11.10	11.55	11.34	10.45	8.94	7.15	5.49	4.67	8.39	kWh/m ² /day
Clearness Index	0.478	0.479	0.539	0.583	0.560	0.661	0.683	0.667	0.627	0.578	0.526	0.492	0.590	ratio
Ambient Temper.	14.7	14.7	15.2	17.8	20.8	25.4	27.4	29.2	27.5	22.9	16.9	16.7	20.8	°C
Wind Velocity	4.0	4.6	4.0	3.6	3.2	3.1	4.3	3.7	3.4	2.8	3.5	3.7	3.7	m/s

Figure 3.28: Average Daily Meteo Data in Nicosia

Considering for the year 2022, the monthly average for 255.1 kWh/m^2 and a daily average energy radiation of 8.5 kWh/m^2 .

To calculate the solar panel power peak, the formula

$$P_p = \frac{ER_{std}}{\eta R_{avgD}} \quad (8)$$

$E(\text{kWh})$ - Energy from the battery capacity

η - PV yield and efficiency

$R_{std}(\text{kWh/m}^2)$ - Standard value of irradiance

$R_{avgD}(\text{kWh/m}^2)$ - Average daily solar irradiance.

Therefore, the peak power for the Nicosia region is

$$P_p = \frac{81000 \times 1}{0.8 \times 8.5} = 11.91 \text{ kW}$$

To regulate the power transmitted from solar panel to the battery, a charge controller is utilized. To do so we multiply the current by 1.25 for variable accountability in the power output.

$$I = 1.25 \frac{P_p}{v} = 1.25 \frac{11911}{12} = 1240 \text{ A}$$

3.5 Pv Design Analysis

The intended load from the modelling of the SEV is 4960Wh for 7 hours, making 17000Wh per day (24 hours). To design the technical data for the PV, the following steps are followed.

Step 1: the total DC Amp-hours/ day

$$\frac{\text{load}}{\text{system nominal voltage}} = \frac{4960}{12} = 413.33\text{Ah/day}$$

Step 2: total amp-hour/day with batteries

$$\text{total } \frac{\text{Ah}}{\text{day}} \times 1.2(\text{losses and safety factor}) = 413.33 \times 1.2 = 496\text{Ah/day}$$

Step 3: total pv array current

$$\frac{\text{total daily Ah required}}{\text{design isolaton (isoaltion based on optimum tilt for season)}} = \frac{496}{5} = 99.2\text{A}$$

Step 4:using pv model SunPower SPR-X21-345 for its high efficiency and high-grade silicon. The following are the specifications for the panel.

Table 3.5 Solar Panel Specification for SunPower X- Series(Ndyamukama;, 2017)

Description	Values
Type	Monocrystalline Silicon (72 cells)
STC Power rating	345 W
STC Power per unit area	211.6 W/m ²
Peak Efficiency	21.16%
Maximum voltage	57.30 V
Maximum current	6.02 A
Open circuit voltage	68.2 V
Short circuit current	6.39 A
NOCT	41.5 °C
Weight	18.6 kg
Temperature coefficient of voltage	-0.164 V/K
Temperature coefficient of power	-0.3%/K
Temperature coefficient of current	0.05%/K

Step 5: based on the above table , the number of modules in parallel is calculated as

$$\frac{\text{total pv array current}}{\text{module operating current} \times \text{module derate factor}} = \frac{99.2}{6.02 \times 0.9} = 18 \text{ modules}(1318 \text{ cells})$$

Step 6: number of modules in series

$$\frac{\text{system nominal voltage}}{\text{module nominal voltage}} = \frac{12}{12} = 1 \text{ module}$$

Step 7: Total number of modules= parallel modules \times series modules = 18 \times 1 = 18

Step 8: minimum battery capacity

$$\frac{\text{total daily } \frac{Ah}{\text{day}} \text{ with batteries} \times \text{autonomous days}}{SOC} = \frac{496 \times 4}{0.8} = 2480Ah$$

battery type specification

3.6 Solar Energy mathematical model for Nicosia

As seen in the figure below, the geographical parameter of Nicosia is used in the determination of the solar irradiance input used in Pvsyst and for simulation in this Simulink model design for this study. The amount of solar radiation reaching the earth's horizontal surface, known as solar irradiance, was obtained from the Solcast database. Pvsyst calculates the average daily radiation based on the clearness index and the latitude. The coordinates for Nicosia, with a latitude of 35°17'31" N and longitude of 33°36'42.", were used to obtain the daily radiation data.

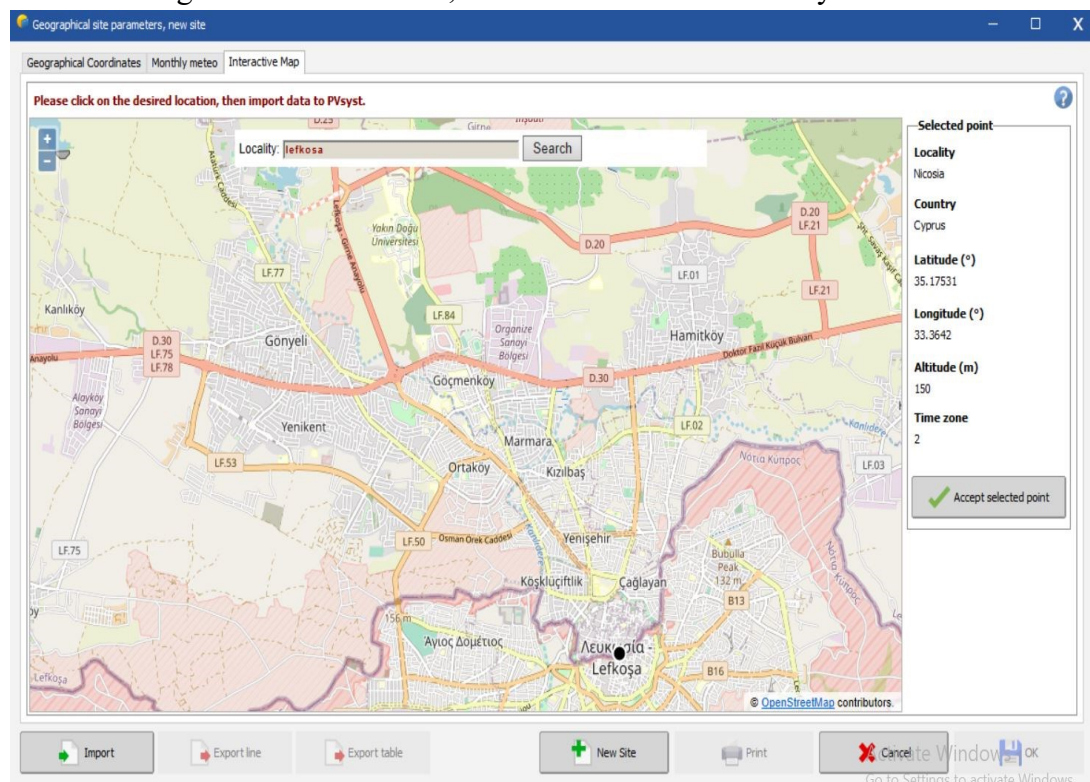


Figure 3.29: Nicosia Geographical Area

The clearness index is a measure of the atmospheric clarity, and Pvsyst calculates the monthly average clearness index, K_T , which is a dimensionless value ranging from 0 to 1. It represents the fraction of solar radiation that reaches the

earth's surface after passing through the atmosphere, starting from the top of the atmosphere. Pvsyst calculates the clearness index using the equation:

$$K_T = \frac{G}{G_o} \quad (9)$$

where:

G = global average radiation that strikes the horizontal surface of the earth (kWh/m²/day)

G_o = the radiation striking a horizontal surface at the top of the earth's atmosphere also known as extraterrestrial horizontal radiation (kWh/m²/day)

The clearness index values are generally high on sunny and clear days, and low on cloudy days. The extraterrestrial radiation, G_o , can be calculated for any month of the year based on the given latitude. So, by knowing the clearness index and extraterrestrial horizontal radiation, the global radiation on the horizontal surface, G , can be calculated using equation 9. The extraterrestrial normal radiation, which is the radiation at the top of the earth's atmosphere striking the surface perpendicular to the sun's rays, is calculated in Pvsyst using equation 10.

$$G_{on} = G_{sc} \left(1 + 0.033 \cdot \cos \frac{360n}{365} \right) \quad (10)$$

where:

$G_{sc} = 1.367 \text{ kW/m}^2$ (Solar constant)

G_{on} = extraterrestrial normal radiation [kW/m²]

n = day of the year (ranging between 1 to 365)

In this study, the focus is on the extraterrestrial radiation on a horizontal surface and Pvsyst uses equation 11 to calculate this value. This equation is used by Pvsyst to calculate the extraterrestrial radiation on a horizontal surface.

$$G_o = G_{on} \cos \theta_z \quad (11)$$

θ_z = zenith angle [°]

The zenith angle is calculated using equation below.

$$\cos \theta_z = \cos \phi \cos \delta \cos \omega + \sin \phi \sin \delta \quad (12)$$

ϕ = Latitude [°]

δ = Solar declination [°]

ω = Hour angle [°]

The solar declination angle is calculated by Pvsyst using equation 13.

$$\delta = 23.45^\circ \sin\left(360^\circ \frac{284 + n}{365}\right) \quad (13)$$

The daily extraterrestrial radiation per square meter is calculated by integrating equation 11 for the solar radiation intensity at the top of the earth's atmosphere from sunrise to sunset. The result of this integration is equation 14.

$$G_o = \frac{24}{\pi} G_{on} \left[\cos \phi \cos \delta \sin \omega_s + \frac{\pi \omega_s}{180^\circ} \sin \phi \sin \delta \right] \quad (14)$$

G_o = daily average extraterrestrial horizontal radiation [kWh/m²/day]

ω_s = sunset hour angle [°]

Also, the sunset hour angle is calculated as below:

$$\cos \omega_s = -\tan \phi \tan \delta$$

Pvsyst calculates the monthly average extraterrestrial horizontal radiation by using the daily average extraterrestrial horizontal radiation, H_o as follows.

$$G_{o,ave} = \frac{\sum_{n=1}^N G_o}{N} \quad (15)$$

where:

$G_{o,ave}$ = Monthly average extraterrestrial horizontal radiation [kWh/m²/day]

N = Number of days in the month

The solar PV output calculated by Pvsyst is based on the amount of solar radiation that reaches the PV surface/array. There are two types of solar radiation that reach the earth's surface - beam or direct radiation and diffuse radiation. Beam radiation doesn't scatter and travels directly from the sun to the earth's surface, while diffuse radiation scatters and originates from all parts of the sky. The global horizontal radiation on the earth's surface is the sum of beam radiation and diffuse radiation.

$$G = G_b + G_d \quad (16)$$

where:

G_b = beam radiation (kW/m²)

G_d = diffuse radiation (kW/m²)

Pvsyst uses the data on global horizontal radiation, obtained from the NASA database, to calculate the amount of solar radiation that falls on the PV panel/array. The software first splits the global radiation into its beam and diffuse components, and then uses this information to determine the total solar radiation incident on the panel.

3.6.1 Mathematical of the Temperature input from irradiance to PV Panel

Based on the location Nicosia, the average ambient temperature in the year 2022 is 20.8 degrees Celsius. The temperature effect on the photovoltaic (PV) system is taken into consideration in the input parameters of Pvsyst. The program calculates the temperature of the PV cells based on the ambient temperature at each time step, which is then used to determine the power output of the PV array. During night-time, the PV cell temperature is typically the same as the ambient temperature, but during the day, when the sun is shining, the cell temperature can rise to 30°C or higher above the ambient temperature. The calculation of the PV cell temperature is based on the energy balance of the PV panel/array, using the equation from Duffie and Beckman (1991).

$$\tau\alpha G_T = \eta_c G_T + U_L(T_c - T_a) \quad (17)$$

where:

τ = solar transmittance of any cover over the PV array [%]

α = solar absorptance of the PV array [%]

T_c = cell temperature of the PV [°C]

T_a = ambient temperature [°C]

G_T = solar radiation striking the PV panel (kW/m²)

U_L = Heat transfer coefficient to the surroundings (kW/m²°C)

η_c = PV array electrical conversion efficiency [%]

Equation 17 demonstrates an equilibrium between the amount of solar energy absorbed by the photovoltaic array and its electrical output, including heat transfer to

the environment. Equation 18 is used to determine the temperature of the cells.

$$T_c = T_a + G_T \left(\frac{\tau\alpha}{U_L} \right) \left(1 - \frac{\eta_c}{\tau\alpha} \right) \quad (18)$$

NOCT (Nominal Operating Cell Temperature) $\left(\frac{\tau\alpha}{U_L} \right)$ is frequently cited by manufacturers as it is challenging to measure directly. NOCT represents the temperature of the cell when the ambient temperature is 20°C, the incident radiation is 0.8 kW/m², and no load is being used (i.e., $\eta = 0$). Equation 18 can be transformed into equation 19 by substituting these values.

$$\frac{\tau\alpha}{U_L} = \frac{T_{c,NOCT} - T_{a,NOCT}}{G_{T,NOCT}} \quad (19)$$

where:

$T_{c,NOCT}$ = Nominal Operating Cell Temperature [°C]

$T_{a,NOCT}$ = Ambient temperature at which the NOCT has been defined [20 °C]

$G_{T,NOCT}$ = Solar radiation at which the NOCT has been defined [0.8 kW/m²]

Assuming a constant value $\left(\frac{\tau\alpha}{U_L} \right)$, Equation 18 can be substituted into Equation 19, resulting in Equation 20.

$$T_c = T_a + G_T \left(\frac{T_{c,NOCT} - T_{a,NOCT}}{G_{T,NOCT}} \right) \left(1 - \frac{\eta_c}{\tau\alpha} \right) \quad (20)$$

PVSYST adopts the proposal by Duffie and Beckman (1991) that the value of $\tau\alpha$ should be 0.9. Furthermore, PVSYST assumes that the photovoltaic array operates at its maximum power point. This is equivalent to the scenario where the photovoltaic array is controlled by a maximum power point tracker. Hence, PVSYST assumes that the maximum power point efficiency is always equal to the cell efficiency.

$$\eta_c = \eta_{mp} \quad (21)$$

where:

η_{mp} = Efficiency of the PV array when it's at maximum power point [%]

Replacing η_c with η_{mp} in eq. 20 to yield:

$$T_c = T_a + (T_{c,NOCT} - T_{a,NOCT}) \left(\frac{G_T}{G_{T,NOCT}} \right) \left(1 - \frac{\eta_{mp}}{\tau\alpha} \right) \quad (22)$$

However, the efficiency of the photovoltaic array at its maximum power point, η_{mp} , is dependent on the cell temperature, T_c . PVSYST assumes a linear relationship between efficiency and temperature, as described in Equation 23.

$$\eta_{mp} = \eta_{mp,STC} [1 + \alpha_p (T_c - T_{c,STC})] \quad (23)$$

where:

$T_{c,STC}$ = cell temperature at STC [25 °C]

$\eta_{mp,STC}$ = maximum power point efficiency at STC [%]

α_p = temperature coefficient of power [%/°C]

Typically, the temperature coefficient of power has a negative value, meaning that as the cell temperature rises, the efficiency of the photovoltaic array decreases. Equation 3.21 for efficiency is then substituted into the cell temperature equation 3.18, resulting in Equation 3.24.

$$T_c = \frac{T_a + (T_{c,NOCT} - T_{a,NOCT}) \left(\frac{G_T}{G_{T,NOCT}} \right) \left[1 - \frac{\eta_{mp,STC} (1 - \alpha_p T_{c,STC})}{\tau \alpha} \right]}{1 + (T_{c,NOCT} - T_{a,NOCT}) \left(\frac{G_T}{G_{T,NOCT}} \right) \left(\frac{\alpha_p \eta_{mp,STC}}{\tau \alpha} \right)} \quad (24)$$

In Equation 3.24, all temperatures must be expressed in Kelvin. This is the equation utilized by PVSYST in each time step to compute the cell temperature. Finally, PVSYST calculates the power output of the photovoltaic array using Equation 3.25 as follows:

$$P_{PV} = Y_{PV} f_{PV} \left(\frac{G_T}{G_{T,STC}} \right) [1 + \alpha_p (T_c - T_{c,STC})] \quad (25)$$

where:

P_{PV} = Power output of the PV array [kW]

T_c = cell temperature of the PV [°C]

$T_{c,STC}$ = cell temperature of the PV at STC [25 °C]

G_T = solar radiation striking the PV array [kW/m²]

$G_{T,STC}$ = Incident radiation at STC [1 kW/m²]

f_{PV} = Derating factor of the PV [%]

α_p = temperature coefficient of power [%/°C]

Y_{PV} = PV Power output at STC [kW]

3.6.2 Solar panel General Mathematical Model

The I-V output behavior of a photovoltaic (PV) cell can be represented by a mathematical model based on an equivalent circuit. This model is commonly used to monitor and evaluate the performance of PV cells and to examine various Maximum Power Point Tracking (MPPT) techniques. The equivalent circuit, shown in Figure 3.30, is comprised of a photogenerated current source, a diode, a resistor representing leakage current in parallel, and a resistor that represents the cell's internal resistance to current flow. The I-V characteristic equation for a PV cell can be expressed as follows:

$$I = I_{PH} - I_S \left(\exp \left[\frac{q(V+IR_S)}{kTA} \right] - 1 \right) - \frac{(V+IR_S)}{R_{SH}} \quad (26)$$

The photocurrent (I_{PH}) is generated by light and is influenced by the solar insolation and cell operating temperature, as expressed by the following equation:

I_s represents the saturation of dark current, q is the electron charge (1.6×10^{-19} C), k is the Boltzmann constant (1.38×10^{-23} J/K), T is the cell temperature, A is the ideal factor, R_{sH} represents the shunt resistance, and R_{SRS} is the series resistance.

$$I_{PH} = \lambda (I_{SC} + K_I (T - T_r)) \quad (27)$$

The cells short-circuit current (I_{SC}) at a temperature of 25°C and an insolation of 1 kW/m² is represented by the following equation:

In this equation, K_I is the temperature coefficient of the cell's short-circuit current, T_r is the cell's reference temperature, and λ represents the solar insolation

in kW/m^2 . Meanwhile, the saturation current of the cell varies with temperature and can be described as follows:

$$I_S = I_{RS} \left(\frac{T}{T_r} \right)^3 \exp \left[q E_G \frac{\left(\frac{1}{T_r} - \frac{1}{T} \right)}{kA} \right] \quad (28)$$

The reverse saturation current (I_{RS}) of the cell at the reference temperature and solar radiation is described by the following equation:

In this equation, I_{RS} is the cell's reverse saturation current at the reference temperature and solar radiation, and E_G is the band-gap energy of the semiconductor used in the cell. The ideal factor A is specific to the PV technology and is listed in Table 6 according to (Hua & Shen, 1998).

The reverse saturation current at the reference temperature can be estimated using the following equation:

$$I_{RS} = \frac{I_{sc}}{\exp \left[\frac{qV_{oc}}{N_s k A T} \right] - 1} \quad (29)$$

where the open-circuit voltage of the photovoltaic (PV) cell at the reference temperature can be represented by V_{oc}

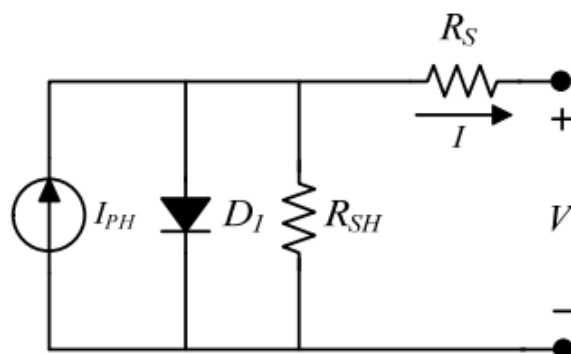


Figure 3.30: PV cell circuit diagram

Table 3.6: PV technology as regarded to Factor A dependency.

Technology	A
Si-mono	1.2
Si-poly	1.3
A-Si:H	1.8
A-Si:H tandem	3.3
A-Si:H triple	5
CdTe	1.5
CIS	1.5
AsGa	1.3

3.7 Dc-Dc Boost Converter

The energy management system of a Solar Electric Vehicle (SEV) is shown in Figure 3.31. This system is responsible for directing the input energy into the vehicle's motors, allowing the vehicle to move. All energy inputs into the vehicle are managed by this system.

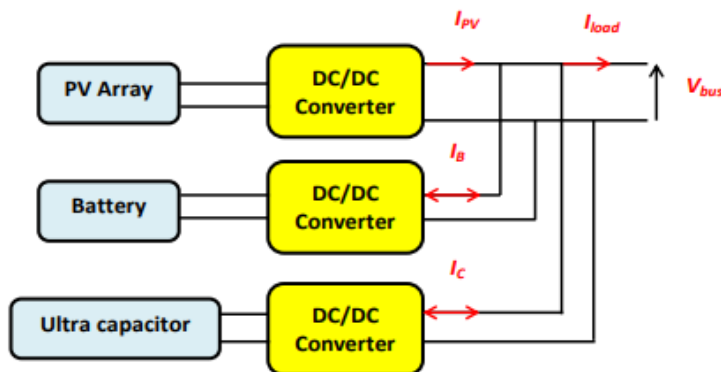


Figure 3.31: energy management system of three sourced input

The Multiport DC-DC converter is used in taking all three input energies, battery as related to the brake energy, supercapacitor and Pv to the electric motor. As illustrated in the figure 3.32 below

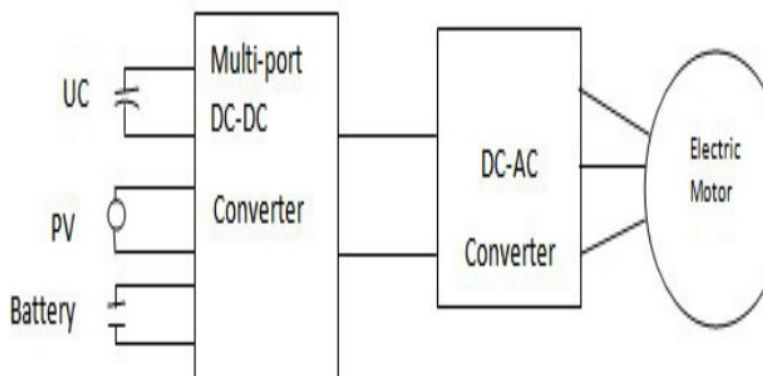


Figure 3.32: DC-DC Converter

In modeling the mathematical formula for this conversion, the model diagram below is illustrated below for a three-input dc-dc converter.

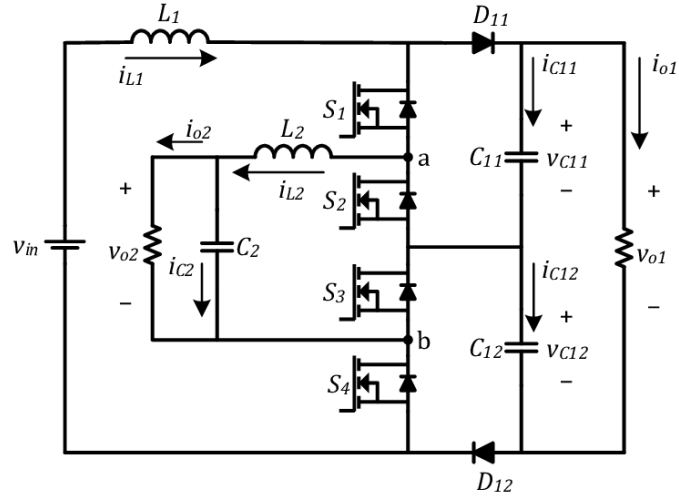


Figure 3.33: Three Input converter model

The output can be as follows.

$$L_1 = d_1 \{V_{pv} - r_1 i_{L1}\} + (d_2 - d_1) \{V_{pv} - r_1 i_{L1} - V_{C1}\} + (1 - d_2) \{V_{pv} - r_1 i_{L1}\} \quad (30)$$

$$V_{C1} = \frac{V_{pv} - r_1 i_{L1}}{d_2 - d_1} \quad (31)$$

$$L_2 = (1 - d_2) \{V_{uc} + V_{C1} + r_2 i_{L2} - V_0\} + d_2 \{V_u - r_2 i_{L2}\} = 0 \quad (32)$$

$$V_0 = \frac{(1 - d_2) \{V_{pv} - r_1 i_{L1}\} + d_2 \{V_u - r_2 i_{L2}\}}{d_2 - d_1 (1 - d_2)} \quad (33)$$

The current second equilibrium is low more than the capacitors C1 and C0, the voltage of the C1 is

$$C_1 = d_2 - d_1 - (1 - d_2) i_{L2} = 0 \quad (34)$$

$$C_0 = (1 - d_2) i_{L2} = \frac{V_0}{R_{load}} \quad (35)$$

When the battery is not used

$$P_{battery} = 0$$

$$I_{battery} = 0$$

3.8 Mppt Modelling Design

In previous sections of the solar panel modelling, it was stated that the solar car must be able to efficiently absorb the maximum energy from the panels while in motion. To achieve this, the orientation and design of the panels must allow for fast Maximum Power Point Tracking (MPPT) algorithms to be used. A brief overview of MPPT was described in Chapter 2.

The Maximum Power Point Tracking (MPPT) algorithm is used to ensure that the energy from the solar panels is efficiently transmitted to the battery and motor.

According to the Lightyear0 design, a 5m^2 surface of 782 cells can generate a power of 130 kW.

The dc - dc converter as designed in the previous subchapter influences the output of the type of connection done on the solar panels wither series, parallel or mixed mounting on the SEV. Therefore, the power depends on the irradiance and temp as regards the location of vehicle usage. Figure 3.34 below shows the characteristics output of the power and voltage as regards to the irradiance and temp in this study design with the use of Simulink.

The energy management system in the Lightyear0 design includes a solar photovoltaic (PV) array, a DC-DC converter, a battery, and an MPPT charge controller block. The MPPT charge controller block comprises of a Perturb & Observe MPPT algorithm and a lithium-ion battery three-stage charge controller, as seen in Fig. This is a common design used in many commercial solar PV MPPT battery charge controllers. The MPPT charge controller block outputs a Pulse Width Modulation (PWM) control signal to switch the switching device in the DC-DC converter. The models for the solar PV array and battery were directly obtained from the Simulink Simscape Electrical block set library.

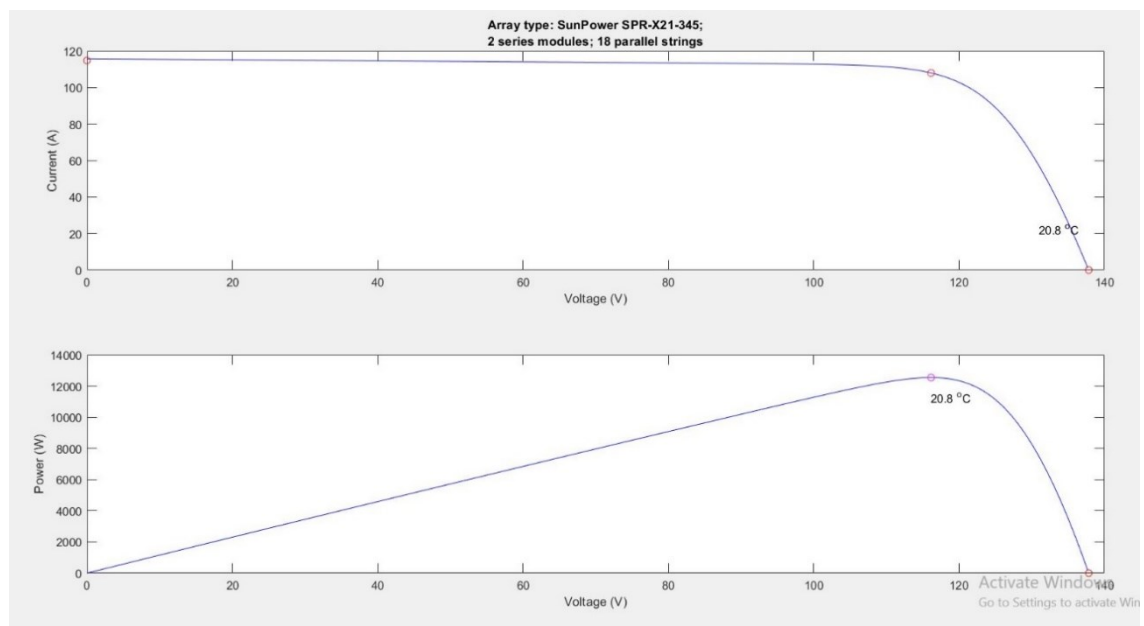


Figure 3.34: I,V irradiance characteristics graph

The MPPT is found using the DC-DC converter and controlled by the "Perturb and Observe" (P&O) algorithm in Fig 3.35. The current and voltage of the PV cells are measured, and the sign of dP (the derivative of power) is used to determine the location of the MPPT. Based on this information, a decision is made to increase or decrease the duty cycle (D).

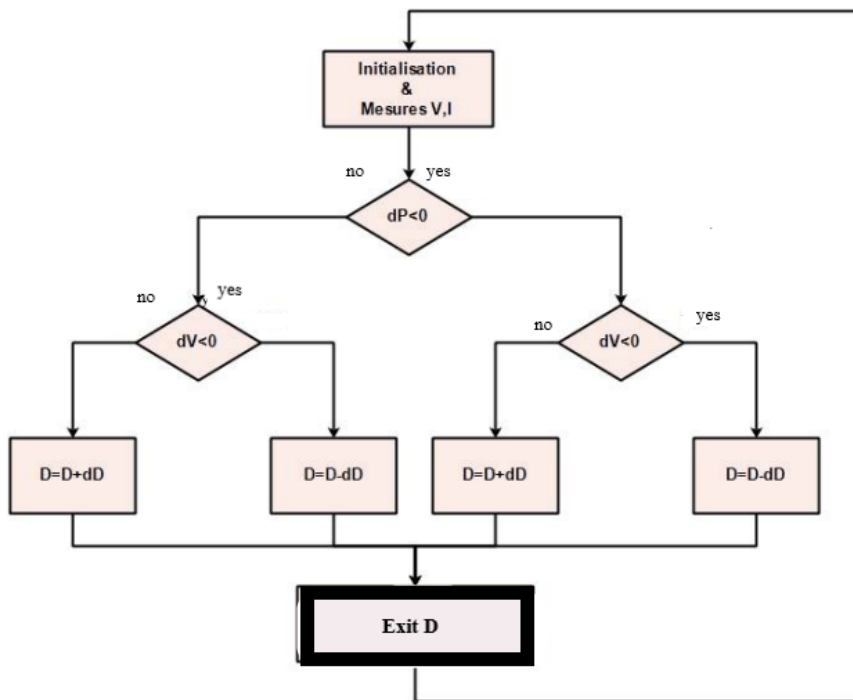


Figure 3.35: P & O Mppt Algorithm

In this study , two types of Mppt control strategy are designed . The purpose is to compare the output voltages . The second uses fuzzy logic inference(explained in appendix B) to derive voltage load in comparison to the first design . This determines uncertainties in the design based on a variation of conditions that may be involved in the motion of the vehicle and power transmitted to the batteries and motor from the solar panels.

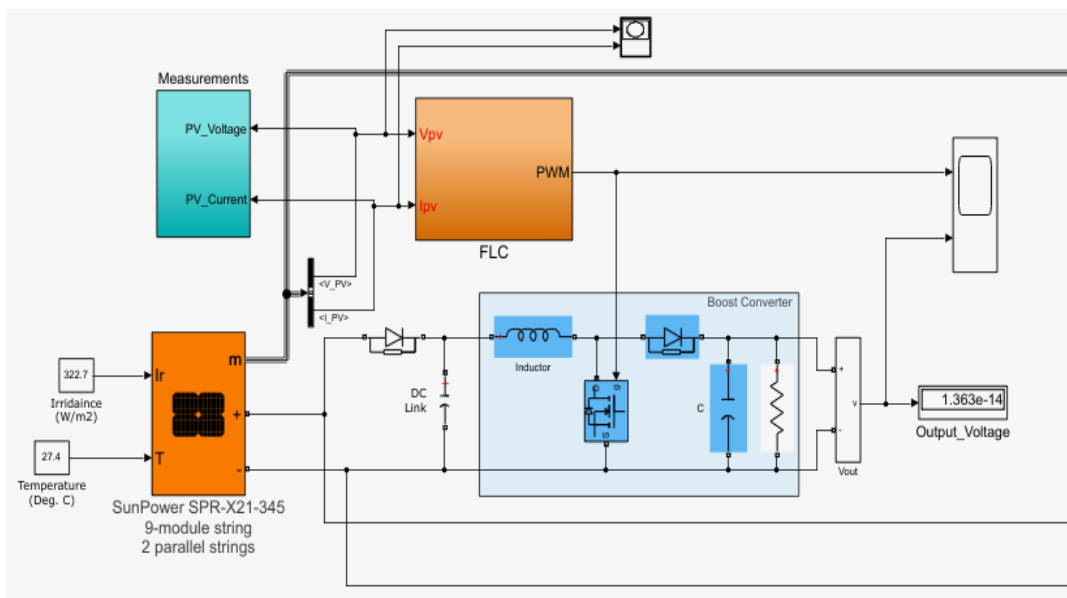


Figure 3.36: Fuzzy logic MPPT design model

3.9 Energy Management System

An Energy Storage System (ESS) is used to either store excess energy generated during high irradiances or maintain a consistent power supply during low irradiances. Traditional energy storage systems consisted of battery banks, but their high energy density results in a short lifespan when providing large bursts of power. A hybrid system that combines batteries with high-power-density sources, such as super capacitors, offers a solution. The battery in the system provides a constant energy source, while the supercapacitor supplies short bursts of power to the load. This combination of a battery and supercapacitor is known as a Stand-alone Photovoltaic Battery-Supercapacitor Hybrid Energy Storage System and is controlled by an energy management system to manage the flow of energy. The energy management system is depicted in the diagram below.

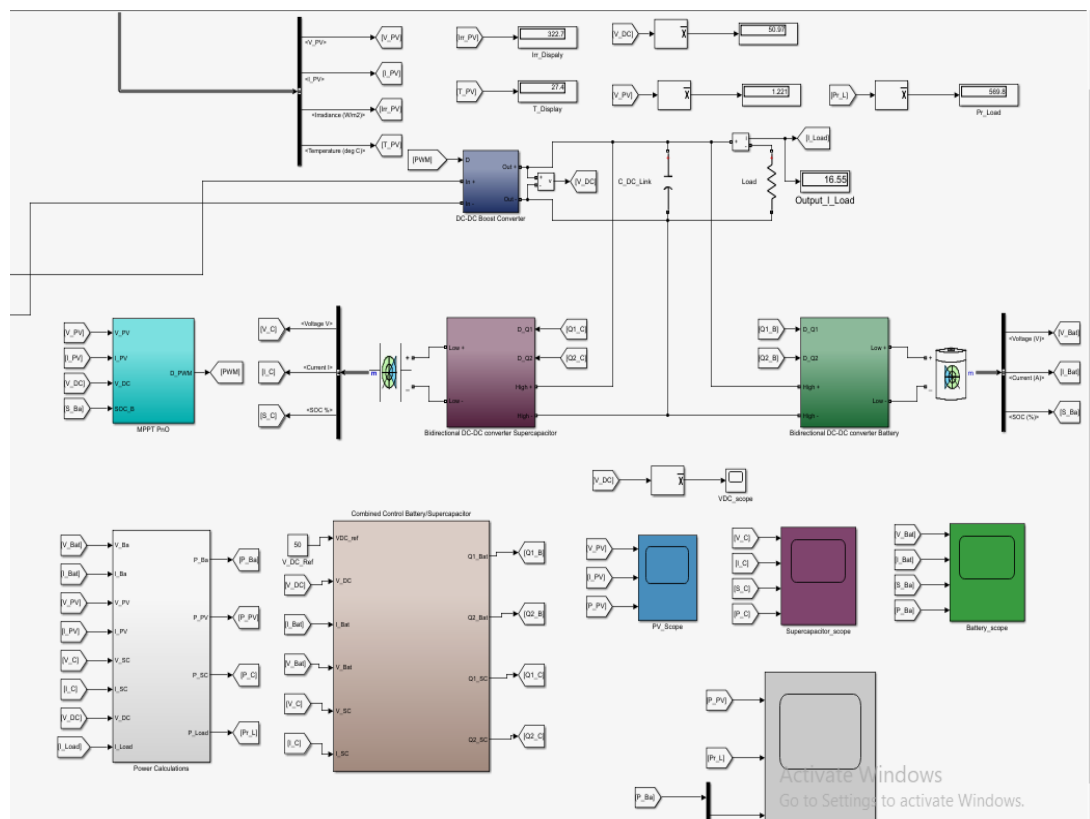


Figure 3.37: Simulink energy management system design

In the design model, the input comes from the solar irradiance of 349W/m² of average year energy in Nicosia, 2022, and an average temperature of 20.8 degrees Celsius. The module is based on the mathematical model output designed in the beginning of the chapter to select SunPower x-series panels based on their high efficiency.

As discussed, for the DC-DC converters, the PWM switches the boost converter which outputs the voltage load. The PWM is determined by the input of the battery SOC, the irradiance, temperature, and voltage load.

The bidirectional DC-DC boost converter is designed for a continuous cycle, in which the voltage load determined is multiplied by the load current to give the output load power. The output load power is transmitted to charge the supercapacitors and the lithium-ion battery.

3.10 Brake Design

The proposed design aims to conserve energy in electric vehicles by incorporating an Anti-lock Braking System (ABS) and a Regenerative Braking System (RBS) for maximum energy conversion during braking. The main goal of the design is to create an energy-saving braking system for use in electric vehicles. The design would incorporate an Anti-lock braking system (ABS) as well as a regenerative braking system (RBS) for maximum conversion of the energy generated into useful energy.

3.10.1 ABS Mathematical modelling using third vehicle dynamics / analysis.

The vehicle dynamics and mathematical models are assumed to simplify the process of deriving the braking system model. Instead of trying to derive a complex and difficult-to-obtain physical model of the electric vehicle, a third-party vehicle dynamics model is used. This allows for the differentiation of the partial differential equations governing the behavior of the brakes.

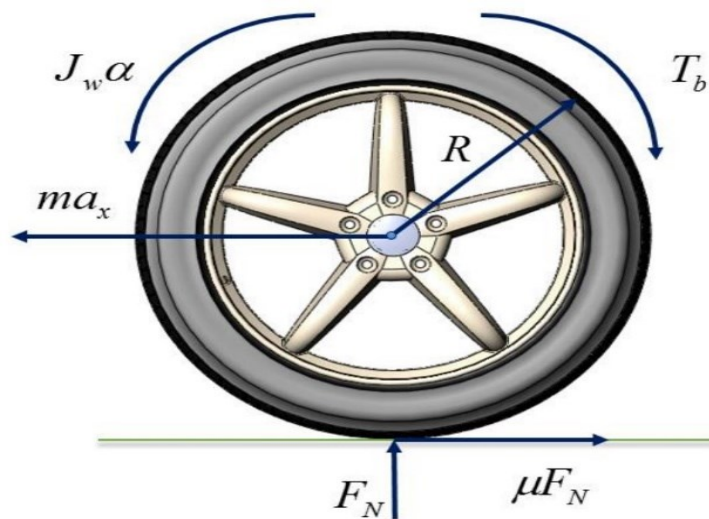


Figure 3.38: *Third vehicle model*

Assuming braking was applied to a wheel of a third electric car that was initially moving at linear speed $v(t_0)$ at time $t = t_0 = 0$

The electric vehicle decelerates slowly through stopping time $t = t_f = 0$ until it comes to a complete stop at final linear velocity $v(t_f) = 0$

The dynamic model equations of the system's motion in linear (x) and vertical (y) directions, respectively, are obtained by applying Newton's second law of motion to the free body diagram previously shown.

$$\sum f_x = m \times a_x \quad (36)$$

Since $a = \frac{dv}{dt}$, $a_x = \dot{v}_x$

$$\therefore \sum f_x = m \times \dot{v}_x \quad (37)$$

Since $\sum f_x = -\mu \times F_N$, $m \times \dot{v}_x = -\mu \times F_N$

$$\therefore \dot{v}_x = -\mu \times \frac{F_N}{m} \quad (38)$$

Where,

m = a percentage of the mass of all electric vehicles that are wheels

v_x = Vehicle's linear speed changes over time.

μ = frictional factor between the tire and the road

F_N = the wheel's normal road reaction force

a_x = time-varying linear deceleration of the vehicle

Since g =gravitational acceleration,

Given as follows is the wheels vertical equilibrium equation: $\sum f_y = 0$

Putting $F_N = m \times g$ into (37), $\dot{v}_x = -\mu \left(\frac{m \times g}{m} \right)$

$$\therefore \dot{v}_x = -\mu \times g \quad (39)$$

Newton's second law of motion application to electric vehicles deceleration, equilibrium equation is given as.

$$\sum M = J_w \times \alpha$$

Since $\alpha = \frac{d\omega}{dt}$, $\alpha = \dot{\omega}$

$$\therefore \sum M = J_w \times \dot{\omega} \quad (40)$$

Since $\sum M = \mu \times R \times F_N - T_b$, $J_w \times \dot{\omega} = \mu \times R \times F_N - T_b$

$$\therefore \dot{\omega} = \frac{\mu \times R \times F_N - T_b}{J_w} \quad (41)$$

Where,

α = amount of electric vehicles deceleration

T_b = applied brake force to the radius wheel

R = wheel radius

J_w = moment of inertia

ω = angular velocity of wheel

Changes in the proportionality between the vehicle's linear velocity and the wheels angular velocity are caused by the application of braking torque to the wheel, which results in a reduction in wheel velocity and the generation of a frictional force between the tyre and the road as the vehicle continues with its linear velocity. The result is the slip ratio, which is the difference in ratio between the electric vehicle's linear velocity and the wheels angular velocity.

$$\lambda = \frac{(v_x - \omega) \times R}{v_x} \quad (42)$$

Where,

λ = slip ratio

The aforementioned equation is differentiated with respect to time t,

$$\dot{\lambda} = \frac{\dot{v}_x(1-\lambda) - \dot{\omega} \times R}{v_x} \quad (43)$$

Substituting values of \dot{v}_x and $\dot{\omega}$,

$$\dot{\lambda} = \frac{\frac{-\mu \times F_N}{m} (1 - \lambda) - \left[\frac{\mu \times R \times F_N - T_b}{J_w} \right] \times R}{v_x}$$

$$\dot{\lambda} = \frac{-\mu \times F_N}{v_x} \left[\frac{(1-\lambda)}{m} + \frac{R^2}{J_w} \right] + \frac{R}{J_w \times v_x} \times T_b \quad (44)$$

The primary variables to be adjusted are the stopping distance, the vehicle's linear velocity, and the slip ratio because the ABS directs the braking operation by controlling the input torque produced by the actuator in the hydraulic system.

Using Burckhardt friction model to model tyre forces,

$$\mu(\lambda, v_x) = [C_1(1 - e^{-C_2\lambda}) - C_3\lambda]e^{-C_4v_x} \quad (45)$$

Where,

C_1 = the friction curve's maximum value

C_2 = shape of the friction curve

C_3 = Friction curve discrepancy between maximum value and value at 1

C_4 = Value of the wetness characteristic

At a specific magnitude of the wheel slip ratio, the effective coefficient of friction between the tire and the road reaches its maximum value; however, this value varies depending on the type of road.

Table 3.7: Variation in the ratio of wheel slip to the coefficient of traction on the road

Surface Types	C_1	C_2	C_3	C_4
Dry Asphalt	1.2801	23.99	0.52	0.03
Wet Asphalt	0.857	33.822	0.347	0.03
Dry Concrete	1.1973	25.168	0.5373	0.03
Snow	0.1946	94.129	0.0646	0.03

Substituting the information in the table above into and the Burckhardt friction model, the graph below shows the variation between the wheel slip ratio and the road coefficient of friction.

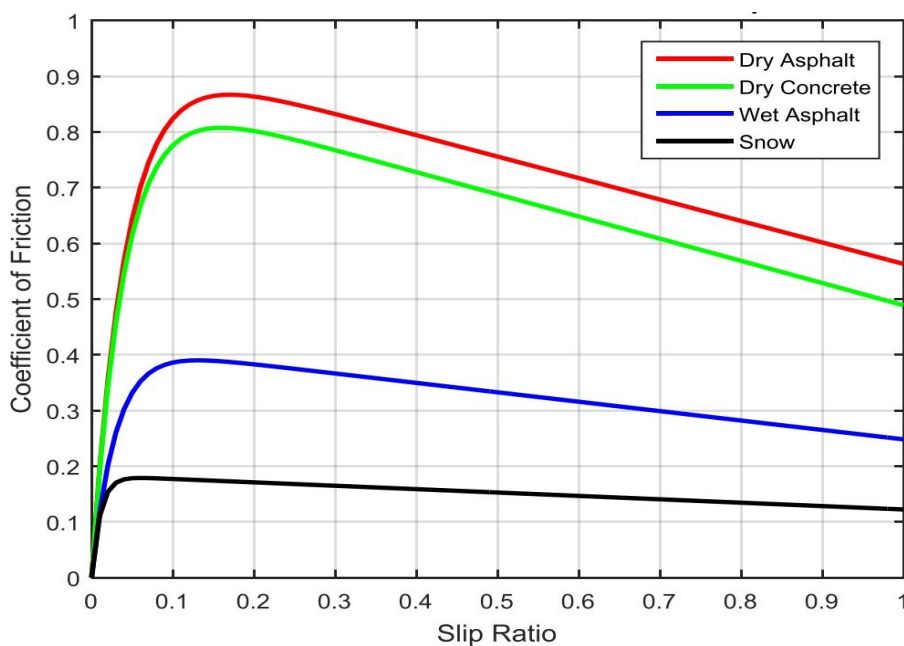


Figure 3.39: Road friction coefficient versus wheel slip ratio (Zhang & Cai, 2018)

Based on the simulation above, the objective of the ABS controller is to use the block diagram below to control the wheel slip ratio (λ) to fix on the estimated value of 0.1 to obtain the maximum frictional coefficient (μ) for different types of road surfaces;

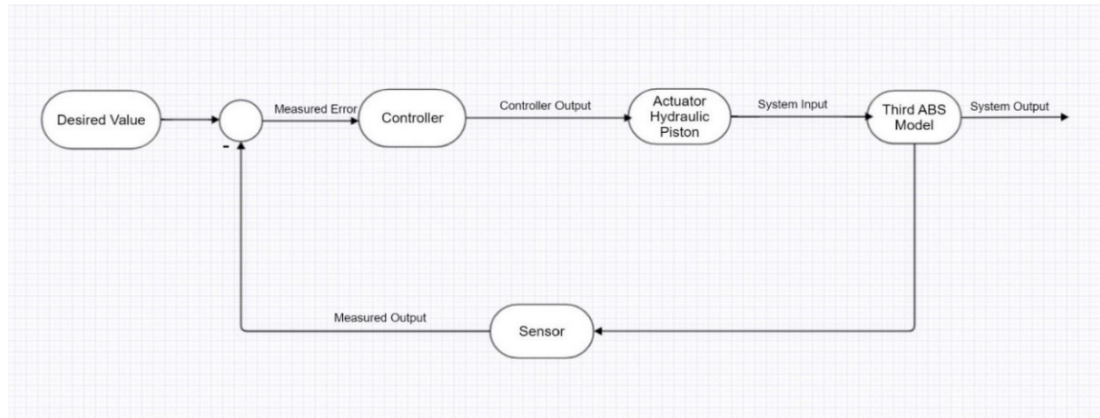


Figure 3.40: *System for Feedback Control in ABS Block Diagram*

The sensor continuously monitors and measures the slip ratio, which is the system's output, and feeds that information back to the system to generate the error signal by comparing it to the desired slip ratio value, which is the system's input. A Proportional-Integral-Derivative (PID) controller or discrete time controller receives this error signal and, depending on the error's sign, assigns the output. The PID controller's output response, which is composed of three stages—proportional, integral, and derivative terms—results from processing the error signal.

As shown below, the controller's transfer function;

$$G(s) = K_p + \frac{K_I}{s} + K_D s \quad (46)$$

Where,

K_p = gain for the proportional term

K_I = gain for the integral term

K_D = gain for the derivative term

The main parameters of the ABS are adjusted by a discrete-time controller by controlling the slip ratio because the ABS is a non-linear feedback model.

The difference equation describes a first-order discrete-time system.

$$y_{k+1} + ay_k = bu_k \quad (47)$$

The difference equation gives a description of a second-order discrete-time system,

$$y_{k+2} + a_1 y_{k+1} + a_2 y_k = b_1 u_{k+1} + b_2 u_k \quad (48)$$

Where,

y_k = discrete-time system output

u_k = discrete-time system input

K = constant

a_1, a_2, a_3 = controller gain

The desired slip ratio is considered when determining the appropriate values of the gains using the time discrete Simulink blocks tool.

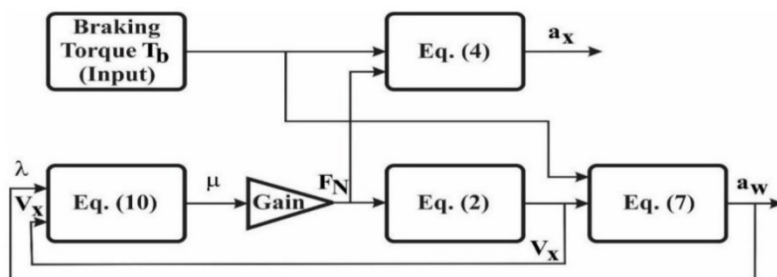


Figure 3.41: Simulation of ABS governing equations.

The dynamic model equations derived in (38), (39), (42), and are then applied to the simulation of the anti-lock braking system described above (45). Two subgroups are used to reduce interference and streamline the simulation.

The slip ratio λ described in (43) is simulated below.

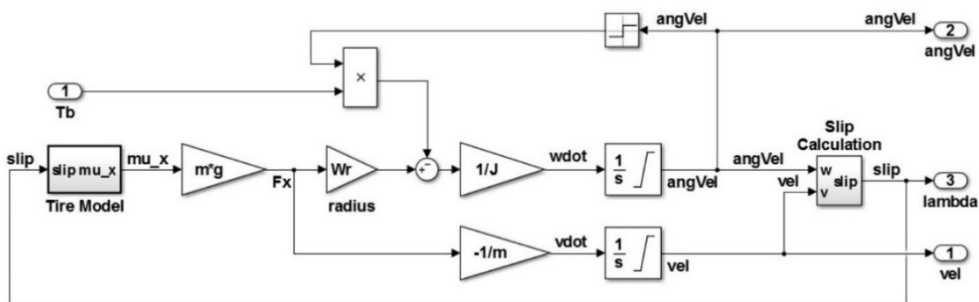


Figure 3.42: Calculation of Slip Ratio Subgroup

The road frictional coefficient μ described in (45) is simulated below.

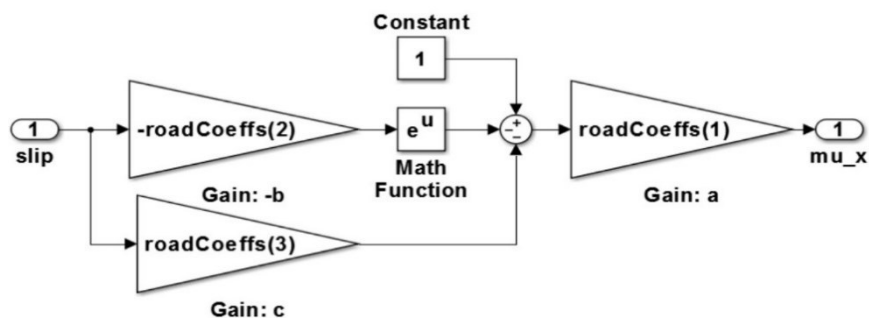


Figure 3.43: Coefficient of friction Computation Subgroup

Given as a function of the braking constant torques T_b and u , the total affected torque used to stop the wheels' rotation is as follows:

$$T = u + T_b \quad (49)$$

Where,

T = total effected torque to stop wheel rotation

u = control manipulating variable

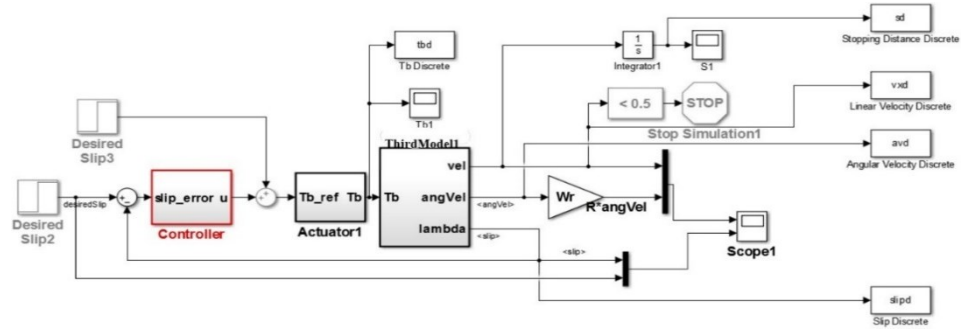


Figure 3.44: Model for the ABS Feedback Control system

3.10.2 Parallel RBS Mathematical modelling

Optimal brake torque requirements, anti-lock braking system and regenerative braking system braking torques, and allocation controls are all considered.

The electric motor provides the regenerative braking torque necessary for the regenerative braking system to function while decelerating. The electric motor powering the electric car under consideration is a three-phase permanent magnet brushless DC motor.

The motor torque is set as a first order reaction regarding electric vehicle dynamics.

$$T_M + (\tau_M + \tau_E)T_M' = T_{MR} \quad (50)$$

Where,

τ_M = Mechanical time constant

τ_E = Electric time constant

T_M = Actual value of motor torque

T_{MR} = Motor reference torque

The axle drive unit and differential distribute the electric motor's output torque during the regenerative deceleration process. The torque for regenerative braking on a driven wheel is therefore given as,

$$T_{br} = T_M \cdot \frac{i_a i_d}{2} \quad (51)$$

Where,

i_a = ratio of the axle's drive

i_d = the transmission's gear ratio

The braking slip ratio can be defined as,

$$\dot{\omega} I_w = \mu F_N R + \frac{C_D A v_x^2 R}{21.15} - T_b \quad (52)$$

$$m_o \dot{v}_x = \frac{C_D A v_x^2}{21.15 v_x} + \mu F_N \quad (53)$$

Where,

I_w = Wheel's inertia

A = Frontal Area

m_o = Wheel's vertical load

The ideal braking torque can be obtained by combining (42), (52), and (53), and this quickly drives the wheel slip ratio to its ideal value.

$$T_{bo} = \frac{\dot{\mu}I_w}{r_o} \left[\left(\lambda - \frac{v_x - \omega R}{v_x} \right) + \left(\frac{m_o R^2}{I_w} + \frac{C_D A v_x^2 R^2}{21.15 v_x I_w} + \frac{\omega R}{v_x} \right) \right] \quad (54)$$

Where,

T_{bo} = Optimal braking torque of wheel

Due to its precise control and quick response, the motor torque is desired at high frequency in dynamics control. Due to the existing lag between pressure variation and brake line valve action, it is impossible to adjust the hydraulic braking force accurately and quickly. As a result, the desired high frequency brake torque cannot be provided by the hydraulic brake.

The optimal brake torque (T_{bo}) is divided into two parts based on the dynamics of the hydraulic and regenerative brakes that were examined.

$$T_{bo} = T_{bd} + T_{bs} \quad (55)$$

Where,

T_{bd} = Dynamic part of braking torque

T_{bs} = Steady part of braking torque

The necessary, T_{bs} is calculated based on the wheel-road adhesion that maintains the slip ratio in equilibrium. As long as the brake torque remains constant and is equal to T_{bs} , then;

$$\dot{\lambda} = \frac{v_x(1-\lambda) - \dot{\omega} \times R}{v_x} = 0 \quad (56)$$

Combining first two equations from earlier and most recent two,

$$T_{bs} = \dot{v}_x m_o R + \frac{C_D A v_x^2 R}{21.15} + \frac{v_x I_w}{R} (1 - \lambda) \quad (57)$$

To provide the dynamically demanding brake torque, T_{bd} is required as slip ratio deviates from the ideal slip ratio, λ_o . It works in conjunction with T_{bs} to capacitively adjust the total torque to the ideal value and the slip ratio to the ideal value. As a result, the necessary dynamical braking torque can be calculated by combining the last four equations as follows:

$$T_{bd} = \frac{\lambda^2 + \lambda(\Delta - 1)}{1 - \lambda} \cdot \frac{v_x I_w}{R} \quad (58)$$

Where ideal slip ratio $\lambda_o = \frac{\Delta \lambda}{1 - \lambda}$,

Δ = Correction factor of slip ratio

Two parameters are suggested to assess the braking energy efficiency performed by the ABS and RBS brakes to enhance the vehicle's energy efficiency during safety-critical driving situations;

ε_s = contribution percentage to the efficiency of steady braking

ε_d = ratio of the dynamic braking system's energy efficiency

It is clear that, E-bs. given the energy consumption of the ABS while braking, optimal brake energy consumption (E-bo), and steady brake energy consumption (E-bs). The contribution ratio to steady braking energy efficiency,-s. during braking is therefore given as,

$$\varepsilon_s = \frac{E_{bs}}{E_{bo}} = \frac{E_{fw_brk} + E_{rw_brk} + E_{mot_brk}}{E_{fw_brk} + E_{rw_brk} + E_{mot_brk} + E_{regen}} \quad (59)$$

$$\therefore \varepsilon_s = \frac{\int_{P_{regen} < 0} (F_{fw_brk} + F_{rw_brk} + F_{mot_brk}) u dt}{\int_{P_{regen} < 0} (F_{fw_brk} + F_{rw_brk} + F_{mot_brk}) u dt + \int_{P_{regen} < 0} U_{bat} I_{bat} dt} \quad (60)$$

Where,

E_{fw_brk} = energy use by the front wheel while braking

E_{rw_brk} = energy use by the rear wheel while braking

E_{mot_brk} = motor's energy usage while braking

E_{regen} = consumption of regenerative energy while braking

$P_{regen} < 0$ = a sign that the motor acts as a generator when the vehicle is braking efficiently

U_{bat} = Voltage during braking

I_{bat} = Battery current during braking

F_{fw_brk} = force of the front wheel's brakes

F_{rw_brk} = rear wheel braking power

F_{mot_brk} = Motor braking force

It is clear that E-bd. when considering the energy consumption of the ABS during braking, the energy consumption of the optimal brake, and the energy consumption of the dynamic brake. Consequently, the contribution ratio to the energy efficiency of dynamic braking,-d. during braking is given as,

$$\varepsilon_d = \frac{E_{bd}}{E_{bo}} = \frac{E_{mot_brk} + E_{regen}}{E_{fw_brk} + E_{rw_brk} + E_{mot_brk} + E_{regen}} \quad (61)$$

$$\therefore \varepsilon_d = \frac{\int_{P_{regen} < 0} F_{mot_brk} u dt + \int_{P_{regen} < 0} U_{bat} I_{bat} dt}{\int_{P_{regen} < 0} (F_{fw_brk} + F_{rw_brk} + F_{mot_brk}) u dt + \int_{P_{regen} < 0} U_{bat} I_{bat} dt} \quad (62)$$

The difference in the vehicle's energy consumption between ABS and RBS can be seen by analysing the energy efficiency of regenerative braking with the help of the parameters, ε_s . and ε_d . The percentage of regenerative steady braking energy efficiency is described by parameter, ε_s , whereas the percentage of regenerative dynamic braking energy efficiency is described by parameter ε_d .

Combining from $T_{bo} = T_{bd} + T_{bs}$ to the most recent equation, the required steady brake torque which is to be supplied by the ABS can be obtained by;

$$T_{b_fric} = T_{bs}\varepsilon_s + T_{bd}(1 - \varepsilon_d) \quad (63)$$

$$\therefore T_{b_fric} = \frac{v_x I_w}{R} (1 - \lambda)\varepsilon_s + v_x m_o R \varepsilon_s + \frac{C_D A v_x^2 R \varepsilon_s}{21.15} + \frac{v_x I_w (1 - \varepsilon_d)}{R} \cdot \frac{\lambda^2 + (\Delta - 1)\lambda}{1 - \lambda} \quad (64)$$

Combining from $T_{bo} = T_{bd} + T_{bs}$ to $\therefore T_{b_fric}$ equation, the following methods can be used to obtain the intended electric motor's regenerative braking torque:

$$T_{b_regen} = T_{bs}(1 - \varepsilon_s) + T_{bd}\varepsilon_d \quad (65)$$

$$\therefore T_{b_regen} = \frac{v_x I_w}{R} (1 - \lambda)(1 - \varepsilon_s) + v_x m_o R (1 - \varepsilon_s) + \frac{C_D A v_x^2 R}{21.15} (1 - \varepsilon_s) + \frac{v_x I_w \varepsilon_d}{R} \cdot \frac{\lambda^2 + (\Delta - 1)\lambda}{1 - \lambda} \quad (66)$$

3.10.3 Novel Regenerative Braking Control Strategy

The novel serial regenerative braking control strategy being proposed for electric vehicles involves an affixing an ultrasonic sensor to the front of the electric vehicle to detect obstructions that could cause collisions. An ultrasonic sensor is one that measures distance by using ultrasonic sound waves. Ultrasonic pulses are periodically emitted by the sensor head, which then picks up the waves reflected from the target. By measuring the interval between the pulse's emission and reception, the sensor can then deduce the target's distance. The calculation of the object's distance from the sensor is shown below.

$$L = \frac{1}{2} \times T \times C \quad (67)$$

Where,

L = Object distance

T = Time between pulse emission and reception

C = Speed of sound in air

The value is multiplied by $\frac{1}{2}$ because T is the total time of pulse travel.

elapsed time between sending and receiving a pulse.

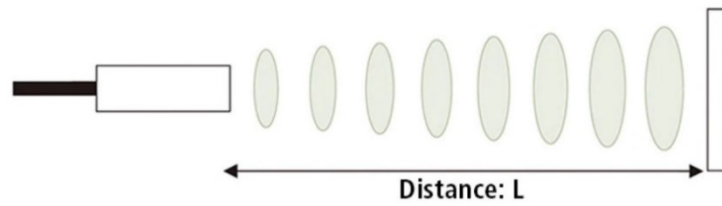


Figure 3.45: Distance covered by ultrasonic pulse [Source: maxbotix.com]



Figure 3.46: Ultrasonic Sensor Operation (Transmission) [Source: maxbotix.com]



Figure 3.47: Ultrasonic Sensor Operation (Receiving) [Source: maxbotix.com]

Texas Instruments' TIDA-00151 reference design, which includes the PGA450-Q1 IC, a system-on-chip (SoC) sensor interface IC for automotive ultrasonic sensors, will be used as the ultrasonic sensor. For the purpose of determining the distance between the transducer and objects as well as signal conditioning and processing for the entire transducer echo signal. The 8051 cores in the MCU and the program memory enable complete configuration for the intended end use. The other systems in the vehicle are connected to this subsystem via a serial Local Interconnection Network (LIN) interface.

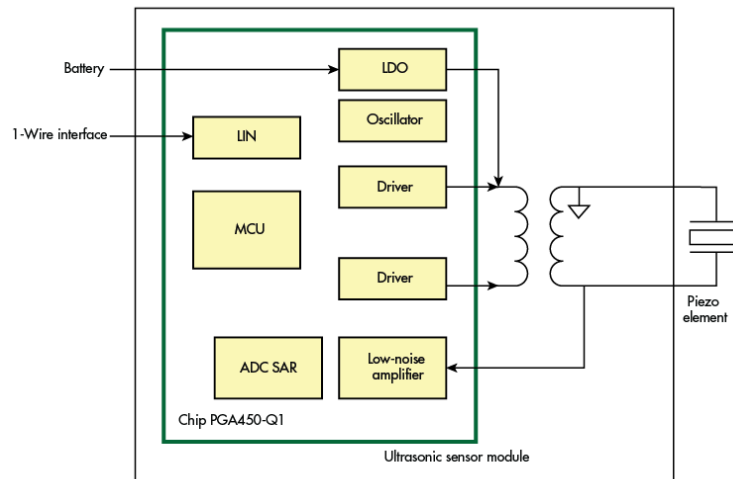


Figure 3.48: TIDA-00151 Ultrasonic sensor circuit diagram [Source: [electronicdesign.com](http://www.electronicdesign.com)]

The object distance to the electric vehicle is then fed to the electric vehicles Overall Control Unit (OCU) to;

1. Determine the braking torque required to bring the electric vehicle to rest within the specified distance.
2. Determine if the already generated rotary kinetic energy of the RBS can generate the required braking torque.
3. Select the RBS to be used for braking if yes.
4. Otherwise apply the ABS to bring about a halt or deceleration of the vehicles motion while preventing its skidding and yawing.
5. To account for cases where direct hard braking is required by the driver to bring the vehicle to rest as soon as possible at his/her discretion, the OCU immediately activates the ABS to bring about this halt by receiving input from a rotary potentiometer installed at the brake pedal. The rotary-type potentiometer senses when the brake pedal is being pressed with more pressure that would give an equivalent brake pedal inclination angle range already calculated and preset by the manufacturer.

To measure angular displacement, rotary-type potentiometers are used. The object whose angular displacement is to be measured is coupled to the shaft of the sensor's rotary knob. The potentiometer's knob can be turned to adjust the electrical resistance between two nodes' leads. It is recommended to use a single turn rotary-type with the circuit diagram below to measure rotations up to one revolution.

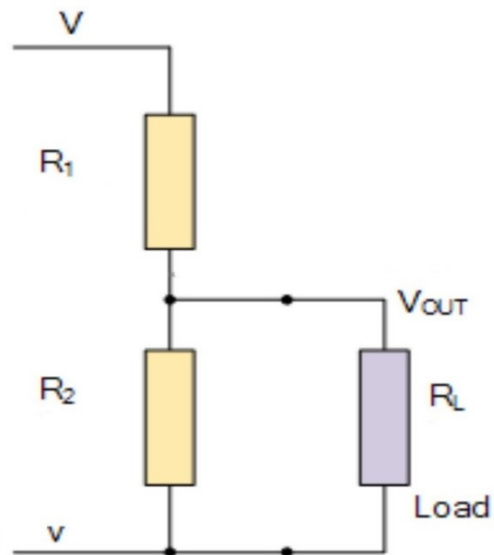


Figure 3.49 : Single turn, rotary-type potentiometer circuit diagram

$$V_{OUT} = \frac{xV_s}{1 + x(1-x)\frac{R_P}{R_L}} \quad (68)$$

$$R_P = R_1 + R_2 \quad (69)$$

$$R_1 = (1 - x)R_P \quad (70)$$

$$R_2 = xR_P \quad (71)$$

Where,

V_{OUT} = Output voltage

x = Slider position

V_s = Supply voltage

R_P = Potentiometer resistance

R_L = Measuring device resistance

The measured angle is obtained by multiplying change in slider position by potentiometer measurement range (θ)

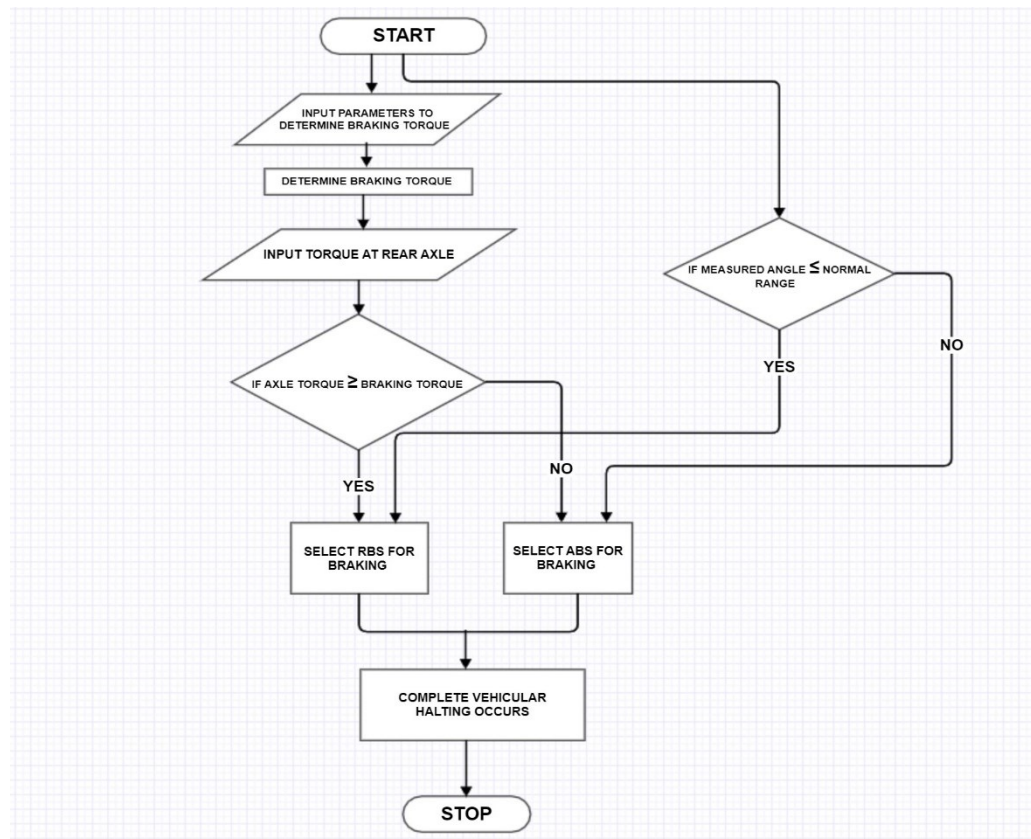


Figure 3.50: OCU flowchart

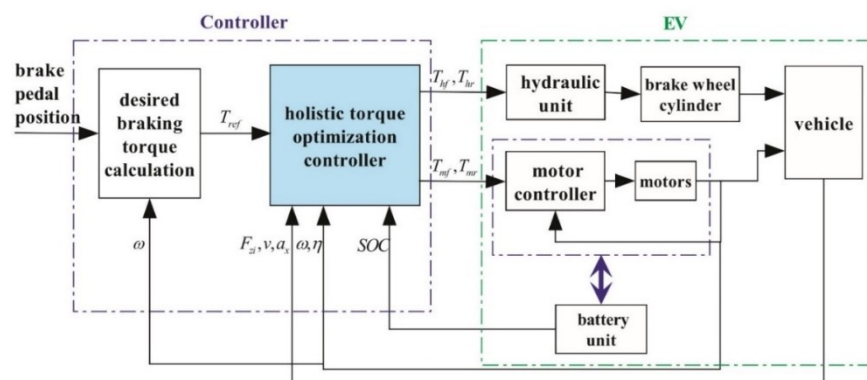


Figure 3.51: OCU Block Diagram

3.10.4 Mathematical Determination of Required Braking Torque

The amount of braking force needed to bring the electric vehicle to rest or in other cases, reduce the velocity of the electric vehicle to a desired amount is an important factor to be obtained by the braking system of the electric vehicle. This novel regenerative system uses the information (distance between the electric vehicle's front and the obstacle to be avoided) gotten from the ultrasonic sensor mounted at the electric vehicles front, as a key component alongside others, to determine how much force should be provided by the system to safely avoid

colliding with whatever obstacles lie in wait, by bringing the electric vehicle to rest before it even reaches said obstacles. The other variables needed for this determination are;

1. The electric car's overall weight (m)
2. the vehicle's speed at the moment (v)

The electric vehicle's speedometer provides the vehicle's velocity, which is then fed to a microprocessor, which converts it using the formula below from the Km/h displayed on the digital speedometer to the m/s required to calculate the braking torque.

$$\text{Velocity in } m/s = \text{Velocity in } Km/h \times 0.2778$$

3. The radius of the tyre (r)
4. The Force which the moving electric vehicle produces (F)

Such that;

$$F = ma \tag{72}$$

$$a = \frac{v^2}{2L} \tag{73}$$

a = Deceleration of Electric vehicle

L = Distance from electric vehicle to obstacle

5. The braking torque needed to bring the electric vehicle to rest (T)

$$T = F \times r \tag{74}$$

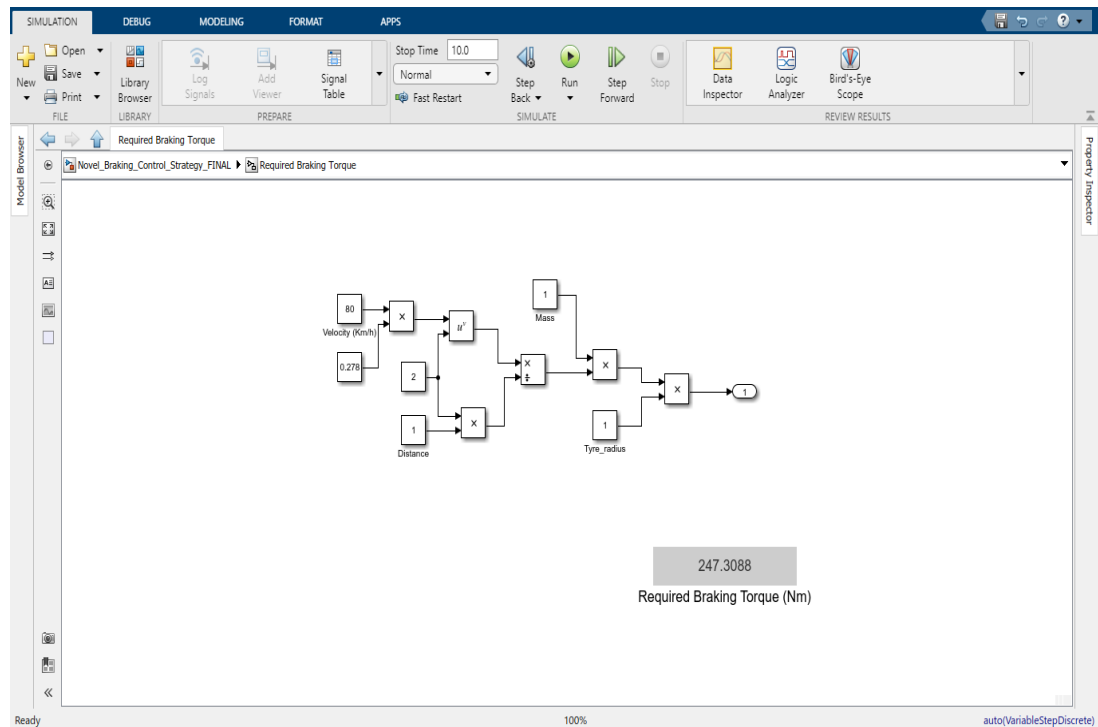


Figure 3.52: *MATLAB SIMULINK Simulation of required braking torque.*

3.10.5 Mathematical Determination of Torque produced by vehicle.

The radius of the wheels, the mass of the electric vehicle, and other factors can all be used to calculate the torque that the electric motor-powered electric vehicle can produce at any given time.

$$T_{bs} = v_x m_o R + \frac{C_D A v_x^2 R}{21.15} + \frac{v_x I_w}{R} (1 - \lambda) \quad (75)$$

Such that;

T_{bs} = Braking Torque produced by RBS

C_D = Coefficient of air resistance

I_w = Moment of inertia of tyre

A = Frontal Area of Electric vehicle

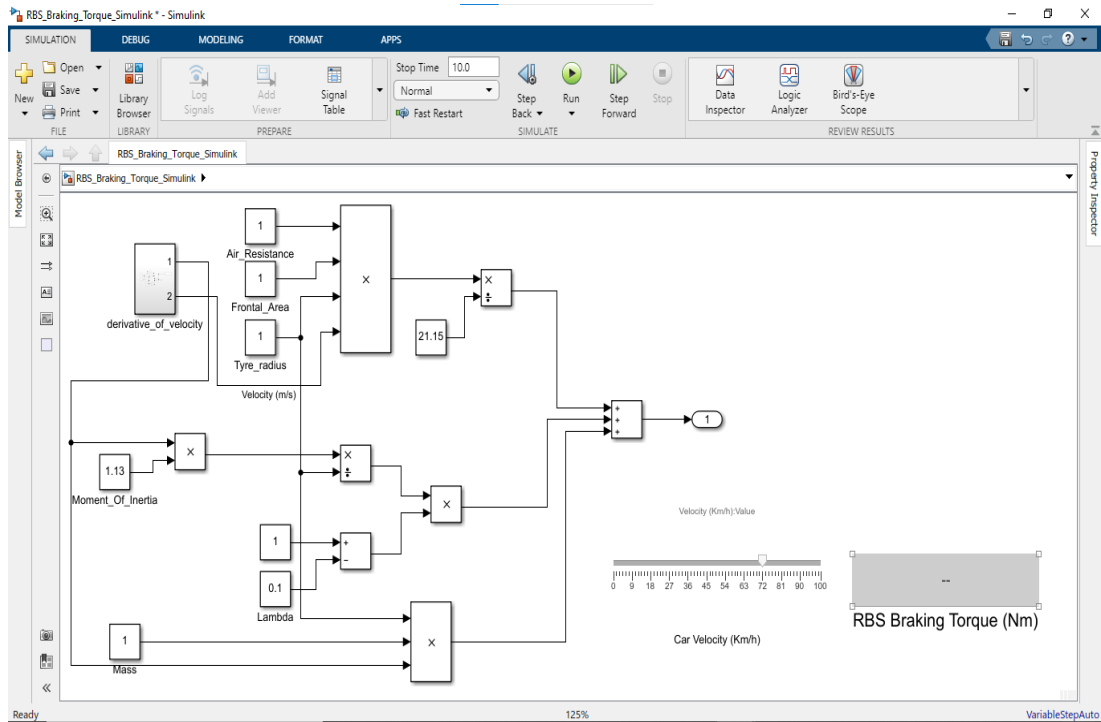


Figure 3.53: *MATLAB SIMULINK Simulation of RBS Braking Torque*

3.10.6 Mathematical Modelling of Novel Regenerative Braking Control Strategy

Implementing the models developed above as subsystems, the designed system is simulated and tested on MATLAB using a SIMULINK model, such that the Lamps labelled “Range Indicator” and “Torque Indicator” represent the systems outcome in terms of choosing either the Anti-lock braking system or the Regenerative braking system to bring about a speed reduction or halt of the moving electric vehicle. The following table shows what the Lamp colours indicate.

Table 3.8: *Table showing meaning of Lamp colours.*

Range Indicator	Torque Indicator	Braking System to be Used
Red	Green	Regenerative Braking System
Green	Red	Anti-lock Braking System
Red	Red	Anti-lock Braking System

The brake pedal angle of operation is represented by a rotary switch that acts as the system's potentiometer output. The position of the pointer indicates the brake pedal's current position (angle) as determined by the potentiometer. The system also includes movable sliders to simulate the current speed of the electric car as determined by the speedometer. Boolean operators, switches, input, and output ports,

if blocks, and if action subsystems are used in the control action to produce the desired results. These components are programmed and connected via wires.

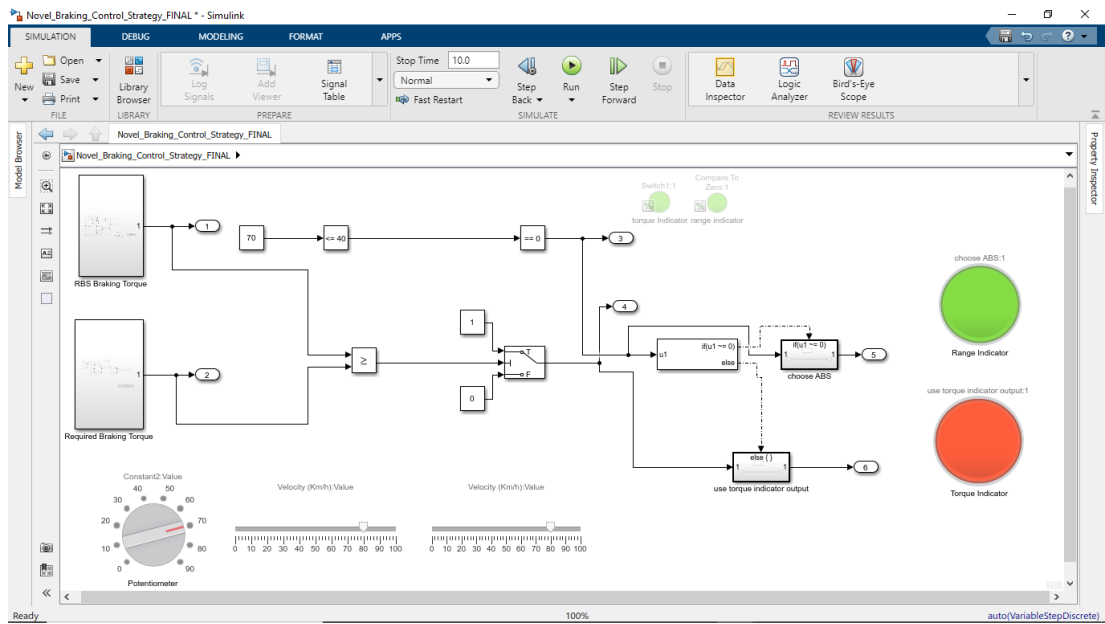


Figure 3.54: MATLAB SIMULINK Simulation of Novel Control Strategy (OCU)

CHAPTER IV

Results and Discussion

In verification of the design analysis in the previous chapter, carrying out a survey analysis of energy potential in north Cyprus , determining the load profile based on the survey , and modelling the forces about the proposed designed solar electric vehicle. The following results are derived from the simulation and survey done in chapter three.

4.1 Forces exerted on the SEV Simulink Model Result

The proposed design speed, hour of usage and total area coverage are 20km/h, 7 hours and 15km range distance for the solar electric vehicle. This is just a basic of what this thesis intends to achieve based on the survey done. Further improvements can be made based on imported survey analysis and other assumptions for the designed vehicle model.

Therefore, the following are the results of the forces acting on the solar electric vehicle based on the designed model ana data provided in chapter 3.

The figure below is a complete model of the forces acting on the designed electric model based on the technical data from the tesla model S and the lightyear0 solar vehicle model.

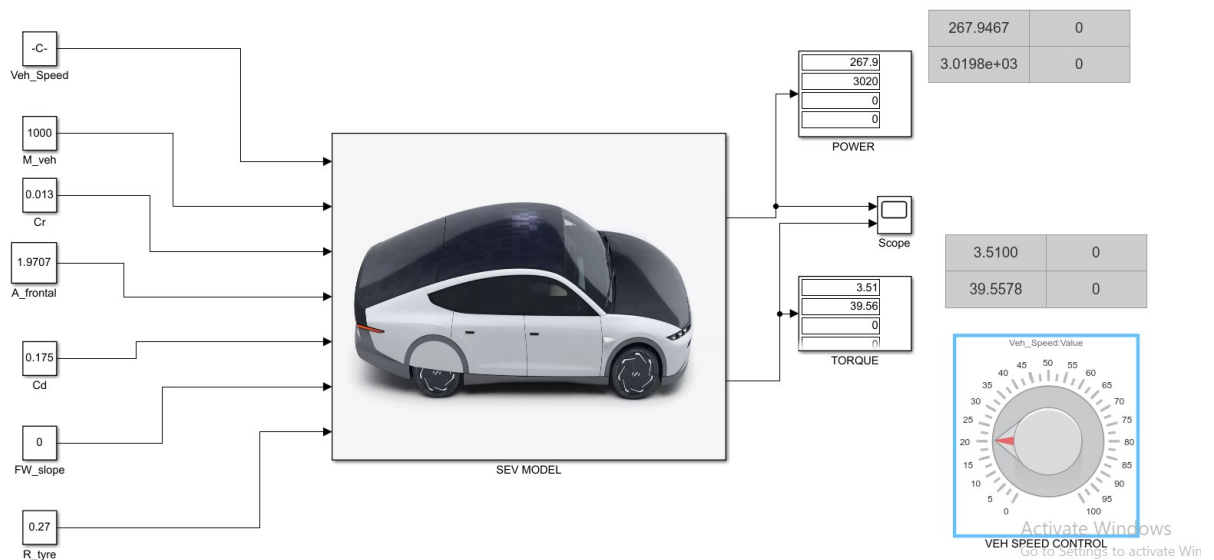


Figure 4.1: Simulink model for the forces about the SEV

Based on the Simulink modelling , the following are the input data in table 4.1 below.

Table 4.1 Technical Input Data for SEV Simulink model

S/NO	INPUTS	VALUE
1	Vehicle speed	20km/h
2	Vehicle Mass	1000Kg
3	Frontal Area	1.9707m ²
4	Tire radius	0.27°
5	Air resistance C_d	0.175
6	Road friction coefficient C_r	0.013
7	Slope force	0

From the modeling the result of the forces acting on the SEV based on the Simulink model is illustrated in the figure below. The power output and torque output from the 20km/h velocity is 3.02Kw and 40Nm respectively.

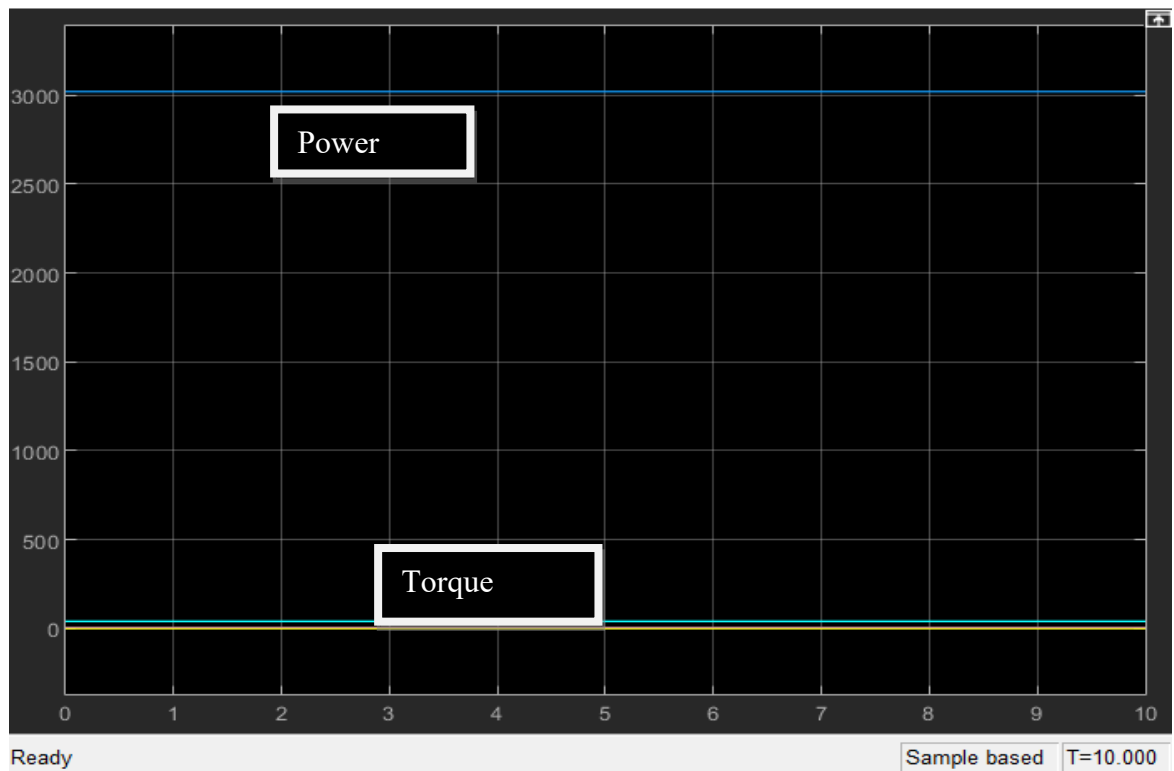


Figure 4.2 Simulink result of SEV required forces.

The blue line indicates power while the green line indicates torque. These are the necessary outputs to power the SEV based on the input data at a constant velocity of 20km/h. The energy required for about 7hours would be 21.14kWh.

4. 2 Energy Management System for Batteries

The temperature and irradiance of Nicosia in 2022 were taken from the battery energy management system design and input into the Simulink model design, as shown in figure 4.2 below.

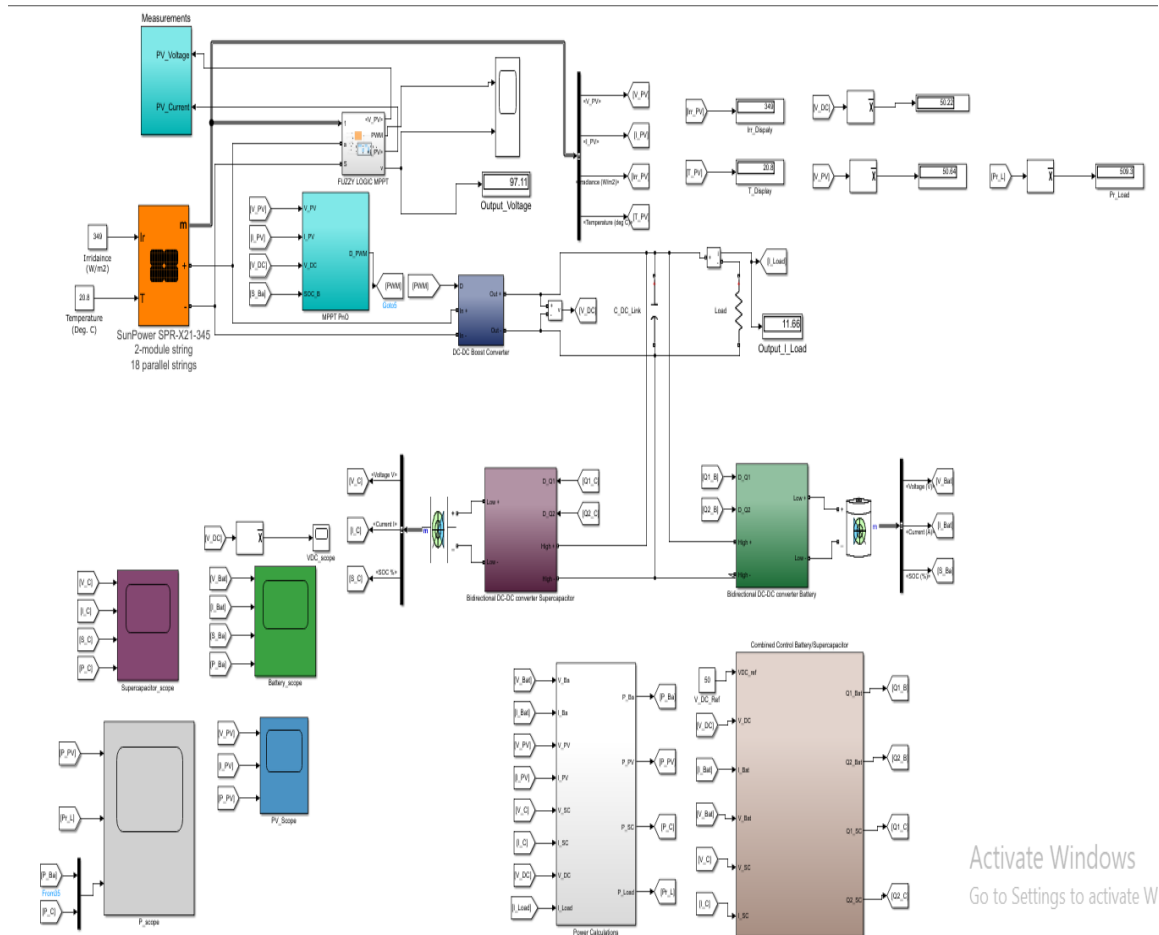


Figure 4.3: Battery Energy Management system

Based on the input data, the average irradiance value for the year, irradiance value for January representing the simulation for energy management system expected in the winter , and the irradiance value for July for the summer energy management system simulation are all simulated to present the expected energy in each of the seasons and the overall energy gotten for the year through the simulation model.

The figures below are results of the simulation for each season and the overall energy for the year. For the average irradiance of the year 2022, the value is 349w/m2 with a temperature of 20.8 degrees Celsius. Figure 4.4 illustrates the overall average power of the average irradiance input.

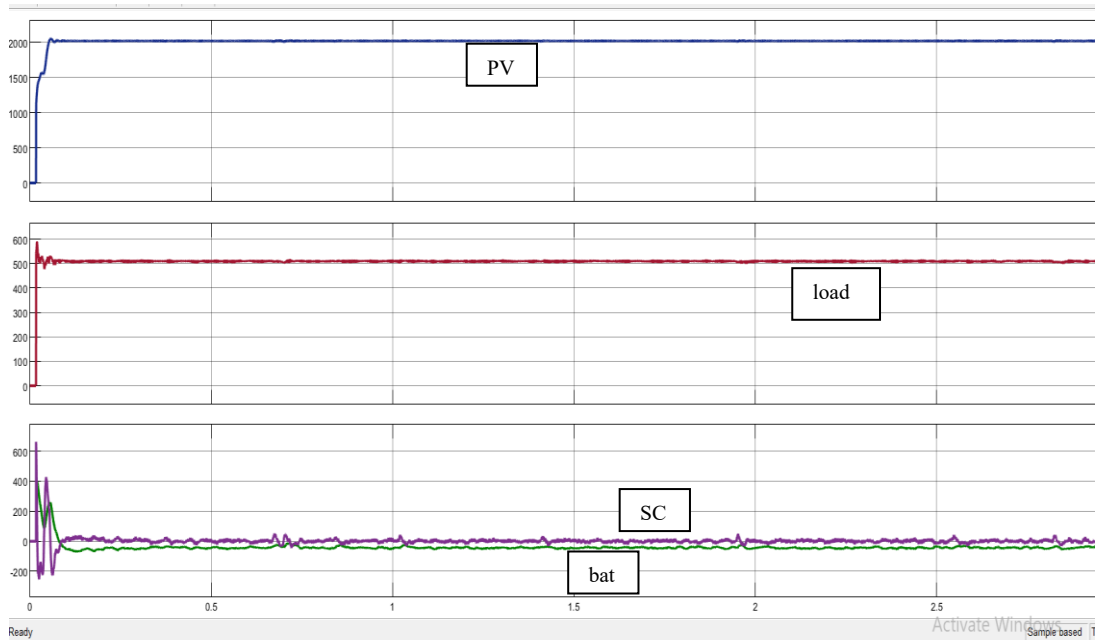


Figure 4.4 Overall Power simulation result from the Average irradiance input

From the figure above, the first graph shows the output power of the PV stabilizing at an output of 2023kW. The third graph is for the storage with the purple line for the energy burst from the supercapacitor and the green line for the battery output power. The supplied load power is 509.3kW as seen in the second phase graph.

Meanwhile for the summer season, with an irradiance value of 473w/m² for the hottest summer month of July, and a temperature of 29.2, the power output is illustrated in figure 4.5 below.

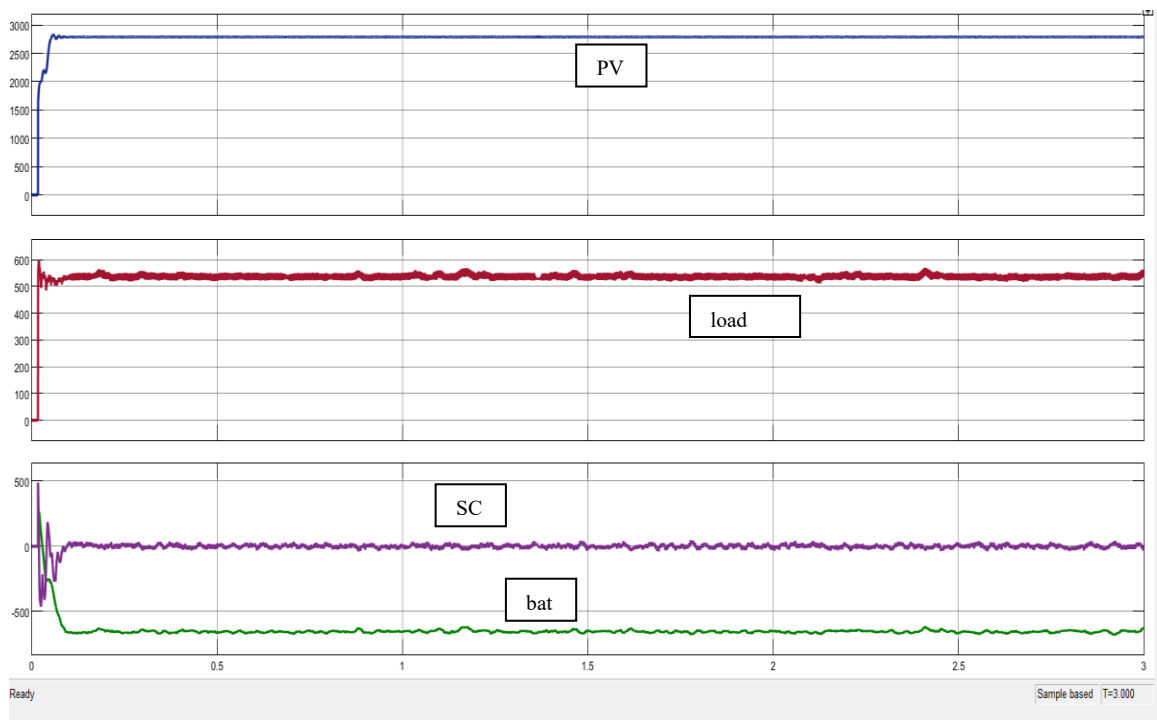


Figure 4.5: Summer Power output

The supplied load is 542.5kW, from an input PV power of 2788kW, while the storage supplied power from supercapacitor and battery are -20.6kW and -632.6kW respectively as seen from their individual graphs.

Finally for the winter month, using the coldest month of January as reference , with an irradiance value of 212w/m² and a temperature of 14.7. Figure 4.6 below is an illustration graph of the power outputs.

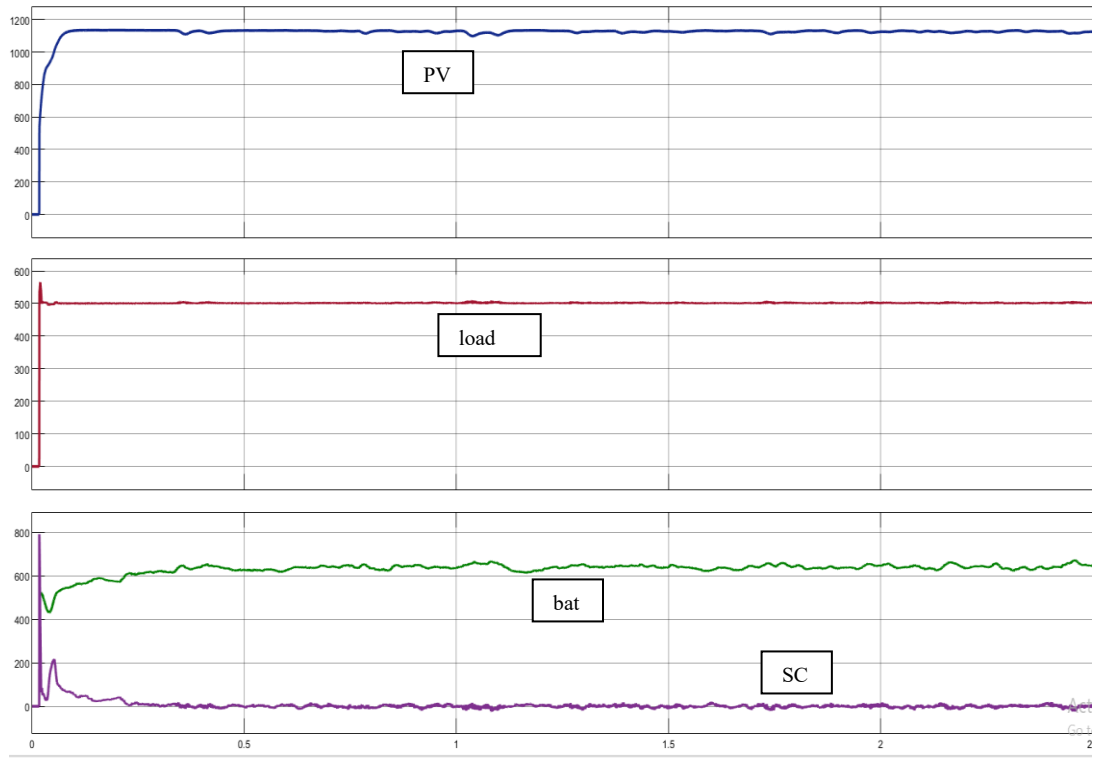


Figure 4.6: Winter power output

In the winter simulation, with less irradiance for PV power supply of 1127kW, the output load power is 501.6kW, with supercapacitor and battery storage output power as -1.099kW and 649.1kW.

The power outputs are illustrated in table 4.2 below. It should be noted that the output powers from the storage when shown negative means the storage is releasing power to the load while charging from the input of the PV.

Table 4.2: Simulink Energy Management Output Power Design

S/NO	DATA	OVERALL AVERAGE	SUMMER	WINTER
1	Irradiance value	349w/m ²	473w/m ²	212w/m ²
2	Temperature value	20.8	29.2	14.7
3	PV Power	2023kW	2788kW	1126kW

4	Battery Power	-48.77kW	-632.6kW	649.1kW
5	Supercapacitor Power	7.89kW	-20.6kW	-1.099kW
6	Load Power	509.3kW	542.5kW	501.6kW

4.3 Braking System Simulink Model Result

To verify the proposed control strategy alongside its effectiveness in bringing about speed reduction to avoid collision and derivation of the converted torque to aid the SEV for longer range coverage, simulations and analysis in MATLAB Simulink software environment were conducted using parameters given in the table below.

Varying road conditions across dry asphalt, wet asphalt, dry concrete, and snow to obtain different slip ratio values i.e., slip ratio values from Figure 3.39 presented in the table below;

Assuming a brake pedal angle range to be measured by the potentiometer $0 - 40^\circ$ as the operating range for the driver's intent to use the Regenerative Braking System, such that anything more than ($40^\circ \leq \theta \leq 90^\circ$) signifies the driver's intent to use the Anti-lock Braking System.

Two sliders are provided to simulate the SEV's speedometer, providing velocity values ranging from 0 – 100 km/h to the system.

The system's output is obtained by reading the light combinations of two Lamps labelled.

Range Indicator and Torque Indicator having either green or red colours. Table 3.7 is referred to for this.

Table 4.3: Table of Parameters

Parameter	Character	Value	Unit
Wheel Radius	R	0.25	m
Initial Velocity	V_x	0 - 100	km/h
Moment of Inertia	I_w	1.13	kgm ²
Vehicle Mass	m	350	kg
Acceleration due to gravity	g	9.81	m/s ²
Coefficient of Air Resistance	C_D	0.75	-
Frontal Area	A	4	m ²
Object Distance	L	100-200	m

Substituting the information in Table 3.6 into and the Burckhardt friction model given in eq (45), the variance of road coefficient of friction to wheel slip ratio based on surface types is plotted below, from which Table 4.4 is gotten.

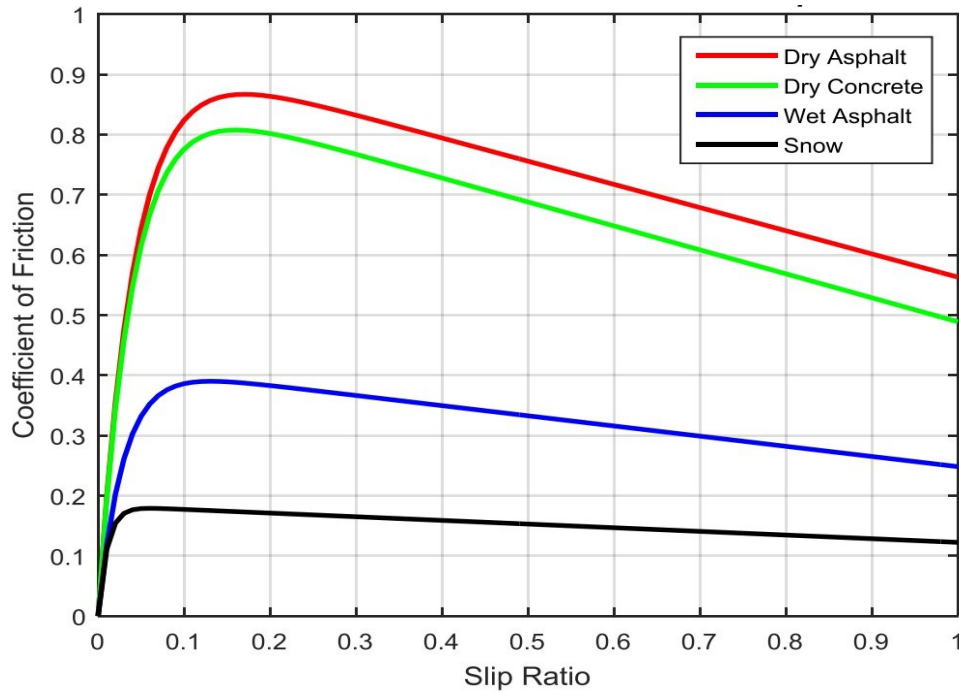


Figure 4.7: Coefficient of road friction against wheel slip ratio

Table 4.4 Road surface type against and corresponding slip ratio

Surface Types	Slip Ratio (λ)
Dry Asphalt	0.17
Wet Asphalt	0.15
Dry Concrete	0.125
Snow	0.03

The simulations for the SEV moving at an assumed velocity of 56km/h, driving in snow with its brake pedal being pressed with an angle of 80° to bring the SEV to rest within 200m are shown below, highlighting the required braking torque to bring the SEV to rest, the braking torque to be provided by the RBS, and the Overall decision of the system in terms of Lamp colours.

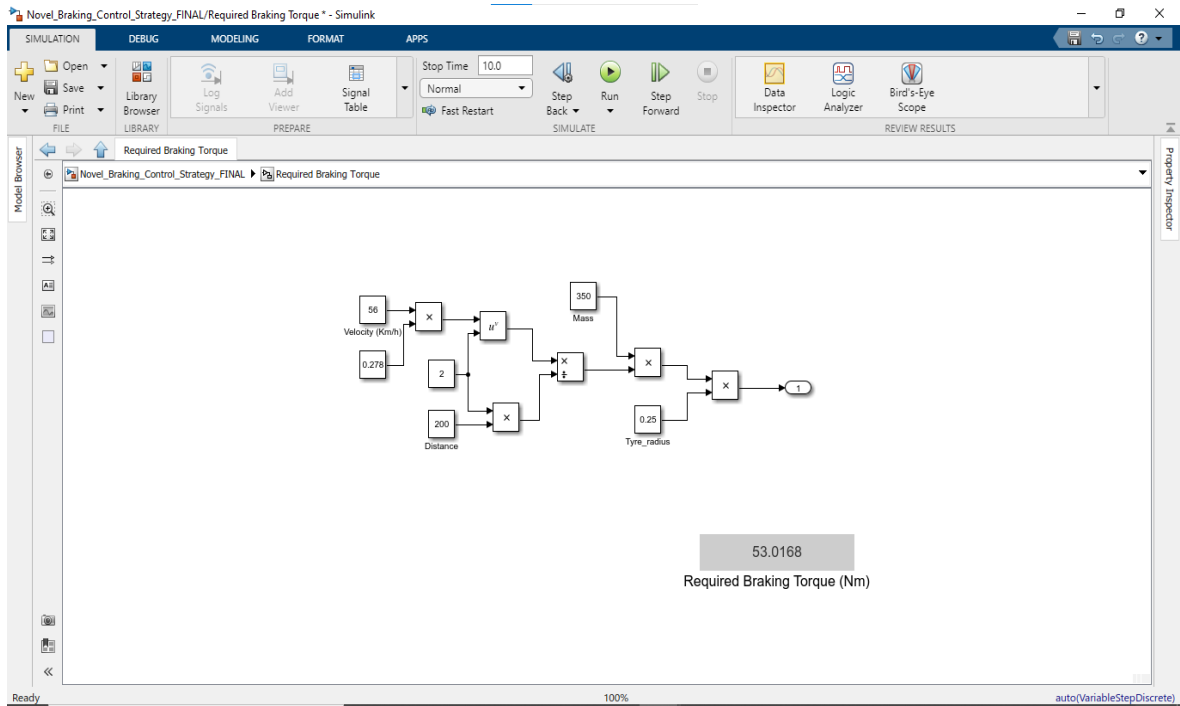


Figure 4.8: MATLAB SIMULINK Simulation of above parameters for Required Braking Torque

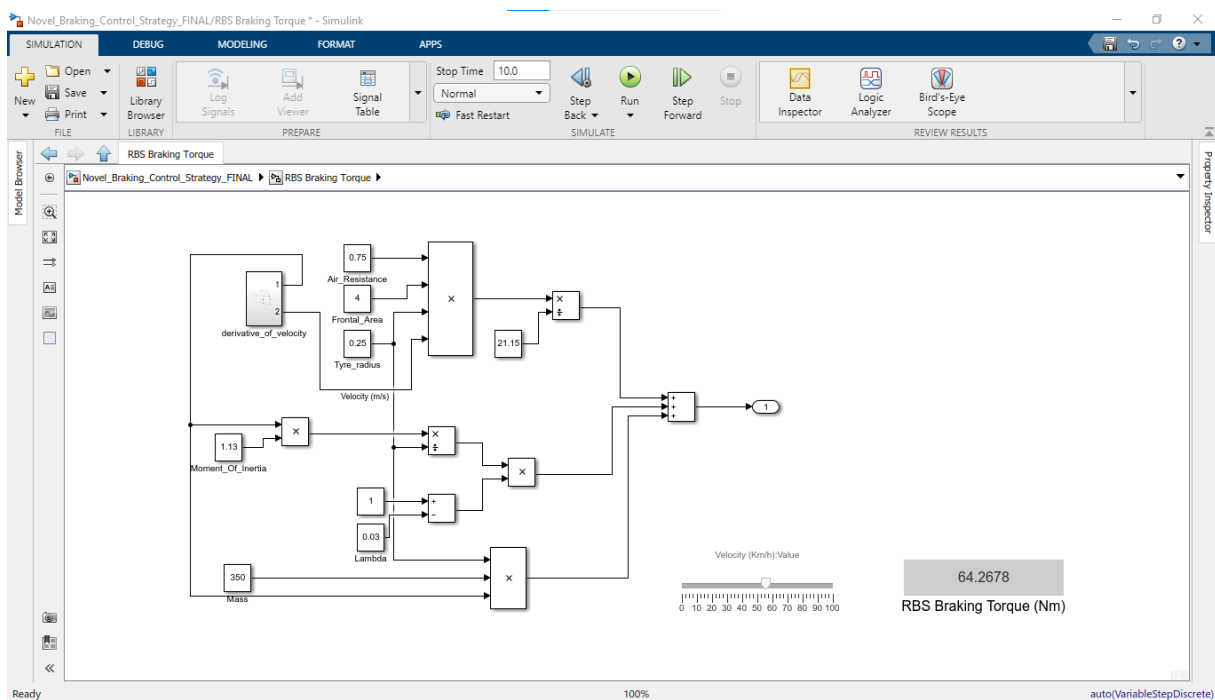


Figure 4.9: MATLAB SIMULINK Simulation of above parameters for RBS Braking Torque

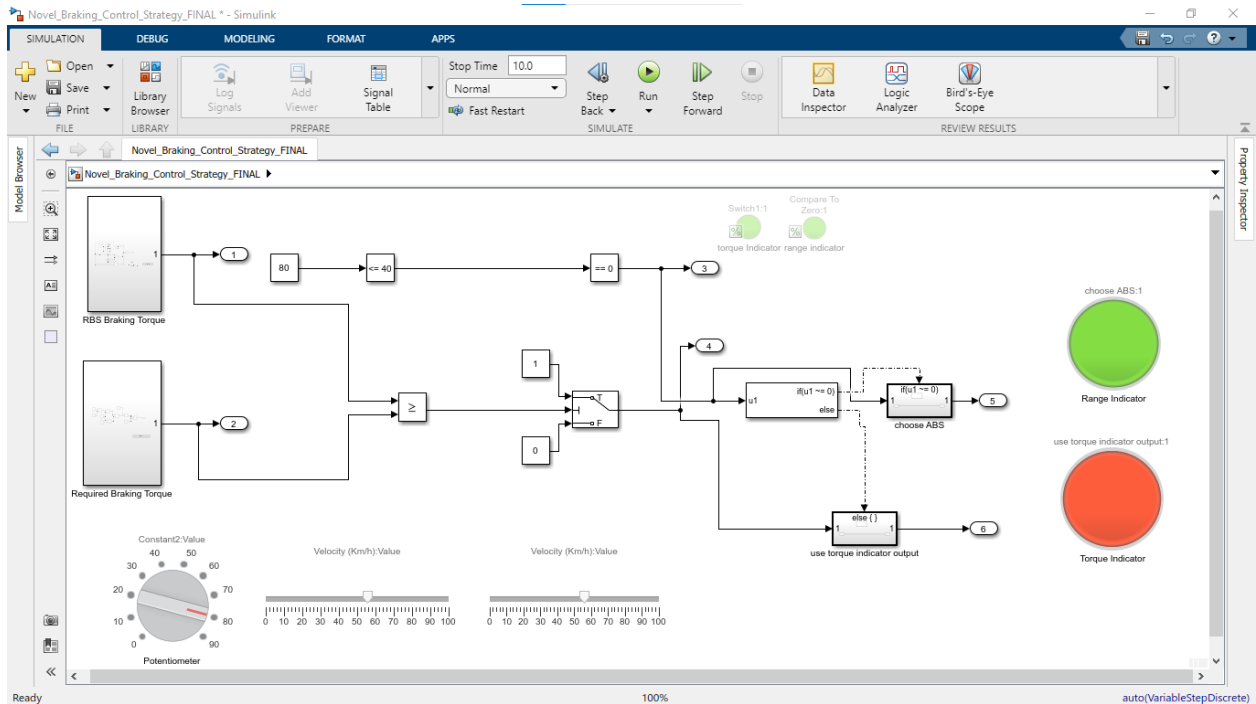


Figure 4.10: MATLAB SIMULINK Simulation of above parameters for proposed system

The parameters are inserted in the simulations such that the ultrasonic sensor output (object distance) is varied from 50m to 200m for the different surface types provided above to obtain Braking torque information, as well as verify the performance, accuracy, and effectiveness of the system. The results are presented in the table below;

Table 4.5: MATLAB SIMULINK Table of Simulation Results

Object Distance (m)	Surface Type	Velocity (km/h)	Pedal Position (°)	Required Braking Torque (Nm)	RBS Braking Torque (Nm)	Lamp Colour	Decision (Braking System)
50	Dry Asphalt	40	50	108.20	117.22	R – Green T - Red	RBS
	Wet Asphalt	50	10	169.10	183.33	R – Red T - Green	RBS
	Dry Concrete	30	45	60.86	66.08	R – Green T - Red	ABS
	Snow	50	25.3	169.06	184.38	R – Red T - Green	RBS

100	Dry Asphalt	49	60	81.18	91.24	R – Green T - Red	ABS
	Wet Asphalt	33	32	36.8	41.42	R – Red T - Green	RBS
	Dry Concrete	76	85	195.30	219.95	R – Green T - Red	ABS
	Snow	45	50	68.47	77.45	R –Green T - Red	ABS
150	Dry Asphalt	89	10	178.55	207.91	R – Red T - Green	RBS
	Wet Asphalt	18	40	7.30	8.51	R – Red T - Green	RBS
	Dry Concrete	34	25.3	26.06	30.40	R – Red T - Green	RBS
	Snow	23	50	11.92	13.97	R – Green T - Red	ABS
200	Dry Asphalt	72	10	87.64	105.60	R – Red T - Green	RBS
	Wet Asphalt	67	45	75.89	91.53	R – Green T - Red	ABS
	Dry Concrete	98	25.3	162.36	196.02	R – Red T - Green	RBS
	Snow	56	80	53.02	64.27	R – Green T - Red	ABS

From the table above we see that the system correctly determines what braking system to use based on the current conditions such that the determination and selection process follows the stipulated operation, we also see that for various values of road type, velocity, and object distance the RBS was able to provide more than the required braking torque to bring the SEV to rest, indicating that not only is the RBS

capable of recharging the SEVs’ batteries, it is also very efficient in braking the vehicle before it reaches or collides with the upcoming obstacle.

4.4 RBS Power Output integration with PV Load Power Output

One of the objectives is integrating the solar energy output with the design braking system output. Having designed the PV and the braking system , a basic integration model is designed as seen in figure 4.11 below. The considered velocity is 5.56m/s as used in all the model designs being the minimal standard safe velocity for any vehicle.

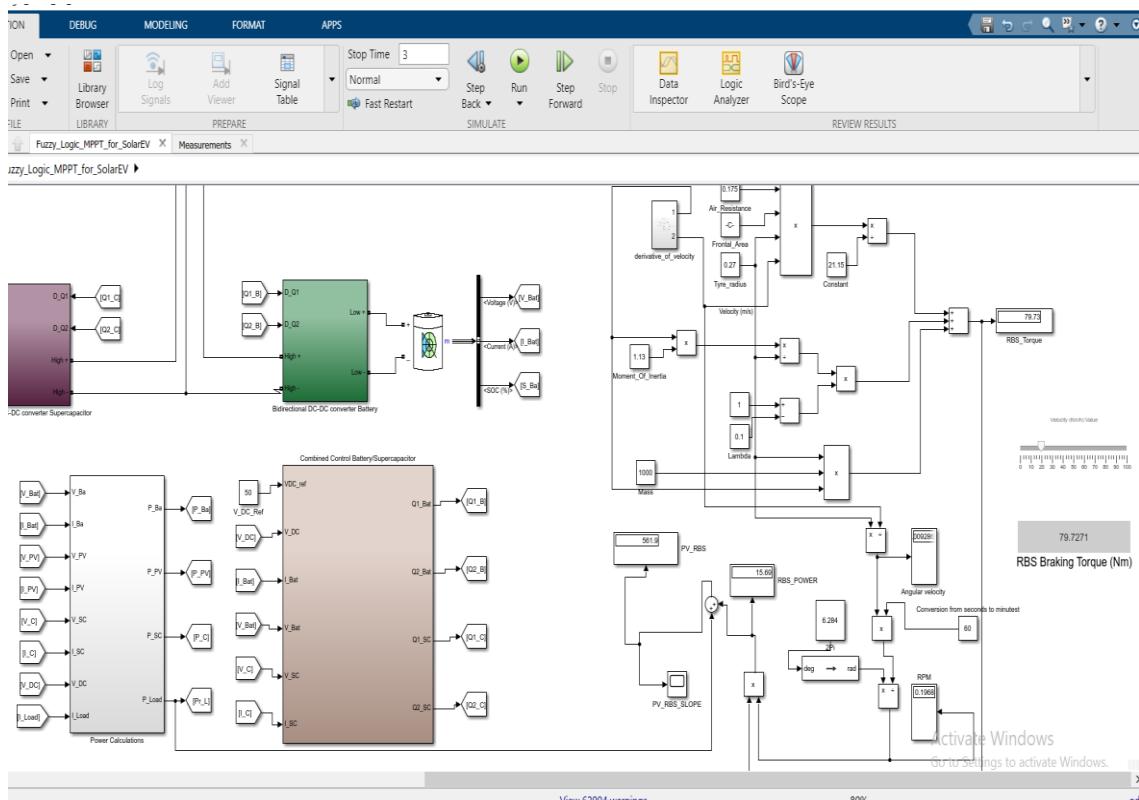


Figure 4.11: Energy sources integration

From the design , the power derived by the RBS is 15.69kW, from a velocity of 5.56m/s. At each braking point and according to the velocity , an addition power is supplied directly to the load for further movement or range of drive.

Modifying table 4.3, after the integration of RBS power at a constant velocity of 5.56m/s at each of the PV irradiance input value, the table becomes

Table 4.6 Integration of PV source Power and RBS Source Power

	DATA	OVERALL AVERAGE	SUMMER	WINTER
	Irradiance value	349w/m ²	473w/m ²	212w/m ²
	Temperature value	20.8	29.2	14.7

	PV Power	2023kW	2788kW	1126kW
	Battery Power	-48.77kW	-632.6kW	649.1kW
	Supercapacitor Power	7.89kW	-20.6kW	-1.099kW
	Load Power	509.3kW	542.5kW	501.6kW
	Load + RBS	524.99kW	558.19kW	517.29kW

CHAPTER V

Conclusion and Recommendations

The integration of PV and braking systems energy for further supply of energy to the electric vehicle has been the main objective of this thesis. This objective is achieved with certain designs made along the way. In a global scenario where environmental hazards from combustion engine vehicles are a problem to mankind, with the fact that , with upcoming designs of electric vehicles and shortage of solar charging stations or high cost of charging electric vehicles, the design of solar electric vehicle is an absolute solution to these crises.

The design started with a collection of travel patterns in Nicosia, and distance covered which influence the decision of this thesis design to be narrowed to the correspondence feedback. Modelling of the forces exerted on the vehicle design was the next approach , by taking technical specifications of the lightyear0 model and the mechanical specification of the tesla model S for the design of the SEV of this thesis. The forces design model , gave an abstract view of the power necessary to move the car at a constant velocity of 5.56m/s.

Further modelling was done about the expected solar energy that can be gotten from the sun for the Nicosia region to power the vehicle based on previous model design when considering forces exerted on the vehicle. The PV design was furthered model in Simulink and done according to each season in the Nicosia region. Pvsyst was the tool for the collection of solar irradiances in the region.

The braking system designed in this thesis has proved that efficient braking systems can be suppliant to aid the SEV for further distance, while still preventing excessive dissipation of heat energy via the brakes, through its conversion and conservation.

Challenges were faced during the design phase in obtaining a 3-D model of the proposed system. The search and installation of a suitable simulation software to test and confirm results from the proposed design took a considerable amount of time and eventually had to be fast-tracked. However, the thesis was completed through all the challenges faced. There were some imprecisions (slight deviations) from the desired interface and interface of the simulation, this however produced similar and desired outputs still.

The solar electric vehicle model design is nearly perfect ,as it requires many calculations and design specifications. In near future , it will be advisable to have a much better design for the mechanical parts, having considered the body materials which should be light weight , the tire of the vehicle which should have smooth friction surface and whose diameter should be reduced for better rolling force.

Furter recommendation is about the solar panel, as most panels are glass natured, research into polymers type of panels and increase in their efficiency will

yield much power and cut off the weight of panels which will be suitable for the design of solar electric vehicles.

References

- Ahmad, S., Mittal, N. R., Bhattacharya, A. B., & Singh, M. (2010). Simulation, output power optimization and comparative study of silicon and thin film solar cell modules. *Proceedings of the 2010 5th IEEE Conference on Industrial Electronics and Applications, ICIEA 2010*, 624–629. <https://doi.org/10.1109/ICIEA.2010.5517028>
- Aksu, U., & Halicioglu, R. (2018). A review study on energy harvesting systems for vehicles. *Tehnički Glasnik*, 12(4), 251–259. <https://doi.org/10.31803/tg-20180210153816>
- Al-rawashdeh, H. (2019). *Design of Solar Photovoltaic for Electric Vehicles Charging Design of Solar Photovoltaic for Electric*. 12(December), 522–531.
- Alnun, N., Said, S., Al-Sharman, S., Al-Ibrahimi, A., Abdulaziz, A., Al Hellabi, M., Touati, F., Ghani, S., Mahdi, E. S., & Benammar, M. (2012). Design of Qatar University's first solar car for Shell Eco-marathon competition. *2012 1st International Conference on Renewable Energies and Vehicular Technology, REVET 2012*, 49–54. <https://doi.org/10.1109/REVET.2012.6195247>
- Alqahtani, S. (2016). *Effects of Social Networking on Higher Education in Saudi Arabia*. 291–304. https://doi.org/10.1007/978-3-319-17716-8_18
- Armaroli, N., & V Balzani. (2011). Towards an electricity-powered world. *Pubs.Rsc.Org-Energy & Environmental*. <https://pubs.rsc.org/en/content/articlehtml/2011/ee/c1ee01249e>
- Basrah, M. S. (2017). INTEGRATION OF ANTI-LOCK BRAKING SYSTEM AND REGENERATIVE BRAKING FOR HYBRID/ELECTRIC VEHICLES. In *Cranfield University 2017*. (Issue 8.5.2017).
- Benboubker, G. (2020). *School of Science and Engineering Engineering of a Solar-Powered Electric Vehicle for on-Campus Use*.
- Bhasin, K. (2019). A Review Paper on Anti-Lock Braking System (ABS) and its Future Scope. *International Journal for Research in Applied Science and Engineering Technology*, 7(8), 372–375. <https://doi.org/10.22214/ijraset.2019.8053>
- Bhatti, A. R., & Salam, Z. (2013). Photovoltaic (PV) Charging of Electric Vehicle (EV). In *Electrical Engineering Research Colloquium For Electronics, Power, Instrumentation & Control And Communication (EERC-2013)* (Vol. 1, pp. 102–103). https://www.researchgate.net/profile/Abdul-Bhatti-6/publication/299580574_Photovoltaic_PV_Charging_of_Electric_Vehicle_EV/links/570079ee08aea6b77469b8ad/Photovoltaic-PV-Charging-of-Electric-Vehicle-EV.pdf
- Bhusal, N. (2018). *The Combined Effect of Photovoltaic and Electric Vehicle Penetration on Conservation Voltage Reduction in Distribution System*. May,

101. <https://digitalscholarship.unlv.edu/thesisdissertations/3218>
- Buchmann, I. (2009). Will Lithium-Ion batteries power the new millennium. *Cadex Electronics Inc., Richmond, BC*, 1–9.
http://members.optusnet.com.au/printing_with_chemistry/Articles/NA_Li-ion1.pdf
- Connors, J. (2007). On the subject of solar vehicles and the benefits of the technology. *2007 International Conference on Clean Electrical Power, ICCEP '07*, 700–705. <https://doi.org/10.1109/ICCEP.2007.384287>
- Chukwuka, C. (2013). *A study of the solar energy systems and storage devices*. <https://open.uct.ac.za/handle/11427/5263>
- Elmenschawy, M., Elmenschawy, M., Massoud, A., & Gastli, A. (2016). Solar car efficient power converters' design. *ISCAIE 2016 - 2016 IEEE Symposium on Computer Applications and Industrial Electronics*, 177–182.
<https://doi.org/10.1109/ISCAIE.2016.7575059>
- Emadi, A., Ehsani, M., & Miller, J. (2003). *Vehicular Electric Power Systems: Land, Sea, Air, and Space Vehicles*. 516.
<https://www.taylorfrancis.com/books/mono/10.1201/9780203913468/vehicular-electric-power-systems-ali-emadi-mehrdad-ehsani-john-miller>
- Fouad, E. (2014). *Charging Station for Electric Vehicles*.
- Han, X., Liang, Y., Ai, Y., & Li, J. (2018). Economic evaluation of a PV combined energy storage charging station based on cost estimation of second-use batteries. *Energy*, *165*, 326–339. <https://doi.org/10.1016/j.energy.2018.09.022>
- Hill, C. A., Such, M. C., Chen, D., Gonzalez, J., & Grady, W. M. K. (2012). Battery energy storage for enabling integration of distributed solar power generation. *IEEE Transactions on Smart Grid*, *3*(2), 850–857.
<https://doi.org/10.1109/TSG.2012.2190113>
- Kayisoglu, G., Canpolat, S., Dilara AYDIN, A., Kucuktas, N., & Huner, M. (2019). Acceleration Logger and Analyzer. *Dergipark.Org.Tr*.
<https://dergipark.org.tr/en/pub/epstem/issue/50288/650446>
- Kirubakaran, A., Jain, S., & Nema, R. K. (2009). A review on fuel cell technologies and power electronic interface. In *Renewable and Sustainable Energy Reviews* (Vol. 13, Issue 9, pp. 2430–2440). <https://doi.org/10.1016/j.rser.2009.04.004>
- Kretchmer, B., Monahan, R., Garcia, A., & ..., E Garner -, U. (2017). Solar Powered Electric Vehicle. *Pnw.Edu*. https://www.pnw.edu/wp-content/uploads/2020/03/Solar_Vehicle_ME439_Final_Paper_v2.pdf
- Kumar, M., Sinha, P., Pal, T., & Kar, K. K. (2020). Materials for supercapacitors. In *Springer Series in Materials Science* (Vol. 302, pp. 29–70).
https://doi.org/10.1007/978-3-030-52359-6_2

- Latha, M., Michahail, S., Apoorva, K. S., Pooja, S. K., Prafulla, P. S., & Sharvani, B. C. (2014). Electric Vehicle Charging Method for Automobiles Using Photovoltaic Cells. *Researchgate.Net*, 3(11), 128–132.
https://www.researchgate.net/profile/Stafford-Michahial/publication/304382645_Electric_Vehicle_Charging_Method_for_Automobiles_Using_Photovoltaic_Cells/links/576dd3df08ae10de6395d635/Electric-Vehicle-Charging-Method-for-Automobiles-Using-Photovoltaic-Cell
- Larminie, J., & Dicks, A. (2013). Fuel cell systems explained: Second edition. In *Fuel Cell Systems Explained: Second Edition*.
<https://doi.org/10.1002/9781118878330>
- Li, W., Long, R., Chen, H., Energy, J. G., & Undefined. (2017). A review of factors influencing consumer intentions to adopt battery electric vehicles. *Elsevier-Renewable and Sustainable*.
https://www.sciencedirect.com/science/article/pii/S1364032117305798?casa_token=yeEPP_40s2kAAAAA:DI9ijMT1LJag-iSGHmnsnauYnnGeJTUE8hyo-56DN_-OsO9Lg4NbAPzqGFaD_Nx_ZIPZqKPx
- M. Sabri, M. F., Danapalasingam, K. A., & Rahmat, M. F. (2016). A review on hybrid electric vehicles architecture and energy management strategies. In *Renewable and Sustainable Energy Reviews* (Vol. 53, pp. 1433–1442).
<https://doi.org/10.1016/j.rser.2015.09.036>
- Mahato, N., Banerjee, A., Gupta, A., Omar, S., & Balani, K. (2015). Progress in material selection for solid oxide fuel cell technology: A review. In *Progress in Materials Science* (Vol. 72, pp. 141–337).
<https://doi.org/10.1016/j.pmatsci.2015.01.001>
- Mandal, S., Sarker, M. R. I., Rahman, M. S., & Beg, M. R. A. (2017). An analysis of braking energy regeneration in electric vehicles. *International Journal of Renewable Energy Research*, 7(3), 999–1006.
<https://doi.org/10.20508/ijrer.v7i3.5770.g7130>
- Mangu, R., Prayaga, K., Nadimpally, B., & Nicaise, S. (2010). Design, development, and optimization of highly efficient solar cars: Gato del Sol I-IV. *2010 IEEE Green Technologies*.
<https://doi.org/10.1109/GREEN.2010.5453800>
- Manivannan, S., & Kaleeswaran, E. (2017). Solar powered electric vehicle. *2016 1st International Conference on Sustainable Green Buildings and Communities, SGBC 2016*. <https://doi.org/10.1109/SGBC.2016.7936074>
- Menasce, D., Grobler, M., & Van Rensburg, P. J. (2013). High power electrical systems design for a solar car: Designing and building the solar car Ilanga.I. *IEEE AFRICON Conference*. <https://doi.org/10.1109/AFRCON.2013.6757697>
- Mills, A., & Stumpges, E. (2013). The American solar challenge 2012. *IEEE*

- Potentials*, 32(2), 10–16. <https://doi.org/10.1109/MPOT.2012.2223831>
- Mohan, H. M., Nair, A. M., Chandran, A. B., & Chandran, A. B. (2019). Solar Powered Plug-in Electric Vehicle. *International Journal of Engineering Research & Technology*, 8(5), 968–971. www.ijert.org
- Nawaz, A. R., Al-brahim, A., Momen, A. Al, Qahtani, A. Al, & Aishah, A. A. (2017). *Fully Electric Car with Solar Cells as a Secondary Source of Power*.
- Ndyamukama, E. F. (2017). *LUT SCHOOL OF ENERGY SYSTEMS ENERGY TECHNOLOGY OPTIMIZATION OF SOLAR POWER SYSTEM FOR Examiners : Professor Jero Ahola Associate Professor Antti Kosonen Abstract*.
- Poullikkas, A. (2015). Sustainable options for electric vehicle technologies. In *Renewable and Sustainable Energy Reviews* (Vol. 41, pp. 1277–1287). <https://doi.org/10.1016/j.rser.2014.09.016>
- Raghavan, A. K. (2018). *PV enabled net zero EV charging station : system design and simulation studies*. <https://uwspace.uwaterloo.ca/handle/10012/13893>
- Rama, S. K. B. S. S. V. R. C. D. Y. A. R. V. P. . (2019). Regenerative Braking System. *International Journal of Trend in Scientific Research and Development, Volume-3*(Issue-4), 298–300. <https://doi.org/10.31142/ijtsrd23546>
- Robinson, J., Brase, G., Griswold, W., Jackson, C., & Erickson, L. (2014). Business models for solar powered charging stations to develop infrastructure for electric vehicles. *Sustainability (Switzerland)*, 6(10), 7358–7387. <https://doi.org/10.3390/su6107358>
- Said, S., Massoud, A., Benammar, M., & Ahmed, S. (2012). A Matlab/Simulink-Based Photovoltaic Array Model Employing SimPowerSystems Toolbox. *Journal of Energy and Power Engineering*, 6, 1965–1975. <https://www.academia.edu/download/30819960/2012123070352113.pdf>
- Sandalow, D. (2009). *Plug-in electric vehicles: what role for Washington?* <https://books.google.com/books?hl=en&lr=&id=i9XEgUchZzgC&oi=fnd&pg=PP1&dq=D.+B.+Sandalow,+Plug-in+electric+vehicles:+what+role+for+Washington%3F+Brookings+Institution+Press,++2009.&ots=uXPQh6a6JV&sig=AJcFdQseYkXA01ClBzkCLHzjmK4>
- Sandy Thomas, C. E. (2009). Transportation options in a carbon-constrained world: Hybrids, plug-in hybrids, biofuels, fuel cell electric vehicles, and battery electric vehicles. *International Journal of Hydrogen Energy*, 34(23), 9279–9296. <https://doi.org/10.1016/j.ijhydene.2009.09.058>
- Schuller, A., Dietz, B., Flath, C. M., & Weinhardt, C. (2014). Charging strategies for battery electric vehicles: Economic benchmark and V2G potential. *IEEE*

- Transactions on Power Systems*, 29(5), 2014–2222.
<https://doi.org/10.1109/TPWRS.2014.2301024>
- Scibioh, M. A., & Viswanathan, B. (2020). Materials for supercapacitor applications. In *Materials for Supercapacitor Applications*.
<https://doi.org/10.1016/c2019-0-00454-2>
- Selvan, V. T. S., A.Sunil, Vignesh.P, & V.Vigneshwar. (2018). *Smart Solar Vehicle*.
- Sperling, D. (1995). Future drive: electric vehicles and sustainable transportation. *Choice Reviews Online*, 32(11), 32-6255-32–6255.
<https://doi.org/10.5860/choice.32-6255>
- Taylor, A. M. K. P. (2008). Science review of internal combustion engines. *Energy Policy*, 36(12), 4657–4667. <https://doi.org/10.1016/j.enpol.2008.09.001>
- Tinnemeyer, J. A. (2011). New advances in li-ion battery monitoring. *Battery Power 2011*, 467–486.
https://www.cadex.com/_content/New_Advances_in_Lithium_Ion_Battery_Fuel_Gauging_Final.pdf
- Uddin, H. M., Jerin, N. H., Sultana, A., & others. (2018). To Study the Solar Irradiation Pattern of Bangladesh for Electricity Generation. In *Daffodil International University*.
https://scholar.google.com/scholar?hl=en&as_sdt=0%2C5&q=H.+M.+Uddin%2C+N.+H.+Jerin%2C+and+A.+Sultana%2C+“To+Study+the+Solar+Irradiation+Pattern+of+Bangladesh++for+Electricity+Generation%2C”+PhD+Thesis%2C+Daffodil+International+University%2C+2018.+&btnG=
- Valero, S., Senabre, C., & López, D. (2013). Feasibility of Recharging Electric Vehicles with Photovoltaic Solar Panels. *52.196.142.242*, 6(2), 24–30.
<http://52.196.142.242/index.php/est/article/view/j.est.1923847920130602.2344>
- Wang, Y., Song, Y., & Reviews, Y. X. (2016). Electrochemical capacitors: mechanism, materials, systems, characterization and applications. *Pubs.Rsc.Org*. <https://pubs.rsc.org/en/content/articlehtml/2016/cs/c5cs00580a>
- Wilson, G., Al-Jassim, M., & WK Metzger. (2020). *The 2020 photovoltaic technologies roadmap - IOPscience*. Iopscience.Iop.Org- Journal of Physics D Undefined. <https://iopscience.iop.org/article/10.1088/1361-6463/ab9c6a/meta>
- Wisniewski, D. (2010). Solar flare: An open-road challenge. *Ieeexplore.Ieee.Org*, 29(1), pp.6-9. <https://ieeexplore.ieee.org/abstract/document/5379684/>
- Wu, B., Zhuo, F., Long, F., Gu, W., Qing, Y., & Liu, Y. (2011). A management strategy for solar panel battery super capacitor hybrid energy system in solar car. *8th International Conference on Power Electronics - ECCE Asia: “Green World with Power Electronics”*, ICPE 2011-ECCE Asia, 1682–1687.
<https://doi.org/10.1109/ICPE.2011.5944438>

Zhang, L., & Cai, X. (2018). Control strategy of regenerative braking system in electric vehicles. *Energy Procedia*, 152, 496–501.
<https://doi.org/10.1016/j.egypro.2018.09.200>

Zhao, J., Materials, A. B., & Undefined. (2021). Electrochemical capacitors: Materials, technologies, and performance. *Elsevier- Energy Storage*.
https://www.sciencedirect.com/science/article/pii/S2405829720304761?casa_token=o5sYmpLFgG8AAAAA:rlqvS0JkGM_SmwsUVB8Fi47fnZzRG3eI2l64ylqLfp5tPUNfZeK0urb3tvMW_oDnv7MYWJAT

Appendices

The following extra information as regards the thesis are attached to the appendices separately from the main report.

Appendix A (Answers from the Survey)

From the E-questionnaire created from google forms, the link below is an attachment to the result gotten from the correspondence of the survey.

https://drive.google.com/file/d/1fhKOh5CXu8VdbDz41wa-Mb5f1CIMp_6Q/view?usp=sharing

Appendix B (Fuzzy Logic Inference for MPPT model)

Fuzzy Logic Controller Design Model

Fuzzy controllers are based on rule bases and membership functions for their design aspect. They are effective because they consider grey areas of design aspects. Fuzzy controllers are more robust and easier to implement as compared to classical control schemes. This is the main reason why fuzzy controller schemes are implemented in artificial intelligence papers because they cover the grey area aspects of design.

In this thesis , I proposed fuzzy controller with two inputs, P_v and I_v and one output, PWM, to create the duty circle resulting in the control by the MPPT.

Our fuzzy logic design is consisting of inputs, output, and Mamdani-Fuzzy inference engine. The output is the Duty cycle and is defuzzified using the centroid method. The block diagram below depicts that.

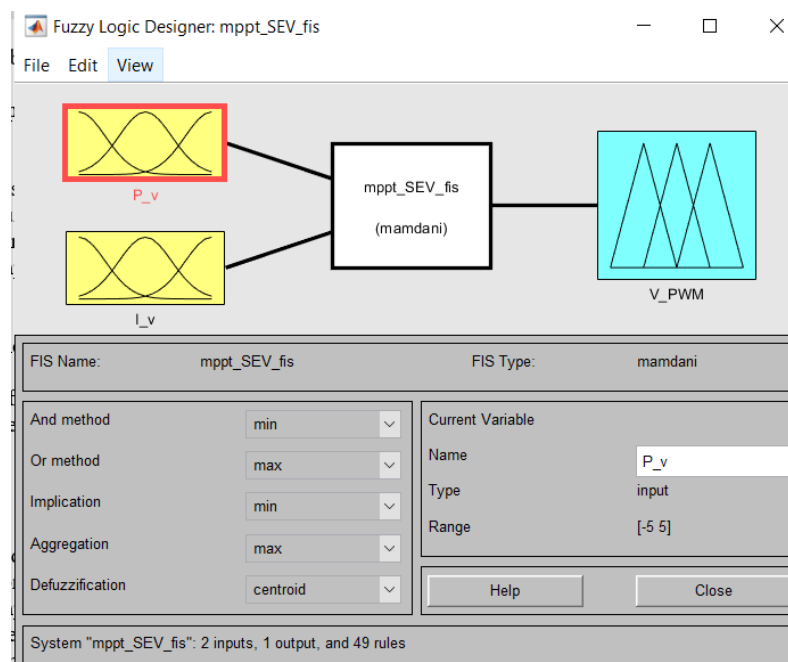


Figure 1: *Design Variables*

Membership Functions

It is very important we implement the membership function in the fuzzification and the defuzzification steps of the FLC because it must perform evaluation of the non-fuzzy input values to the fuzzy linguistic terms and vice versa. More so, we implement the membership function to measure these linguistic terms. Below are the

membership function of the inputs and the output values showing their respective ranges.

P_V – The power derived from the solar irradiance and temperature of the region into the simulation.

Then, we divide the power from -5 to 5 to 7 different ranges as follows:

- Negative big (1,2,-5), gbellmf.
- Negative medium (-4 ,2) trimf.
- Negative medium (-3 ,1) trimf.
- Zero (-0.5 ,0.5) trimf.
- Positive small (1 ,3) trimf.
- Positive medium (2 ,4) trimf.
- Positive big (1,2,5) , gbellmf.

I_V – The current derived from the solar irradiance and temperature of the region into the simulation.

Then, we divide the current from -5 to 5 to 7 different ranges as follows:

- Negative big (1,2,-5), gbellmf.
- Negative medium (-4 ,2) trimf.
- Negative medium (-3 ,1) trimf.
- Zero (-0.5 ,0.5) trimf.
- Positive small (1 ,3) trimf.
- Positive medium (2 ,4) trimf.
- Positive big (1,2,5) , gbellmf.

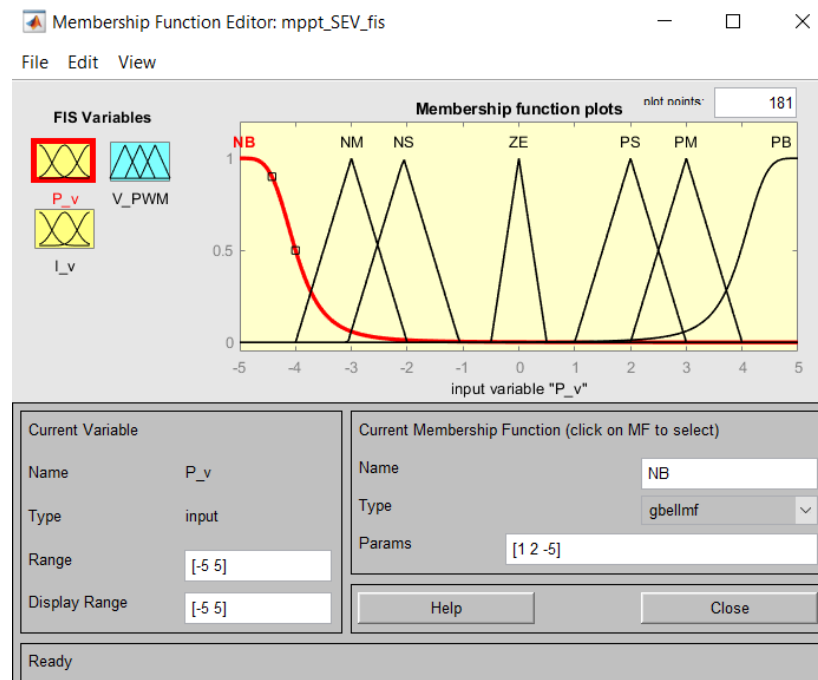
PWM – Now for the output membership function, The Output is regarded as the duty cycle that is controlled by the MPPT to results to the boosting of the voltage. The PWM serves as the transducer for switching the pulses.

The membership functions are classified as.

- Negative big (-1, -0.6), trimf.
- Negative medium (-0.8, -0.4) trimf.
- Negative medium (-0.6 , -0.2) trimf.
- Zero (-1.5 ,1.5) trimf.
- Positive small (0.2 ,0.6) trimf.
- Positive medium (0.4 ,0.8) trimf.
- Positive big (0.6, 1) , trimf.

Table 1: *Membership Functions*

Input/output	Parameters	Membership Functions	Ranges
INPUT	P_V	NB, NM, NS, ZE, PS, PM, PB	-5 to 5
	I_V	NB, NM, NS, ZE, PS, PM, PB	-5 to 5
OUTPUT	PWM	DL, DS, NBT, IS, IL	-1 to 1

Figure 2: *Membership function P_v*

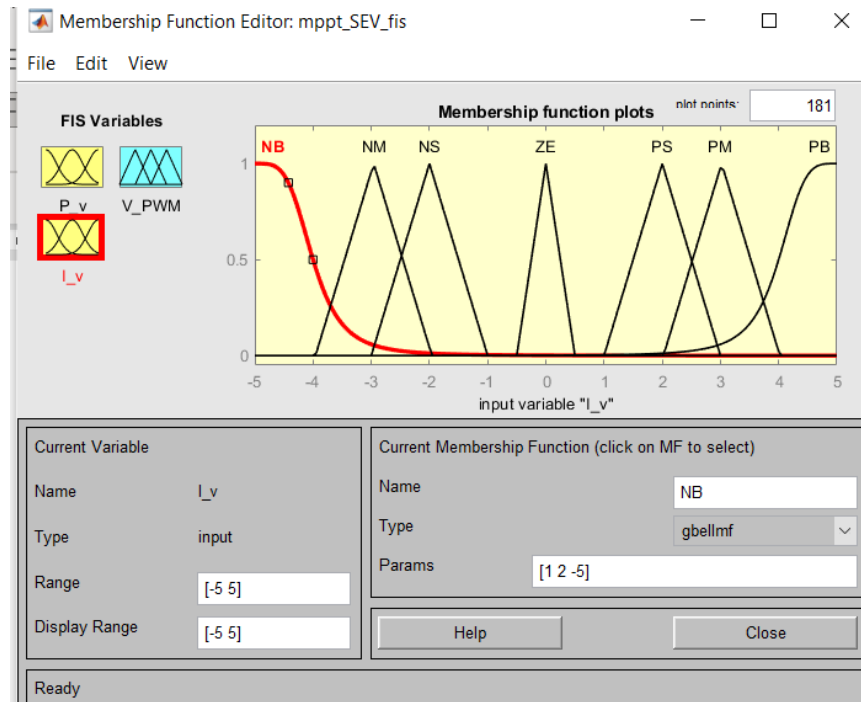


Figure 3: *Membership function I_v*

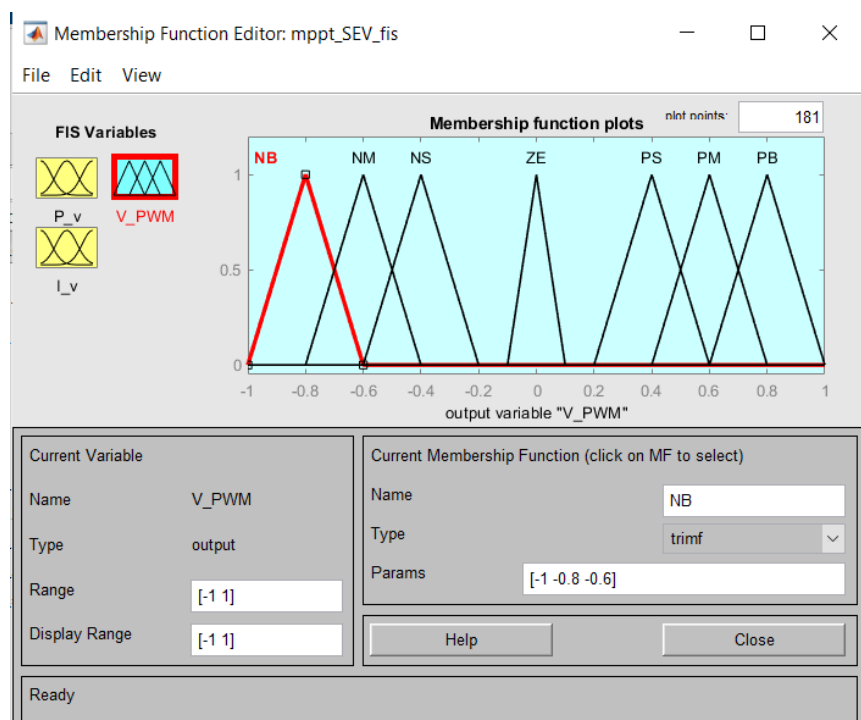


Figure 4: *Output Membership function PWM*

Design Rules base

Therefore, the fuzzy rules for training with an IF-THEN condition and a conclusion used for this design is shown in Table 3.2 and Figure 3.4 below. The fuzzy rules are designed to track the maximum power point of the Pv system under

changing weather conditions. Rapid changing solar radiation is taken into account while designing these rules.

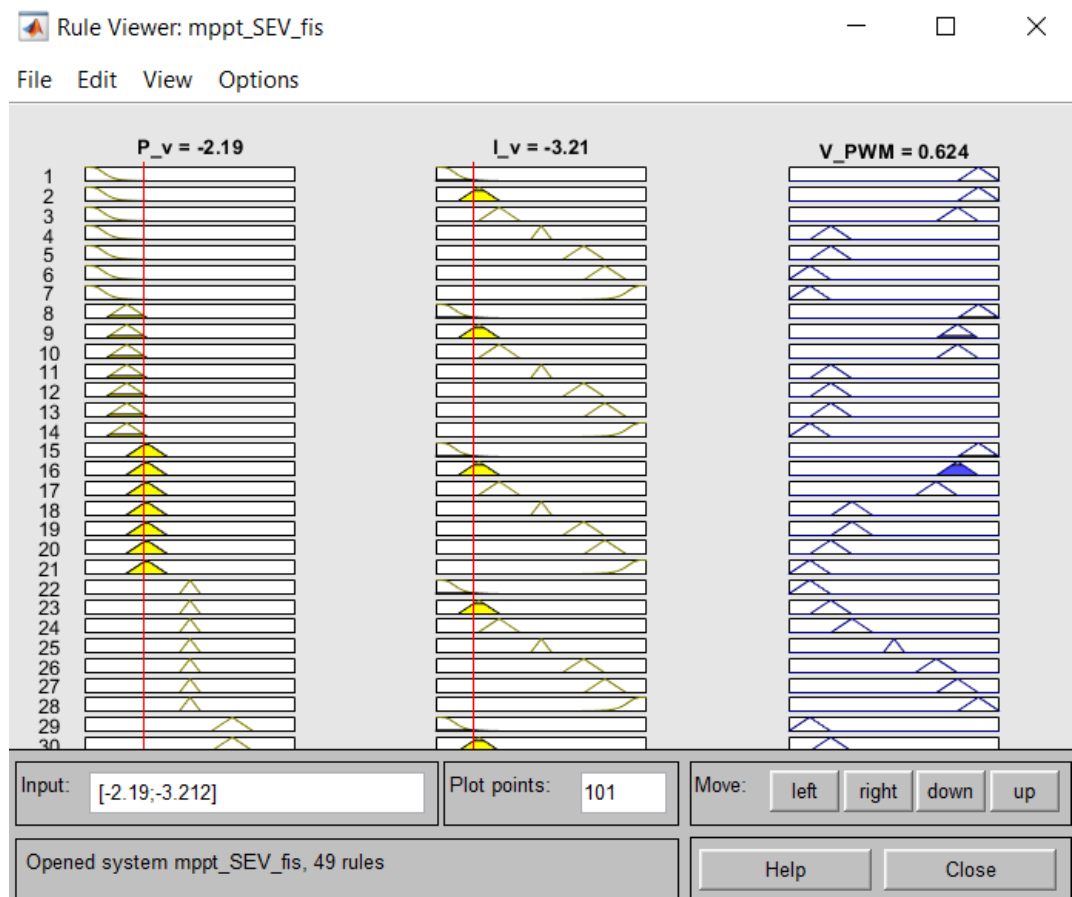
Table 2: *Fuzzy Rule based training*

$\Delta P_v / \Delta I_v$	NB	NM	NM	ZE	PS	PM	PB
NB	PB	PB	PM	NM	NM	NB	NB
NM	PB	PM	PM	NM	NM	NM	NB
NS	PB	PM	PS	NS	NS	NM	NB
ZE	NB	NM	NS	ZE	PS	PM	PB
PS	NB	NM	NS	PS	PS	PM	PB
PM	NB	NM	PM	PM	PM	PM	PB
PB	NB	NM	NM	PM	PM	PB	PB

Defuzzification

Finally, the process of defuzzification. The defuzzification process is a procedure of the quantitative outcome of the fuzzy logic design, the stated fuzzy sets, and the degrees of the membership function. Basically, it is needed in the arrangements of the fuzzy control and these arrangements contains many rules that will convert some variables into the result of the fuzzy design and then the variables that are converted are called the expressed results that are in the terms of the membership functions in the fuzzy sets. Furthermore, the defuzzification renders the fuzzy set degrees of the membership function into an output in the form of the output like the real values.

Figure 5 :Fuzzy Knowledge Rule base viewer



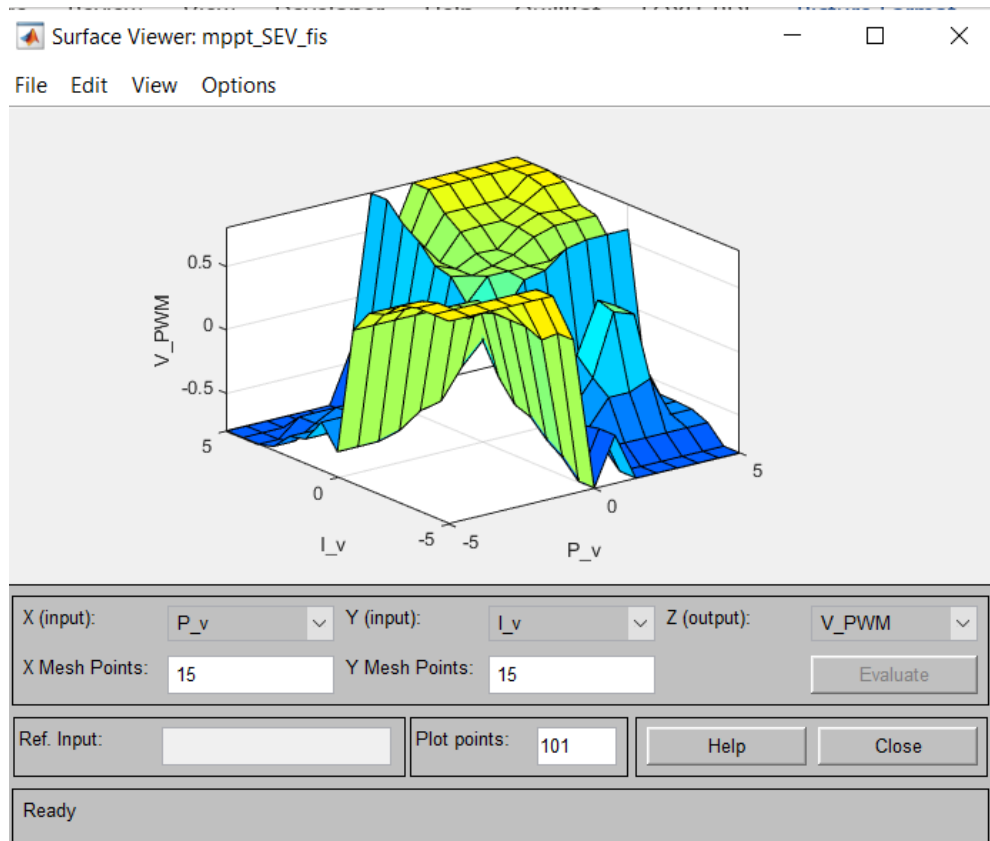


Figure 6: *Surface Viewer* plot

Appendix C (Plagiarism report)

chapter 1

ORIGINALITY REPORT

2 %	1 %	1 %	%
SIMILARITY INDEX	INTERNET SOURCES	PUBLICATIONS	STUDENT PAPERS

PRIMARY SOURCES

1	clock.uclan.ac.uk Internet Source	1 %
2	Muhammad Nouman Aslam Khan, Zeeshan Ul Haq, Hafeez Ullah, Salman Raza Naqvi et al. "Prediction of hydrogen yield from supercritical gasification process of sewage sludge using machine learning and particle swarm hybrid strategy", International Journal of Hydrogen Energy, 2023 Publication	1 %

Exclude quotes Off Exclude matches < 6 words
 Exclude bibliography On

Chapter 2

ORIGINALITY REPORT

11 %	9 %	6 %	%
SIMILARITY INDEX	INTERNET SOURCES	PUBLICATIONS	STUDENT PAPERS

PRIMARY SOURCES

1	www.pnw.edu Internet Source	2 %
2	moam.info Internet Source	2 %
3	Jarapala Ramesh Babu, Manas Ranjan Nayak, B. Mangu. "A Peer Review of Hybrid Electric Vehicle Based on Step-Up Multi-input Dc-Dc Converter and renewable energy source", Journal of Physics: Conference Series, 2021 Publication	2 %
4	www.studymode.com Internet Source	1 %
5	www.doria.fi Internet Source	1 %
6	Mariam ElMenshawy, Mena ElMenshawy, Ahmed Massoud, Adel Gastli. "Solar car efficient power converters' design", 2016 IEEE Symposium on Computer Applications & Industrial Electronics (ISCAIE), 2016 Publication	<1 %

chapter 3

ORIGINALITY REPORT

4%	3%	2%	%
SIMILARITY INDEX	INTERNET SOURCES	PUBLICATIONS	STUDENT PAPERS

PRIMARY SOURCES

1	journalofbabylon.com Internet Source	1%
2	weatherspark.com Internet Source	1%
3	www.researchgate.net Internet Source	<1%
4	www.arrow.com Internet Source	<1%
5	M.E. Glavin. "A stand-alone photovoltaic supercapacitor battery hybrid energy storage system", 2008 13th International Power Electronics and Motion Control Conference, 09/2008 Publication	<1%
6	www.cookcountyclerkil.gov Internet Source	<1%
7	www.hartfieldsite.org.au Internet Source	<1%
8	www.kratki.net.gr Internet Source	

Chapter 4

ORIGINALITY REPORT

1 %	1 %	0 %	%
SIMILARITY INDEX	INTERNET SOURCES	PUBLICATIONS	STUDENT PAPERS

PRIMARY SOURCES

1	www.slideshare.net Internet Source	1 %
2	product.popykpd.com Internet Source	<1 %

Exclude quotes Off

Exclude matches < 6 words

Exclude bibliography On

Chapter V

ORIGINALITY REPORT

0%

SIMILARITY INDEX

0%

INTERNET SOURCES

0%

PUBLICATIONS

%

STUDENT PAPERS

PRIMARY SOURCES

Exclude quotes Off

Exclude bibliography On

Exclude matches < 6 words

Abstract

ORIGINALITY REPORT

0%

SIMILARITY INDEX

0%

INTERNET SOURCES

0%

PUBLICATIONS

%

STUDENT PAPERS

MATCH ALL SOURCES (ONLY SELECTED SOURCE PRINTED)

Exclude quotes Off

Exclude bibliography On

Exclude matches < 6 words